# Repairing impacted thermoplastic composites using ultrasonic welding to restore the compressive strength

J. A. Vreeken

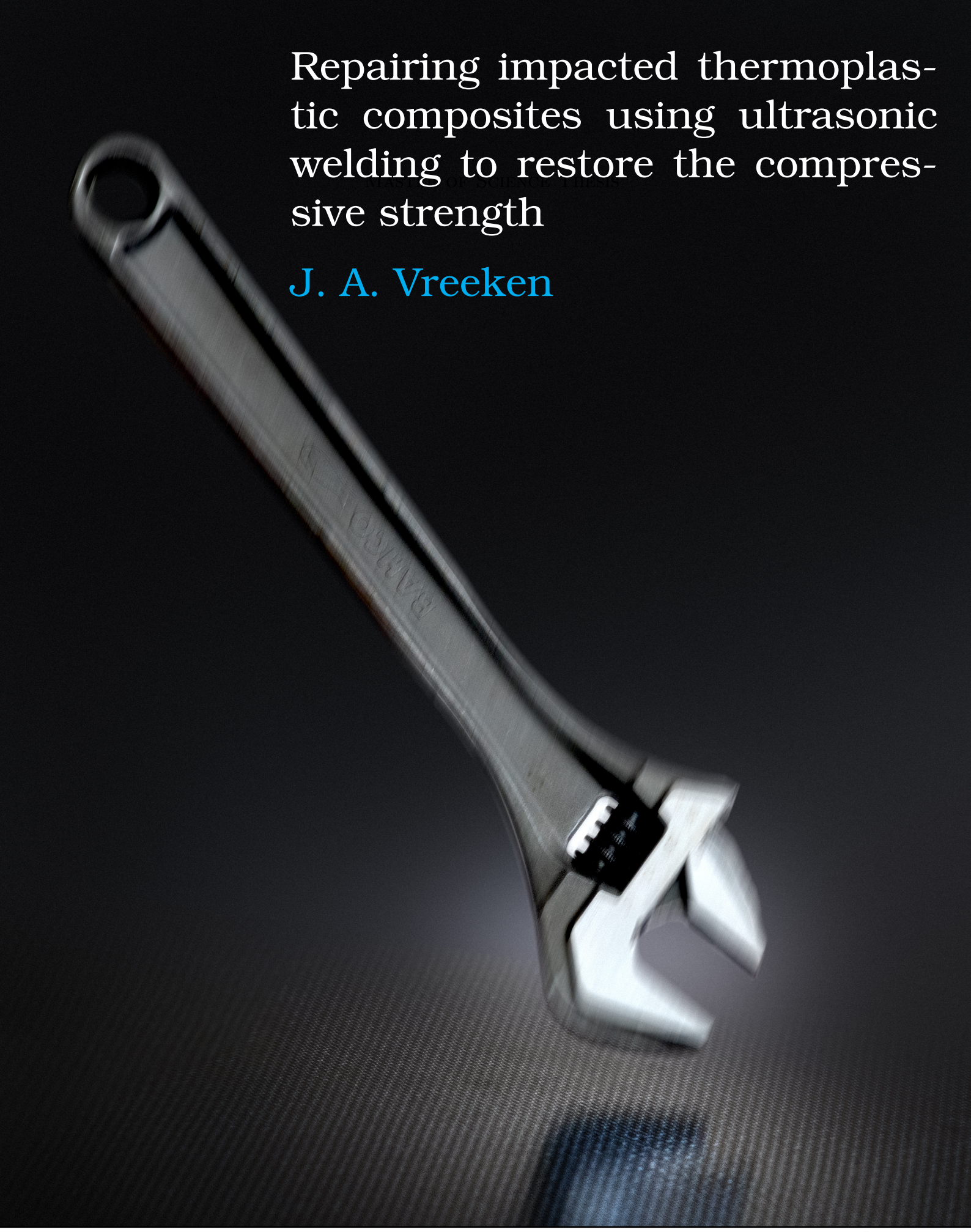

TU Delft Delft University of Technology

# Repairing impacted thermoplastic composites using ultrasonic welding to restore the compressive strength

Master of Science Thesis

For obtaining the degree of Master of Science in Aerospace Engineering
at Delft University of Technology

J. A. Vreeken

22nd of June , 2022

Faculty of Aerospace Engineering · Delft University of Technology

Delft University of Technology
Faculty of Aerospace Engineering
Department of Aerospace Structures and Materials

**GRADUATION COMMITTEE**

Dated: 22nd of June , 2022

Chair holder:

Dr.ir. I. F. Villegas

Committee members:

Dr.ir. J. A. Pascoe

Ir. J. Sinke

Dr.ir. B. C. P. Jongbloed

“A grinder and paint makes you the welder you ain’t”

— *Unkown* —

# Acknowledgments

This thesis not only finalizes my Master's program, it also concludes my time at the faculty of Aerospace Engineering at the Delft University of Technology. Completing this thesis project, and the rest of my studies, would not have been possible without the people around me whom have supported me through the good times and the bad times.

First, I would like to thank my supervisors John-Alan Pascoe and Irene Fernandez Villegas, not only for the opportunity to work on this research project, but also for continuously guiding and supporting me throughout the duration of this project. Without this guidance and support, I would never have been able to make this project a success.

I also would like all the technicians of the DASML lab who helped me during the experimental phase of my project. I would like to specifically thank Dave Ruijtenbeek and Alexander Uithol. Although they might not realize it, at some point, they became an important part of my social contact. During the lockdown period of the pandemic, social contact was very limited, having lunch with them every day during this period really helped me keeping a good spirit.

Furthermore, I would like to take this opportunity to thank Daan Hottentot Cederløf, my friend and unofficial mentor throughout my studies. As he did the same bachelor and master programs as me, and was a few years ahead, he paved away a path keeping me in his wake. All his help, from lending me all his books to all kinds of study related advice, really made my time as a student a lot easier.

Finally, I would like to thank my girlfriend, Lizzie Snijders. She provided me the love and support to help me push through the last phases of my studies. Although the circumstances of the last year were especially challenging, I know for a fact that I could not have done it without her by my side. Most importantly, I would like to thank my mother, Liesbeth Hoetmer. She knows best the challenges I faced and without her lifelong unconditional love and support, I would not be where I am today.

Delft, University of Technology — J. A. Vreeken
22nd of June , 2022

# Abstract

Within aviation, the interest in thermoplastic composites has been growing over the past years and some aircraft components are now being made from thermoplastics. With the use of thermoplastics, there is a need for efficient processes to repair damage, more specifically impact damage, as 75% of the damages is caused by impact events. The aim of this research project is to investigate the potential use of ultrasonic (US) welding as a tool to repair impact damage, which will be compared to the already existing method, hot-pressing.
To investigate the potential of US welding, first, impact damage inside a thermoplastic composite was characterized. This was followed by an investigation on the heating mechanisms inside impact damage during welding and the influence of different welding parameters. This knowledge was used to set up welding parameters for the final repairs. The US repaired specimens, together with pristine, damaged and hot-press repaired specimens which were used as a reference, were tested to determine their compression after impact (CAI) strength.
Investigation into US welding impact damage showed that heat was generated inside the delaminations themselves and that frictional heating between the sonotrode and the surface of the laminate is negligible. It was shown that US welding can cause the delaminations to grow, but can also melt and re-consolidate delaminations decreasing the damaged area. Within this project, using a sonotrode that covered approximately 65% of the damaged area, US welding was able to re-consolidate a maximum of 25% of the damaged area. Even when using the same welding parameters, the process showed large variations between the welds. These variations should be minimized for the process to be usable as a repair process.
CAI testing showed that, for US welded repairs, the repairs can either increase or decrease the CAI strength, which is believed to be related to the variation between the welded repairs. One specimen showed that, although only partially re-consolidated, US welding can fully restore the CAI strength, due to the fact that the re-consolidated area suppressed local buckling inside the damaged area, which normally causes the specimen to fail prematurely. However, it was also shown that specimens with little re-consolidated area or degraded material decreased in CAI strength. Compared to US welding, hot-pressing, although able to re-consolidate the whole damaged area, was not able to increase the CAI strength. This was the case due to the fact that the whole specimen needed to be re-consolidated, which resulted in poor material quality near the edges of the specimen, causing premature failure of the whole specimen.

# Table of Contents

# List of Figures

# List of Tables

# Nomenclature

**Abbreviations**

| | |
|---|---|
| CAI | Compression After Impact |
| CFRP | Carbon Fiber Reinforced Polymer |
| DIC | Digital Image Correlation |
| ED | Energy Director |
| IR | Infra-Red |
| PEEK | Polyetheretherketon |
| TC | Thermocouple |
| TP | Thermoplastic |
| TS | Thermoset |
| UD | Uni-Directional |
| US | Ultrasonic |

**Symbols**

| | | |
|---|---|---|
| $A_{vibr}$ | Vibration amplitude | $\mu m$ |
| $E_k$ | Kinetic energy | $J$ |
| $F_c$ | Consolidation force | $N$ |
| $F_{max}$ | Maximum compression force | $N$ |
| $F_w$ | Welding force | $N$ |
| g | Standard gravity | $9.81 \frac{m}{s^2}$ |
| h | Height | $m$ |
| m | Mass | $kg$ |
| $T_g$ | Glass Transition Temperature | °C |
| $T_m$ | Melting Temperature | °C |
| $U_g$ | Gravitational potential energy | $J$ |
| v | Velocity | $\frac{m}{s}$ |

# Chapter 1

# Introduction

## 1.1 Motivation

As leading aircraft manufactures replace traditional metal materials with advanced composite materials, the full potential of composites can be exploited through innovative structural design. Where carbon fiber-reinforced polymers (CFRP) were first used for secondary or non-load-carrying structures, in recent years they have been replacing traditional materials in primary load-carrying structures as well. As a result, aircraft like the Boeing 787 and Airbus 350 are made from more than 50% of advanced composites when looking at structural weight, while in 1980, the MD-80 used composites in only 5% of its structural weight [9]. Although from the beginning thermosets were most dominantly used, in recent years thermoplastics are becoming more popular [10, 11]. Compared to thermosets, thermoplastics offer advantages like shorter and more cost-effective manufacturing processes and the ability to be remelted and reprocessed or recycled.
With the increasing use of thermoplastics, there is an increasing need for not only efficient and suitable manufacturing processes, but also for maintenance processes like repairing damage. More specifically, as 75% of the damages is caused by impact events, such as collision with ground servicing vehicles, runway debris and tool drops [12], there is a need for efficient repair methodologies to repair impact damaged thermoplastic composites. As the average downtime of a damaged aircraft is 3.5 days which will costs an airline $225,000 (2007) [12], there is a need for a fast and practical solution to reduce repair time and therefore costs.

The aim of this research project is to investigate the potential use of ultrasonic (US) welding as a tool to repair impact damage. Compared to the already existing method, hot-pressing, ultrasonic welding could offer faster processing times, no need for dedicated tooling, smaller and lighter machinery and a smaller heat affected zone. In this research project, the compressive strength will be used to determine the effectiveness of the repair.

## 1.2 Research questions and objectives

The main research objective of this research project is:

**"To evaluate the performance of ultrasonic spot welding to repair impact damage as an alternative to hot-pressing, by means of experimental testing"**

In order to guide the present research, a research question with sub research questions was formulated. The research question and sub research questions are stated below.

Main research question:

*How does ultrasonic spot welding compare to hot-pressing to repair impacted CFRP composites and restore the compressive strength and stiffness?*

Sub research questions:

- What are the damage characteristics of impacted thermoplastic composites?
  - What is the influence of impact energy on the impact damage characteristics?
  - What is the influence of the impactor shape on the impact damage characteristics?
- To what extent can US welding re-consolidate impact damage in thermoplastic composites?
  - What are the heating characteristics of impact damage during US welding?
  - What is the influence of US welding parameters on the ability to re-consolidate the impact damage?
- How much compressive strength and stiffness does hot-pressing restore in case of matrix damage only?
- Which aspects influence the amount of compressive strength restored by hot-pressing?
- How much compressive strength and stiffness does US welding restore in case of matrix damage only?
- Which aspects influence the amount of compressive strength restored by US welding?

## 1.3 Structure of the report

Chapter 2 presents the literature on impact damage, compression after impact and ultrasonic welding. In this project, the experiments are divided into three different parts. Part 1 includes experiments related to impact damage, to determine the influence of different impact parameters and to establish a baseline damage. Part 2 includes experiments related to ultrasonic welding, to determine the heating characteristics of impact damage and the influence

of welding parameters and to create US welded repairs. Part 3 includes experiments related to compression after impact, where first reference repairs were created using hot-pressing after which pristine, damaged, US welded and hot-pressed specimens were tested to determine their CAI strength. Chapter 3 discusses the methodologies and test setups used in each part of the experiments. Chapter 4, 5 and 6 show and discuss the results obtained during each part of this research project. Additionally, these chapters will provide answers to the sub research questions. Finally, the thesis is concluded in chapter 7 and recommendations for further research as well as practical recommendations are given in chapter 8.

# Chapter 2

# Literature review

This chapter provides the literature relevant to this research project. Section 2.1 discusses impact damage. More specifically, it describes the different characteristics of impact damage and the parameters influencing impact damage. Section 2.2 discusses compression after impact. It provides general information, a description of the failure mechanisms and explains the influences of various impact damage characteristics on the residual compressive strength. Finally, section 2.3 discusses the principles of ultrasonic welding.

## 2.1 Impact damage

### 2.1.1 Description of damage

Impact damage in fiber-reinforced polymer composites consists of multiple damage modes. The most common damage modes that can occur are: indentation damage, surface buckling, delamination, matrix cracks due to bending, matrix cracks due to shear and fiber damage. Which damage modes actually occur and their extent is dependent on multiple variables like, impact energy, impactor shape and matrix material. These variables and their influences will be discussed in separate sections. The most typical low-velocity impact damage consists of a small indentation at the location where the impactor hits the laminate. Underneath the surface at the impact location, there are matrix cracks and delaminations which spread over a larger area than the area which is impacted. These matrix cracks and delaminations are present throughout the whole thickness and spread out like a cone from the impacted surface towards the backside of the laminate [13, 14], see figure 2.1. The matrix cracks follow a pattern described by De Freitas et al. as a pine tree, with vertical cracks in the bottom layer [15]. Takeda et al. showed that some of the transverse cracks, perpendicular to the interface, grew into the interface with the start of a delamination as a result but others were not surrounded by delaminations [16]. Cristescu et al. observed that delaminations never occur in two adjacent plies of the same fiber direction but always in between plies with different fiber directions [17]. Clark explains that delaminations between plies most often

have an elongated shape or “peanut” shape, with the longer axis pointing in the direction of the fibers of the lower ply [18], for a quasi-isotropic layup this results in a damage described as a staircase, see figure 2.2. Also, fiber damage is present mostly on the backside of the laminate and, depending on the impact energy, directly underneath the impact location. Beside fiber damage there is also local buckling around the location of the impactor. In case the impactor does not penetrate the laminate, a nearly undamaged cone (only containing micro matrix cracks) can be observed under the impacted area. This cone extends from just below the indentation till the last few plies on the non-impacted side which contain matrix cracks, delaminations and fiber failure [1], see figure 2.3.

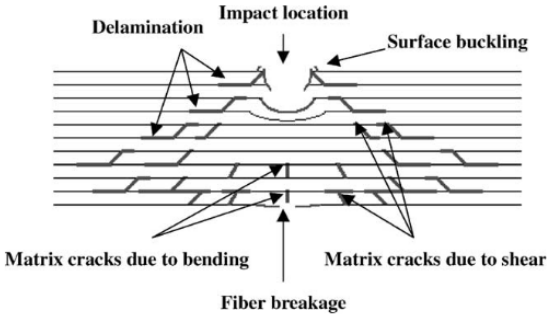


**Figure 2.1:** Schematic representation of impact damage (cross-section). Obtained from [1].

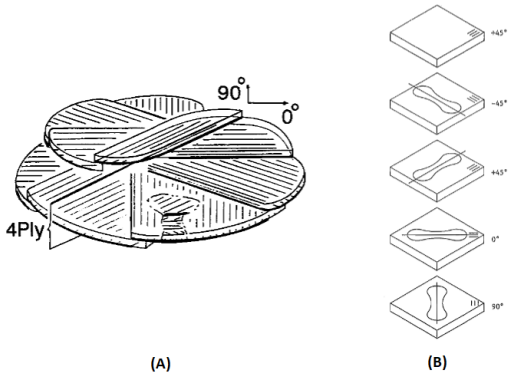


**Figure 2.2:** (a) Delamination "staircase" [2] and (b) "peanut-shaped" delamination (B) [3]

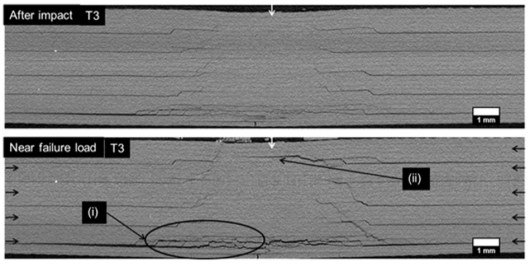


**Figure 2.3:** Cross-section of impact damage containing an undamaged cone [4]

### 2.1.2 Parameters influencing impact damage

#### Influence of impact energy on delamination damage

In order to get a better understanding of the type and extent of damage that can be inflicted by an impact event, it is useful to determine a relationship between impact energy and the extent of the damage. When impacting a composite laminate, there is a threshold energy below which no delaminations will occur [19]. At low energies only matrix cracks and delaminations occur and at higher energies fiber damage starts to occur [1, 20]. It may appear obvious that higher impact energies account for larger damages. However, it is important to determine a relationship. As fiber damage remains relatively local and delaminations can widely spread, it is more useful to determine the relationship between delamination area and impact energy. Numerous researchers evaluated this relationship and came to the conclusion that after the threshold energy the relationship is linear [20–27].

#### Influence of matrix material

Extensive research has been performed on low-velocity impacts on composites. However, most of the research is performed using thermoset composites and limited research has been performed on thermoplastic composites. As Sun et al. [25] and Schimmer et al. [26] already mentioned in their papers, there are a lot of conflicting conclusions about the differences between both Thermoset (TS) and thermoplastic (TP) when looking at low-velocity impact damage. Some claim that (toughened) TS have better impact resistance as, in their studies, (toughened) TS show smaller areas of delaminations compared to TP [28,29]. However, others claim TP are superior at resisting impacts [14, 26, 30, 31]. Although results about the impact resistance of both TS and TP are divided, there are some important trends that can be agreed upon. First, TP generally show a larger permanent indentation compared to TS. This allows for easier detection of impact damage and is therefore beneficial [26, 31]. Secondly, TP tend to show less delamination damage but more fiber damage compared to TS [4, 32]. Finally, TS damage is more elongated in the direction of the fiber on the non-impacted side of the laminate as that side shows more fiber splitting. TP on the other hand show a large bulge on the non-impacted side of the laminate [25, 28]. Lu et al. make an interesting note that TS based laminates show delaminations in almost every interface which is not the case for TP based laminates. Therefore, the total delamination area of TS laminates is considerably larger than TP laminates (more than 10x larger in their research). Because often the projected area of the delaminations as a group is used, instead of the sum of all individual delaminations (due to the use of C-scans, which can not distinguish the presence of separate delaminations in different interfaces when using transmission instead of pulse-echo mode), when comparing the impact performance of TS and TP, the performance of TP is most likely underestimated [31].

#### Influence of impactor shape on the extent and visibility of damage

The impactor shape has a considerable effect on both the damage initiation threshold energy but also on the kind of damage that results from the impact event. Multiple researchers found that, when an impactor has a more blunt shape, the threshold energy increases. A more blunt shaped impactor also results in more delamination damage and less fiber breakage,

whereas sharper impactors tend to cause more fiber damage and a decreased amount of delamination [33–36]. It was also noted that, for the same impact energy, a blunt shaped impactor is less likely to leave a permanent indentation. The effect of impactor shape on the damage initiation threshold is more significant for thinner laminates. Delaney et al. investigated the relationship between visibility of the permanent indent and the internal damage. They found that, for small radius impactors, there is a clear relation between increased visibility and increased internal damage. However, for large radii this relationship vanishes. They made an important remark that all permanent indents show some degree of relaxation over time, especially the indent from large radii. This means that, especially for blunt impacts, visible damage could become barely visible after a certain amount of time [37].

## 2.2 Compression after impact

### 2.2.1 Background information

In order to determine the residual compressive strength (the compressive strength of a laminate with impact damage) after an impact event, a "compression after impact" (CAI) test is performed. Commonly, the ASTM D7137 standard [5] is used with the compliant fixture which is shown in figure 2.4. Although impact damage has limited effect on the tensile strength, it is critical for the compressive strength [38, 39] as the residual strength greatly reduces after moderate impacts (reductions of 50-70% are common [13, 39, 40]). CAI testing is useful to investigate what factors drive premature compressive failure after impact. It is important to understand CAI behavior and failure mechanisms of composites to come up with an effective repair approach. CAI tests are crucial in evaluating the performance of the repair, as CAI testing will indicate to what extent the effects of the impact damage are eliminated.

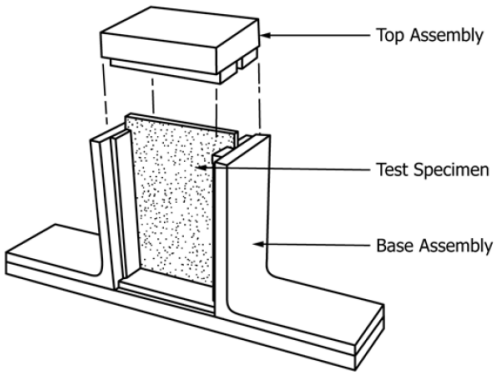


**Figure 2.4:** Schematic of CAI support fixture with specimen in place. Fixture is placed inside a compression load frame. Obtained from [5].

### 2.2.2 Description of failure mechanisms

In order to design an effective repair strategy for repairing impact damage with the aim to restore the compressive strength, the failure mechanisms have to be understood. With this knowledge, the critical factors which lead to premature failure, can be determined. An

effective repair method will eliminate these factors and result in an increase of the residual compressive strength. To describe the failure mechanisms, a rectangular plate is considered with a circular damaged area in the middle. This area contains impact damage such as delaminations in between multiple (or all) plies, matrix cracks along and perpendicular to the fiber directions and fiber damage such as kinking and breakage. When the plate is loaded in compression, the plate tends to behave like a normal undamaged plate until the global buckling load of the plate is approached. Until this point, limited stiffness degradation and damage propagation is observed [40]. After this point, the failure mechanisms drive the CAI behavior.

Depending on the kind of damage obtained during impact (mostly delaminations or fiber damage), two failure mechanisms can occur, which will be explained below. In practice, both mechanisms will occur simultaneously and interact with each other. According to Wisnom and Yang et al. delaminations are the most dominant factor reducing the CAI strength [38, 40]. Vieille concludes that, especially for tough matrix materials with limited delaminations and extensive fiber damage, fiber damage is instrumental in driving CAI behavior [32]. Bull describes it as a competition between load bearing fiber fracture (and associated growth during loading) and loss of constraint from delamination [4].

The first failure mechanism occurs when there is mostly delamination damage and limited fiber damage. Depending on the impact energy, and therefore the presence of a permanent indentation that acts as an eccentricity, the plate starts to globally buckle in direction of the non-impacted side of the plate [32]. The initiation of global buckling is immediately followed by local buckling of the plies in the damaged area. The local buckling first happens in the surface plies and is followed by the rest of the plies [38]. Local buckling in the damaged area degrades the load-bearing ability of this area. This results in the fact that the compressive load is redistributed and the areas next to the impacted area need to take an increased load. The increased load will in its turn lead to propagation of delaminations in direction transverse to the load, and consequently local buckling. The propagation of delamination and local buckling in transverse direction happens fast until the sides are reached and results in the complete failure of the plate.

A second failure mechanism happens when there is a reduced amount of delamination damage and an increased amount of fiber damage. As fibers in the loading direction, which take most of the compressive load, are broken in the impacted area, even before local buckling, the load-bearing ability is reduced. Like the first failure mechanism, the load is redistributed to the surrounding fibers [4]. The load on the surrounding fibers is increased and the fibers will consequently fail. A transverse crack will propagate from the impacted area to the sides of the plate [32]. After initiation of this crack, it propagates fast and results in the complete failure of the plate.

Figure 2.5 shows the three stages [6] of CAI. At stage 1, the plate shows a linear elastic behaviour. At the beginning of stage 2, the stiffness is degraded, indicating the initiation of local buckling (point B) and global buckling (point C). As the propagation of local buckling would further induce delamination growth, matrix damage and eventually fiber damage, at point D the maximum force is reached [38] at which damage rapidly propagates transversely which leads to total failure (stage 3). Tuo et al. concluded that damage always starts from the impact area and propagates suddenly across the laminate to the longitudinal edges. The area of fiber damage was found to be narrow, the matrix damage area was somewhat larger

than the section with fiber damage. The area of delamination damage was the largest and exhibited an irregular shape [6]. The different stages of CAI are shown in figure 2.6 using strain and displacement data which were obtained by digital image correlation (DIC).

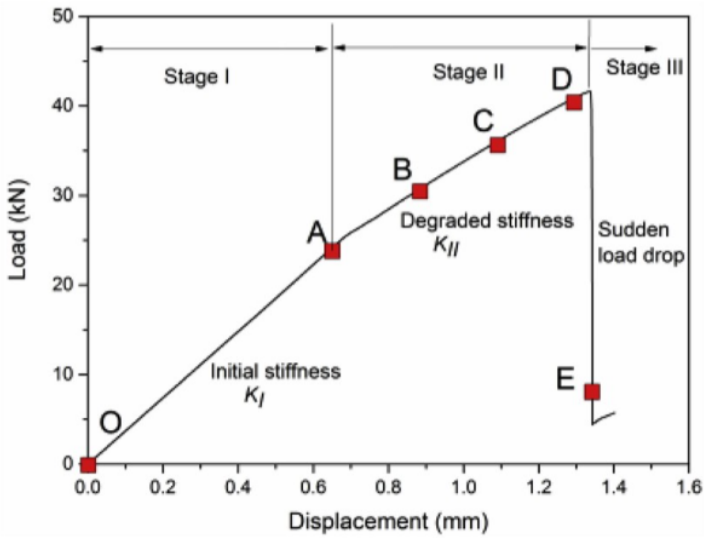


**Figure 2.5:** Stiffness degradation during the three stages of CAI [6]

### 2.2.3 Influence of impact damage on the residual compressive strength

#### Influence of damage area

The relationship between impact damage and residual compressive strength has been widely studied by many researchers. In general, a linear relationship has been found between the impact energy and the compressive strength [4,23,32,41–44]. Although this relationship gives a good estimate, it highly simplifies the situation. The relationship is based on the fact that impact energy is linear with damaged area and the fact that damaged area is linear with CAI strength. Therefore, the relationship between damaged area and CAI strength is also considered to be linear. The relationship only holds when the damaged area is containing damage consisting of mostly delaminations together with matrix cracks and little fiber damage. Others discovered that, instead of using the damaged area, it is more appropriate to use the width of the damage (dimension of damage perpendicular to the loading direction), hence there is a linear relationship between the width of the damage and the residual compressive strength [45].

Soutis [13] observes that, for multi-directional CFRP laminates, the impact damage area is often circular in shape. He proposes an approximation method by replacing the damaged area by a circular hole (with the assumption that most interfaces contain delaminations). The damage development of impact damage under compression is similar to an open hole under compression. Buckling of the 0°-fibers together with delamination and matrix cracking initiate at edges of the hole, hence damaged area, at the two points closest to the two lateral edges of the laminate and propagate across the width of the plate, causing final failure. The

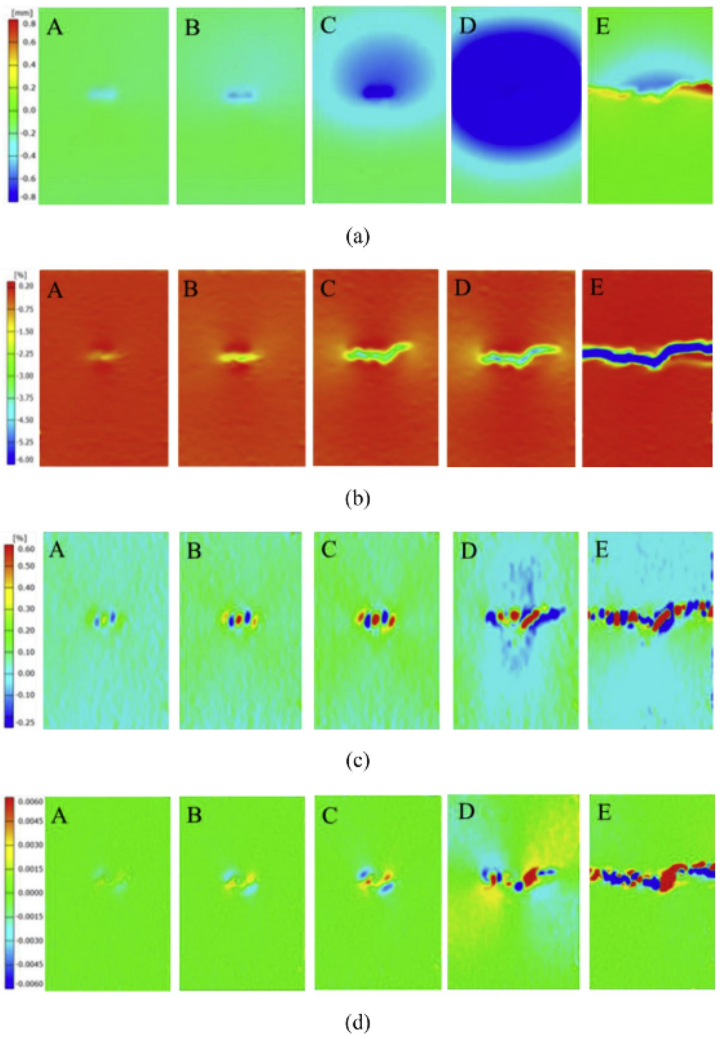


**Figure 2.6:** DIC results at different stages of CAI (A till E, correspond with figure 2.5 ): (a) out-of-plane displacement, (b) strain in vertical direction, (c) strain in horizontal direction and (d) in-plane shear. [6]

model is justified by assuming that the damaged area has no load bearing capacity. The broken fibers cannot transfer the compressive load and the intact fibers will inevitably buckle as all interfaces are delaminated. Although this method gives a good approximation, it, interestingly, overestimates the residual strength. A plate with a hole has a higher residual strength than a plate with impact damage of the same area [44]. This feels counter-intuitive as it is expected that the damaged area still provides some degree of load bearing capacity, resulting in a higher residual strength. However, it turns out that the damaged area helps initiating the damage at the edge of the hole. This happens at a lower load than for the actual hole. As propagation happens fairly abruptly, earlier damage initiation at the edge of the hole, results in a lower failure load.

### Influence of delamination

Delamination is considered to be the most dominant damage influencing the CAI performance [39, 46]. This is due to a combination of two important factors. The first factor is the large extent to which delamination is present in the impacted laminate compared to fiber and matrix damage, for the same impact energy levels. The larger area and through-thickness presence of delamination causes more 0°-fibers to be unable to carry the compressive load. This means a lower load bearing capacity of the laminate as a whole and earlier initiation of damage. The second factor is the fact that unstable propagation of damage is triggered due to local buckling of the adjacent sub-laminates. This propagation is more sudden and catastrophic than that of fiber or matrix damage [32].

### Influence of fiber damage

During an impact event, the laminate can experience 0°-fiber rupture with corresponding matrix damage which can be observed as cracks. These cracks have a negative influence on the CAI performance of the laminate. Around such a crack, stress-concentrations will be present when loaded in compression or a combination of compression and bending when the laminate starts to buckle globally. These stress-concentrations will promote crack propagation and final failure [47].

Fiber damage has a significant effect on the CAI strength [6]. According to Vieille, 0°-fiber (fibers parallel to loading direction) breakage is instrumental in driving CAI behavior and is the reason that carbon fiber/polyetheretherketon (PEEK) material, which shows fewer delaminations but more fiber damage than carbon fiber/epoxy, shows earlier damage propagation and a lower failure load, when compared to carbon fiber/epoxy material with the same damaged area [32]. This propagation of damage is driven by the redistribution of the load to neighboring 0°-fibers, which will inevitably fail under the increased load [4].

### Influence of the permanent indentation

As buckling is induced by imperfections, the permanent indentation has an influence on the local buckling behavior, which in turn has an influence on the CAI behavior. De Freitas et al. showed that, for smaller indentations, both the impacted and non-impacted side of the damaged area buckled to the outside. For larger indentations, both buckled in the same direction, in direction of the non-impacted side. This is caused by the eccentricity induced by the indentation, dictating the buckling direction [23]. Not only is the eccentricity dictating the buckling direction, it also lowers the load at which buckling begins. As the initiation of buckling is associated with propagation of damage and complete failure, a lower buckling load will also mean a lower failure load.

### Influence of the undamaged cone

As described in section 2.1.1, after an impact event, an undamaged cone can be present in the middle of the damaged area. The undamaged cone has an important role in preserving the residual strength. The undamaged cone acts as a support for the surrounding delaminations.

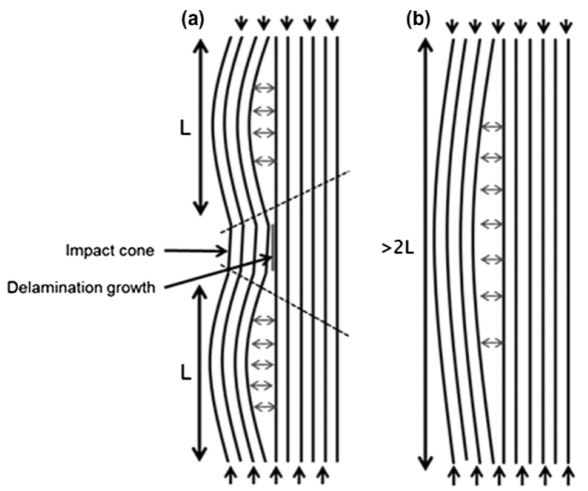


**Figure 2.7:** Schematic representation (cross-section) of the effect of the undamaged cone on the buckling length (L) of the delaminated sub-laminates. (a) shows local buckling of the delaminated area of a laminate with undamaged cone. (b) shows local buckling of the delaminated area of a laminate without undamaged cone. [4]

This will effectively decrease the buckling length of the delaminated sub-laminates by half, see figure 2.7. In theory decreasing the buckling length by half will increase the buckling load by a factor of 4. Decreasing the unsupported length will increase the load at which the sub-laminates start to buckle. Increasing the local buckling load of the delaminated sub-laminates will increase the load at which damage propagates and final failure occurs [4]. Bull et al. observed that, when increasing the compressive load, the outside edge of the delaminated area does not significantly propagate outwards but the delaminations do propagate inside the undamaged cone. Eventually, the undamaged cone disappears as it also becomes delaminated. This means the unsupported length of the delaminated sub-laminates suddenly increases and, because the buckling load becomes lower but the load itself stays the same, causes the sub-laminates to buckle instantaneously. So, shortly after the disappearance of the undamaged cone, damage rapidly propagates and complete failure of the laminate occurs. This process can be seen in figure 2.8, the figure shows damage after impact, damage just before final failure and damage after final failure [4].

### Influence of misaligned fibers

Misalignment of fibers can, under compression, cause micro buckling which negatively contributes to the residual strength. This phenomenon is similar to local buckling caused by the permanent indentation but on a smaller scale. Misalignment of fibers can be within the plane of the laminate or out of plane which can, for example, be observed at the crimps of woven fabrics [32]. Although, this is inevitable when using woven fabrics and will most likely not be an issue when using uni-directional material, it must be taken into account when repairing a laminate. When the repair method results in insufficient quality, misalignments could be present in the laminate, negatively contributing to the CAI behaviour.

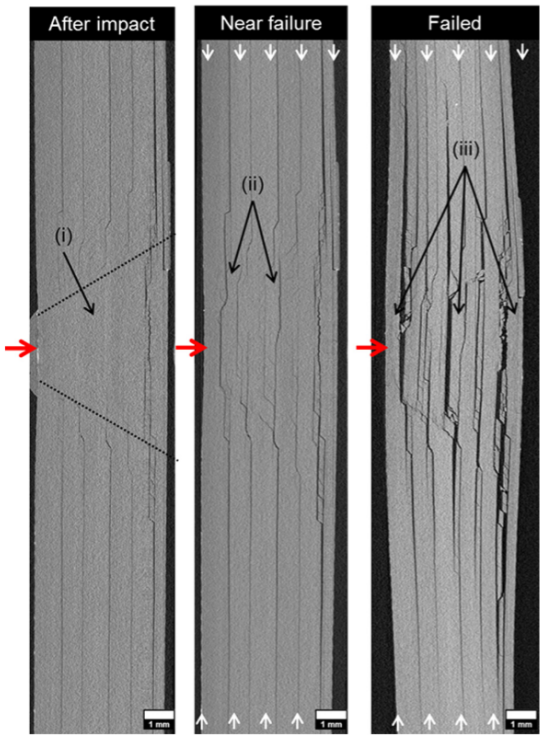


**Figure 2.8:** Cross-section of impact damage with undamaged cone under compressive load: After impact, near failure and after failure. Red arrow indicates location of impact. The figures show how the delaminations grow into the undamaged cone during loading. [4]

## 2.3 Ultrasonic welding

Ultrasonic welding is based on the principle that high frequency and low amplitude mechanical vibrations, together with a static force, are induced into a material, which generates heat. These mechanical vibrations are induced by an ultrasonic welder, which consists of a generator, piezoelectric converter, booster and a sonotrode, see figure 2.9. The generator provides a high frequency electrical signal to the piezoelectric converter which converts this electrical signal into a mechanical vibration. This mechanical vibration is amplified by the booster and sonotrode. The sonotrode is responsible for inducing this mechanical vibration, together with the static force, into the material. For thermoplastic (composite) ultrasonic welding, the vibrations are usually introduced transverse to the welding interface [48].

For ultrasonic welding thermoplastic composites, there are two different heating mechanisms. These two mechanisms consist of frictional heating and viscoelastic heating [49]. Frictional heating is caused by the friction between two surfaces that move relative to each other due to the introduction of the mechanical vibrations. These two surfaces could be the sonotrode and the adherend or, in case of a single lap joint, between the two adherends. Frictional heating is the most important heating mechanisms until the material reaches the glass transition temperature (Tg). After Tg is reached, viscoelastic heating inside the matrix material starts to occur. This becomes the dominant heating mechanism [50], due to its higher heating rates.

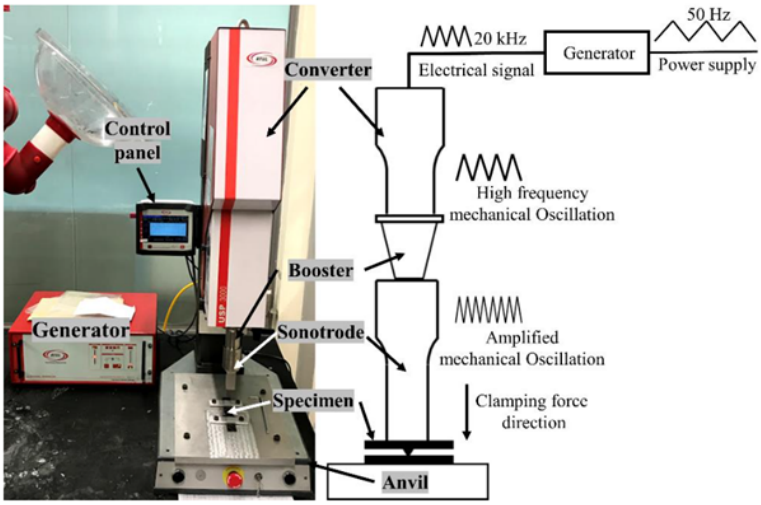


**Figure 2.9:** Left: An ultrasonic welder. Right: A schematic representation of an ultrasonic welder [7].

Considering a lap joint, the ultrasonic vibrations cause relative movement between both adherends and frictional heat is generated [49]. When the surface of the adherends reach Tg, heat is also generated by viscoelastic heating [49]. When heating rates are low, heat could dissipate into the adherends which could affect their material properties. For example, melting of the adherend could promote voids, matrix squeeze out or fiber distortions, which have a negative influence on the adherends. To increase the heating rates and concentrate heat generation at the interface, energy directors (ED) can be used [48]. These energy directors are made from a neat matrix material and exist in a variety of shapes, for example a cone shape or pultruded triangles , and are placed inside the interface. When mechanical vibrations are induced, the relative movement between the ED and one of the adherends will promote friction, hence frictional heating. Due to the geometry of the ED's, frictional heating is concentrated at smaller areas, increasing the heating rate. When the surface of the adherend and the ED reach the glass transition temperature, heat is generated through viscoelastic heating. However, due to the absence of fibers inside the ED and its geometry, the stiffness of the ED is lower, therefore the strain amplitude inside the ED is higher than inside the adherends. Due to the nature of viscoelastic heating, the higher strain amplitude causes more heat to be generated in the ED [51]. This means that the ED will reach the melting temperature before the adherend does, hence most of the heat is concentrated inside the interface. This is beneficial as, for welding a lap joint, a connection between the two adherends has to be made, which only requires melting the material at the interface and, as mentioned before, heat inside the rest of the adherend could have negative effects on its material properties.

For ultrasonic welding a lap joint with a flat ED, it is shown that the welding process consists of five stages [8]. As these different stages represent physical changes inside the ED and adherends, they have an influence on the power and displacement data during the welding process. Therefore, power and displacement curves can be used to distinguish the different stages, see figure 2.10.

Below, the five stages of the welding process are briefly described. In the paper of Fernandez Villegas [8], these stages are described in more detail.

Stage:

1. The temperature of the ED increases without any distinguishable changes to the material. The power increases linearly which corresponds to the increase of the vibration amplitude. There is an upward displacement of the sonotrode to accommodate the vibration. Stage 1 ends when heating of the edge of the ED progresses to the rest of the interface.

2. The ED continues to heat up and melt. This happens through nucleation and growth of random hot spots. Due to the reduction of solid material, hence a reduction of the material's stiffness, the power decreases. As only spots are melting, there is still solid material, which prevents the downward movement of the sonotrode, hence constant displacement. Although the nucleation of these hot spots appears to be random, an increase of welding force seems to increase the number of hot spots.

3. This stage is mostly characterized by squeeze flow of the ED, which causes a downward displacement of the sonotrode. In this stage, only the ED reaches the melting temperature whereas the adherends do not. Due to squeeze out, the two adherends move closer to each other, increasing the mechanical impedance which increases the welding power.

4. The squeeze flow of the ED continues which almost reduces the weld line thickness to zero. At this moment, enough heat has transferred into the adherends for the adherends to start melting locally. As the power decreases due to the melting of the adherends but is counteracted by the presence of molten ED at the interface, it results in a power plateau. It seems that an increase of welding force will decrease the duration of this stage as it increases the rate at which the flow is squeezed out. As the squeeze out continues, there is a downward displacement of the sonotrode throughout this stage.

5. The thickness of the welding line can be considered zero and melting of the adherends is a dominant factor in this stage. Melting of the adherends causes the power to drop and the displacement of the sonotrode to continue downwards. When decreasing the welding force, heat generation and squeeze flow occur at a lower pace. This lower pace, allows for more heat dissipation into the adherends, which results in different heat-affected zones.

The parameters that lead the welding process are welding force, vibration amplitude and vibration time [48]. The heating rate is determined by both the welding force and the vibration amplitude. An increase in the value of either one of the two parameters will result in an increase of the heating rate [52]. This means that, for high welding forces and vibration amplitudes, shorter welding times can be achieved, hence less heat dissipation to the surrounding material and, therefore, a smaller heat affected zone in thickness direction. Important to note is that the welding force should not be too low as this will promote the loss of contact between the sonotrode and the adherend. This loss of contact is also known as hammering and, as the vibrations from the sonotrode are not properly introduced into the adherend, makes the welding process less efficient and less predictable.

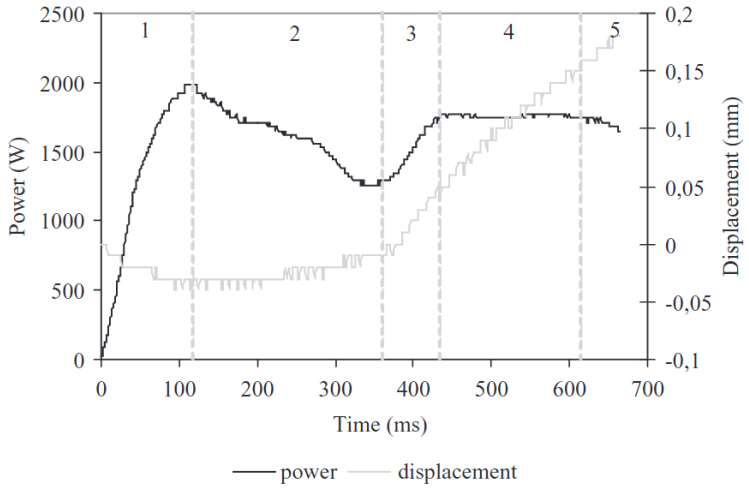


**Figure 2.10:** The 5 different stages during the welding process indicated on the power and displacement curves of a welded lap joint with flat ED. Positive values indicate a downward displacement of the sonotrode. [8]

The vibration time will determine the duration of the welding process and, therefore, the input of energy. The amount of energy that is put in will determine the temperature inside the material and, therefore, the quality of the weld [48]. If the duration is too short, the material in the interface will not sufficiently melt and bond, resulting in a poor quality weld. If the duration is too long, overheating of the material can occur, which also results in a poor quality weld. The ideal duration will ensure the material in the interface (ED and surface of the adherends) will fully melt but will not result in overheating of the matrix or excessive melting in the adherends.

The vibration time can be set to a fixed duration, or be controlled indirectly by using welding energy or vertical sonotrode displacement information to determine when to stop the vibrations. The latter, so called "displacement controlled", has shown to be a method that provides more consistent welds than using time control [8]. Looking at the different stages during the welding process, ideally, the welding process is stopped at stage 4. At stage 4, the interface is completely melted without the adherends being affected too much by the heat. For every weld, the time it takes to reach stage 4 will vary. Variations are introduced by the inevitable random nature of the welding process itself, for example, the time it takes for the unpredictable frictional heat to reach Tg. It can also be influenced by external factors such as variations in clamping. As, at every point in time, the displacement of the sonotrode is linked directly to the physical state of the weld, using this data results in a more robust method to determine when the vibration phase needs to be stopped.

The consolidation phase, which starts after the vibration phase is stopped, allows the material to cool down and consolidate under pressure. This pressure will ensure proper material quality as it suppresses the formation of voids and delaminations. The consolidation force is usually equal to the welding force. Due to the high cooling rates, the consolidation duration is usually set to 2-3 seconds.

For ultrasonic spot welding impact damage, it is expected that the heating behavior inside the material is different than is the case for spot welding a lap joint. A lap joint has one

interface with an energy director and two relatively stiff adherends. Therefore, heat generation mostly happens at the interface and is likely to remain concentrated close to the interface [48]. On the contrary, impact damage (when considering there is no fiber damage) has multiple delaminations, hence multiple interfaces, each interface without an energy director. The effect which these differences have on the welding process are unknown, therefore it is important to investigate the heating characteristics of the damaged area during the ultrasonic welding process before the influences of the welding parameters can be investigated.

# Chapter 3

# Methodology

This chapter will discuss the methodology and experimental setups that were used during the research project as well as the test specimens and inspection equipment. The research project was divided into three different parts. The first part covered impact damage, the second part covered ultrasonic welding and the third part covered compression after impact. The methodology and experimental setup of each part will be discussed in section 3.1, 3.2 and 3.3, respectively.

## 3.1 Part 1 - Impact damage

The purpose of this part of the project was to determine the characteristics of the damage that is caused when a thermoplastic composite is impacted. Determining the damage characteristics was not only important as they dictated the type of damage that needed to be repaired during this project, it would also give insight into what range of impact scenarios this repair method might be suited for. As mentioned in section 2.1, limited research has been performed on impact damage in thermoplastic composites and the available research shows conflicting conclusions. Therefore, it was decided that, instead of using data from literature, impact data was generated during this part of the project by performing impact trials.

This part focused on determining the influences of the impact energy and impactor shape on the impact damage characteristics. Depended on the results, a suitable baseline damage was determined that was used during part 2 and 3 of this research project. As ultrasonic welding is only able to melt and re-consolidate the matrix material and therefore only repairs delaminations and matrix cracks, ideally, the damage consisted only of delaminations and matrix cracks without (or with limited) fiber damage. As only one weld would be performed to repair the impact damage, preferably, the damaged area was similar in size to the sonotrode.

### 3.1.1 Methodology

In order to determine the influence of the impact energy and the impactor shape on the impact damage, impact tests were performed using an impact tower. To determine the effect of the

impactor shape, three different impactors were used. Each impactor had a hemispherical shape with a diameter of 15mm, 20mm or 40mm. To determine the influence of the impact energy on the damage characteristics, with each impactor shape, a range of impacts was performed using different impact energies. For each range, an initial impact energy of 12.5J was used as it was expected this impact energy does not initiate impact damage. After each impact, in the case no damage was obtained, the impact energy was increased by 2J. This was repeated until an impact energy was reached that initiated impact damage inside the specimen. The drop height and impact energy were calculated using the following equations:

$$U_g = m \cdot g \cdot h \tag{3.1}$$

$$E_k = \frac{1}{2} \cdot m \cdot v^2 \tag{3.2}$$

Where $U_g$ is the gravitational potential energy, $E_k$ is the kinetic energy, m is the mass in kg, g is the standard gravity, h is the height in meters and v is the velocity in meters per second.

Equation 3.1 was used to determine the drop height to obtain a certain impact energy and equation 3.2 was used to determine the impact energy of the actual impact using the impact velocity measured by a laser trigger system. Finally, the impact energy was converted into energy per thickness (J/mm) by dividing the impact energy by the specimen thickness.

After each impact, the impacted specimens were visually inspected to check for external signs of matrix cracks and fiber damage. As mentioned in section 2.1, if fiber damage is present, this will at least be located in the outer-ply of the impacted side of the specimen or the outer-ply of the non-impacted side. Therefore, to determine whether a specimen contained fiber damage, performing a visual inspection was sufficient. Additionally, after each impact, the specimens were inspected using an ultrasonic C-scan device, for internal damage such as delaminations. The ultrasonic C-scan procedure will be discussed in section 3.5. If a specimen did not obtain damage during the impact event, the specimen was impacted again.

After the influences of the impact energy and impactor shape were determined, the baseline impact damage, with corresponding impact parameters, was determined. As this damage would be used as a reference for the entirety of the project, this damage was analyzed in more detail using cross-sectional microscopy. The cross-sectional microscopy procedure will be discussed in section 3.5.

### 3.1.2 Experimental setup

The experimental setup that was used for this part of the project was an impact tower connected to a data acquisition unit, which can be seen in figure 3.1. The impact tower was in compliance with the ASTM D7136 standard [53]. A laser trigger system was used to measure the velocity of the impactor before impact. The head of the impactor was interchangeable so other impactor shapes could be used. Additional weights could be added to the impactor to change the total mass of the impactor. For each impactor diameter, the mass of the impactor is listed in table 3.1. Finally, the impactor was equipped with a load cell that measured the impact force. The impact tower had a capturing system that prevented the impactor from

impacting twice, after bouncing up after the first impact. A computer was used to control the impact tower (e.a. controlling the drop height, triggering the drop) and to acquire the data from the load cell.

| Configuration | Impactor diameter [mm] | Impactor mass [g] |
|---|---|---|
| 1 | 40 | 3728 |
| 2 | 20 | 3515 |
| 3 | 15 | 3561 |

**Table 3.1:** Impactor diameter and impactor mass for each configuration

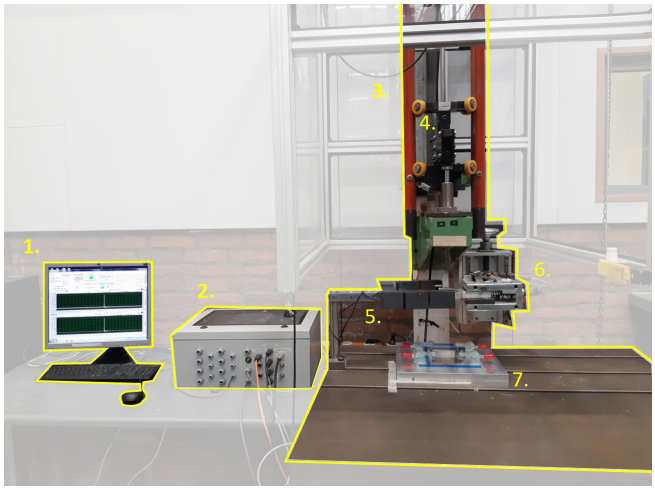


**Figure 3.1:** Experimental setup used for impacting specimens. 1. Computer to control the impact tower 2. Data acquisition unit 3. Impact tower 4. Impactor carrier with impactor 5. Laser trigger system 6. Capturing system 7. Clamping fixture.

## 3.2 Part 2 - Ultrasonic welding

The purpose of this part of the project was to investigate the influence of the welding parameters on the process of welding impact damage. Subsequently, it was determined which welding parameters would be used for repairing the specimens that would be tested for their compressive strength recovery. As mentioned in section 2.3, the heating characteristics of welding impact damage were not known. Therefore, this was determined first, before the influence of the welding parameters was investigated and the welding parameters for the final repairs were determined.

### 3.2.1 Methodology

To investigate the heating characteristics of welding impact damage, welding was performed on specimens with and without damage. Welding specimens without damage would show the heating characteristics of the pristine material. When comparing this with the heating characteristics shown for welding specimens with damage, the influence of the presence of

impact damage on the heating characteristics could be determined. Both welding trials were conducted with a consolidation step where the consolidation force was zero. This was done by lifting the sonotrode after the vibration phase. Letting the specimen consolidate without a consolidation force allowed voids to become present at locations where the material had melted. This would help to determine the melted locations afterwards using cross-sectional microscopy. Also, by lifting the sonotrode during the consolidation step, temperature measurements could be performed of the surface of the specimen using an infrared (IR) camera. Important to note is that, during the entirety of the project, only one spot weld was executed on each specimen. Also, a fixed consolidation time was used throughout the project, set on 60 seconds.

After the heating characteristics were determined, the influence of the different welding parameters were determined. The different welding parameters were welding duration, welding force and vibration amplitude and consolidation force. To determine the influence of each welding parameter, a welding trial was performed for each parameter where this parameter was varied while keeping the other welding parameters constant. Between the different welding trials, the values for the parameters that were kept constant could vary. As this was a preliminary investigation, the gained knowledge was immediately implemented to improve the welding process.

During the welding process, welding data (power and displacement curves) and temperature data were acquired. After each weld, the specimen was inspected using an ultrasonic C-scan to check for changes with respect to the ultrasonic C-scan before welding. This was followed by inspection using cross-sectional microscopy. This data was analysed to determine the influences of each welding parameters as well as to determine the set of welding parameters that would be used to repair the damaged specimens that would be tested for their compression after impact strength.

### 3.2.2 Experimental setup

The experimental setup used for the ultrasonic welding part of this project consisted of an ultrasonic welding machine with built-in data acquisition, external data acquisition unit with thermocouples and an IR-camera. This setup can be seen in figure 3.2. The welding machine was a 20kHz Herrmann Ultraschall Hiq dialog microprocessor-controlled ultrasonic welder with a 15x30mm rectangular titanium sonotrode with custom made rig to clamp specimens. This welder was able to provide in-situ data of the welding force, power and vertical displacement of the sonotrode. This data could be used to control the welding process by, for example, stopping welding if a certain displacement was reached. Although the welding machine had a built-in data acquisition unit, this only recorded for a maximum of 16 seconds before it started overwriting itself. Therefore, for welding processes longer than 16 seconds, the external data acquisition unit was used. Five thermocouples could be used at the same time, which were connected to the external data acquisition unit. The IR-camera was a FLIR A655sc which was capable of recording temperatures up to 650 °C with a resolution of 640 x 480 pixels and a frame rate of 25 frames per second for a maximum of 40 seconds. To clamp the specimens, two bars were used which were tightened using two bolts each. To ensure a consistent clamping force, a torque wrench was used to apply a fixed amount of torque (16Nm). Depending on the type of specimens, which will be discussed in section 3.4, the specimens were clamped in two different ways, see figure 3.3.

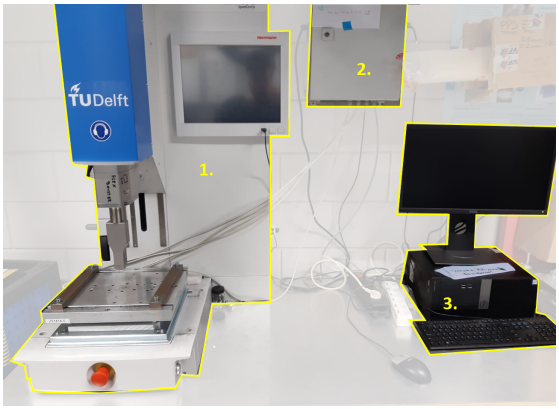


(a) General welding setup

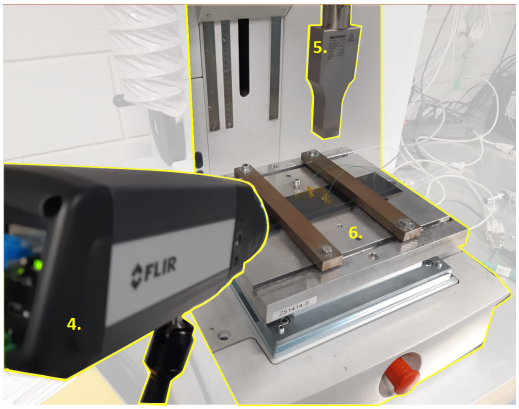


(b) Welding setup including IR-camera showing the angle at which the IR-camera is used

**Figure 3.2:** Experimental setup used for the welding trials. 1. Welding machine 2. External data acquisition unit 3. Computer 4. IR-camera 5. Sonotrode 6. Clamping fixture

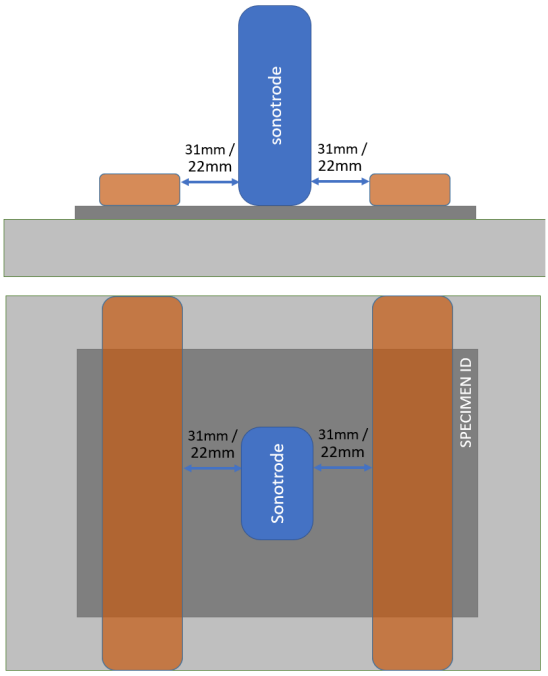


(a) Configuration used for type 1 specimens

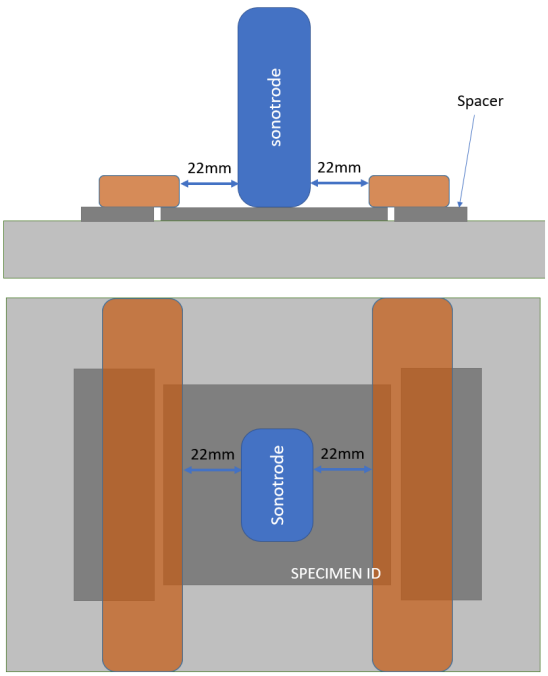


(b) Configuration used for type 2 specimens

**Figure 3.3:** Clamping configurations used for ultrasonic welding. Top row shows a front view and bottom row shows a top view of the clamping configurations.

## 3.3 Part 3 - Compression after impact

The purpose of this part of the project was to determine the recovered compressive strength and stiffness of the specimens which were repaired using ultrasonic welding. Additionally, the performance of these specimens was compared to the performance of pristine specimens, damaged specimens and specimens which were repaired with a reference repair method.

### 3.3.1 Methodology

To determine the compressive strength recovery of the ultrasonic welding repair, four types of specimens were tested for their compressive strength and stiffness using a compression after impact test. The four types consisted of pristine specimens, damaged specimens, specimens repaired by ultrasonic welding and specimens repaired by hot-pressing. The pristine and damaged specimens were used to provide a baseline to compare the repairs with. The hot-press repair was used as a baseline repair, as this is the current alternative for repairing thermoplastic composites.

During the compression after impact tests, the force and cross-head displacement of the compression load frame was monitored. Additionally, a digital image correlation (DIC) system was used to measure local strains and displacement. This would provide a more detailed insight in the behaviour under compressive loading of the different types of specimens.

### 3.3.2 Experimental setup

The experimental setup used for the compression after impact part consisted of a Zwick 250 kN compression load frame with data acquisition unit which captured the force and cross-head displacement. The cross-head had a displacement rate of 1.0mm per minute. The fixture used was according to the ASTM D7137 standard [5]. Additionally, a DIC system was used. The DIC system consisted of two 4 megapixel cameras positioned on a horizontal bar fixed to a tri-pod, connected to a computer which used the VIC-3D software package to control the DIC system and to acquire and post-process the data. The distance between the cameras was approximately 40cm with a relative angle of around 30 degrees between the cameras. The distance from the specimen to the cameras was approximately 100cm. A sample rate of 1 sample per second was used. The total setup can be seen in figure 3.4.

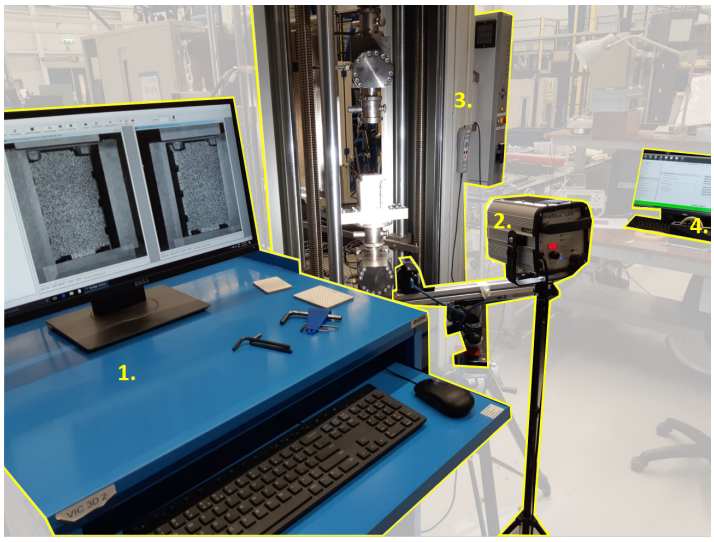


**Figure 3.4:** Setup used for compression after impact testing. 1. Computer to acquire DIC data 2. DIC cameras and spotlight 3. Compression load frame 4. Computer to acquire data from compression load frame.

## 3.4 Test specimens

During the entirety of the research project, two different type of test specimens were used. Type 1 was compliant with both test standards used for impacting and CAI testing. Type 2 specimens were used during the welding part of the project and were similar to the first type but had different dimensions. As the first type of specimens would be unnecessary large for the welding trials, the second type of specimens were made smaller in order to save time and materials.

### 3.4.1 Material, lay-up and dimensions

All specimens used in this research project were made from CFRP. The material used is Toray Cetex® TC1200 utilizing the semi-crystalline thermoplastic polymer PEEK, manufactured by Toray Advanced Composites. The material has a glass transition temperature of 143 °C and a melting temperature of 343 °C. The resin content by weight is 34%. To construct the laminate a uni-directional (UD) pre-preg was used. The laminate consisted of 32 plies with the following quasi-isotropic lay-up: $[45/0/-45/90]_{4S}$. The nominal cured thickness of each ply was 0.137mm, which resulted in a laminate with a nominal total thickness of 4.37mm. Figure 3.5 shows the dimensions of the two types of specimens.

### 3.4.2 Manufacturing of the specimens

To manufacture the specimens, first, large panels were produced by stacking the UD-plies according to the correct lay-up. These plies were then consolidated inside a hot-press. To consolidate the laminates, the press was heated to a temperature of 385 °C with a heating rate

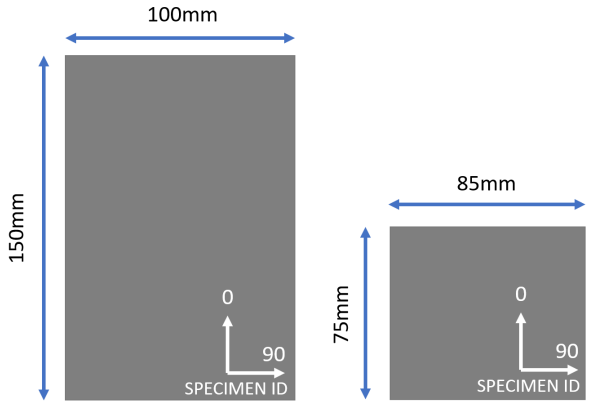


**Figure 3.5:** Left: Specimen type 1 , Right: Specimen type 2

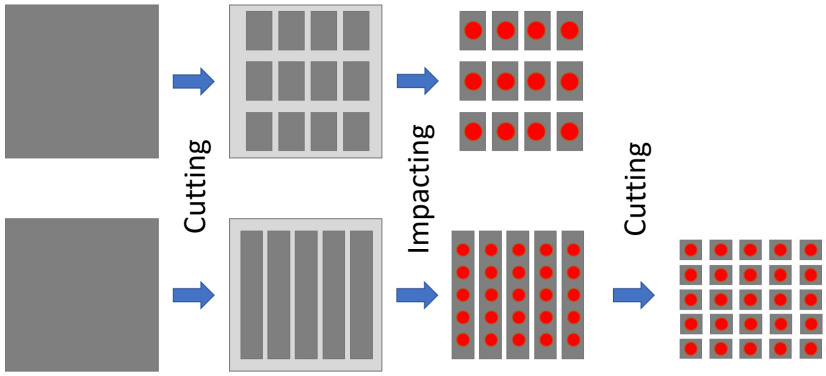


**Figure 3.6:** Figure shows how the panels are cut and impacted to obtain two types of specimens. Top row: type 1 specimens , bottom row: type 2 specimens. Red circles represent impact damage.

of 5°C per second. During this phase, a pressure of 4 bars was applied. After the temperature of 385 °C was reached, the temperature and pressure were kept constant for 30 minutes, after which the pressure was increased to 10 bar while keeping the temperature constant. This was kept constant for 45 minutes, after which the press started cooling down with a cooling rate of 5°C per second until reaching room temperature, while maintaining 10 bars of pressure. The panels had a dimension of 600x600mm. Before the panels were cut to the correct dimensions, they were inspected for flaws by an ultrasonic C-scan. The specimens that would be used for the compression after impact test were cut with an automated cutting machine to ensure a higher precision and consistency in the dimensions as well as making sure the edges were all parallel, which would be beneficial for eliminating variations between the specimens during compression testing. The specimens that would be used for the welding trials were cut using a manual water cooled circular diamond saw. Finally, the type 1 specimens were cut to the final dimensions before impacting, whereas the type 2 specimens were first cut into strips, then impacted, after which they were cut to the final dimensions, see figure 3.6.

## 3.5 Inspection equipment

During this research project, specimens were inspected after manufacturing, after each impact and after each welding process. Depending on the purpose of the specimen, this was mainly done using an ultrasonic C-scan inspection and through cross-sectional microscopy. As with cross-sectional microscopy the specimen had to be sacrificed, this was only used for specimens that were used to establish a baseline damage and specimens used in the welding trials.

### 3.5.1 Ultrasonic C-scan

The ultrasonic C-scan (Called C-scan from here on) device used in this project was an in-house developed (at the Delft university of technology by DASML) device, see figure 3.7, that consisted of an Olympus EPOCH 650 ultrasonic A-scanner where the transmitting and receiving probes were connected to a custom made frame with actuators that could translate the probes on a vertical and horizontal axis while being submerged inside a water tank. An in-house developed software package was used to control the movement of the probes and to collect the signal obtained by the ultrasonic A-scanner and the location of the probes. The software package converted this data to a 2D C-scan image. The type of scanning used was a through transmission type of scanning. This means that it was only capable of measuring the total signal loss of the ultrasonic input signal through the thickness without any depth information. Therefore, the material quality indicated by the C-scan was an average of the quality over the whole thickness. However, when calibrated, the machine was capable of performing consistent scans which could accurately determine the (projected) dimensions of the damaged areas. During the entirety of this project, only C-scans were used to determine the size of the damaged area. As for each location only the average quality was determined, it was easy to determine the damaged (projected) area but more difficult to determine the type of damage at a particular location. Therefore, cross-sectional microscopy was used as much as possible to determine this.

### 3.5.2 Cross-sectional microscopy

In order to prepare the specimens for cross-sectional microscopy, all specimens were cut according to the cutting scheme depicted in figure 3.8. The samples were cut using a Struers Secotom-10 cutting machine with a water cooled diamond coated blade. After the specimens were cut, they were embedded in clear Epofix resin under vacuum conditions and cured for 12 hours. After curing, they were ground and polished using a Struers Tegramin-20 grinding and polishing machine. The second to last polishing step included polishing with a 1 micron diamond solution. The last polishing step included polishing with a colloidal silica suspension. After cleaning the polished specimens, cross-sectional microscopy was performed using a Keyence VK-X laser confocal microscope. Figure 3.9 shows the two different cross-sections with the location of the damaged area and sonotrode. It shows that, in cross-section 1, the damaged area is not completely covered by the sonotrode which is the case in cross-section 2.

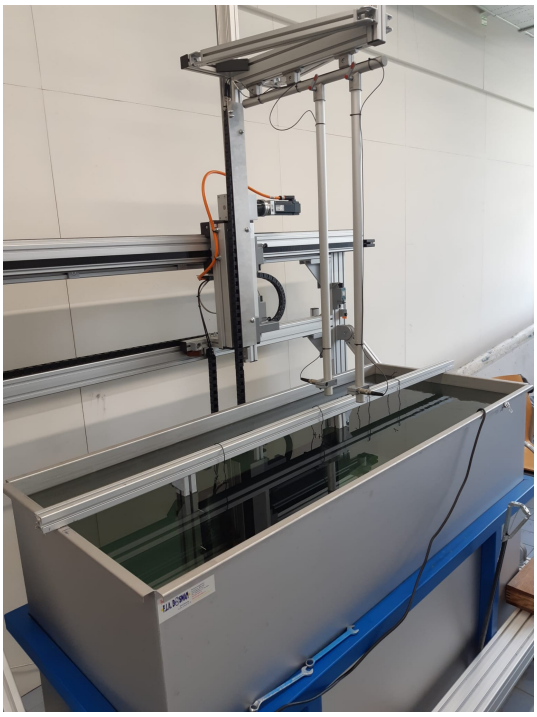

**Figure 3.7:** The ultrasonic C-scan device which was used during this project

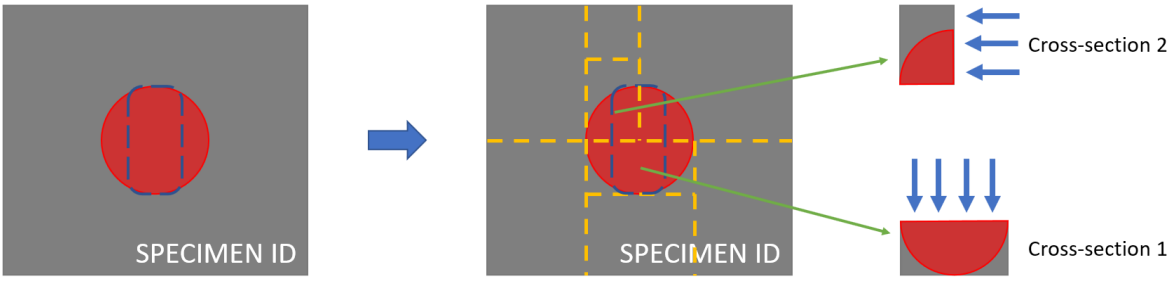


**Figure 3.8:** Schematic of how cross-sectional microscopy samples are cut from the welded specimens. The yellow lines represent the cutting lines. The red areas represent the damaged areas. The blue rectangles represent the location of the sonotrode during the welding process. The blue arrows indicate the surfaces that are observed during cross-sectional microscopy.

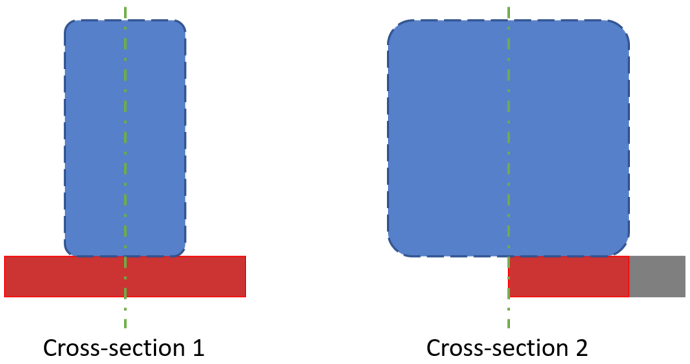


**Figure 3.9:** Schematic of cross-sectional microscopy samples, showing the damaged area in each sample and the location of the sonotrode. The red areas indicate the damaged areas. The blue rectangles represent the location of the sonotrode during the welding process.

# Chapter 4

# Part 1 - Impact damage

In this chapter, the results of part 1 are shown and discussed. Section 4.1.1 shares some general remarks which arose from the impact trials. Section 4.1.2 shows the results of the impact trials to determine the influences of the impact energy and impactor shape. Section 4.1.3 shows the results for the baseline damage that will be used through-out this project. Both the results of the impact trial and of the baseline damage will be discussed in section 4.2.1, 4.2.2 and 4.2.3, respectively. For this report, the resolution of the cross-sectional microscopy images had to be lowered, high resolution images can be found in the database through this link: https://dataverse.nl/dataverse/TPCWeldingRepair

## 4.1 Results

### 4.1.1 General remarks

During the impact trials, the specimens that do not contain damage after impacting were impacted again, which is repeated until they do obtain damage. This should not alter the results as, until the first damage threshold is reached, besides an indent, no damage is obtained [19,54]. However, after looking at the results, it was observed that specimens that are impacted multiple times have a lower damage threshold. Because of this, only impact data is used from specimens that are impacted for the first time. This will eliminate variances in the data. Furthermore, only impact data is used from type 1 specimens. Type 1 specimens are compliant with the ASTM test standard, whereas type 2 specimens are not.

### 4.1.2 Impact trial results

Figure 4.1 shows a graph which plots the impact energy against the damaged area. More detailed impact data of all performed impacts can be found in appendix A.

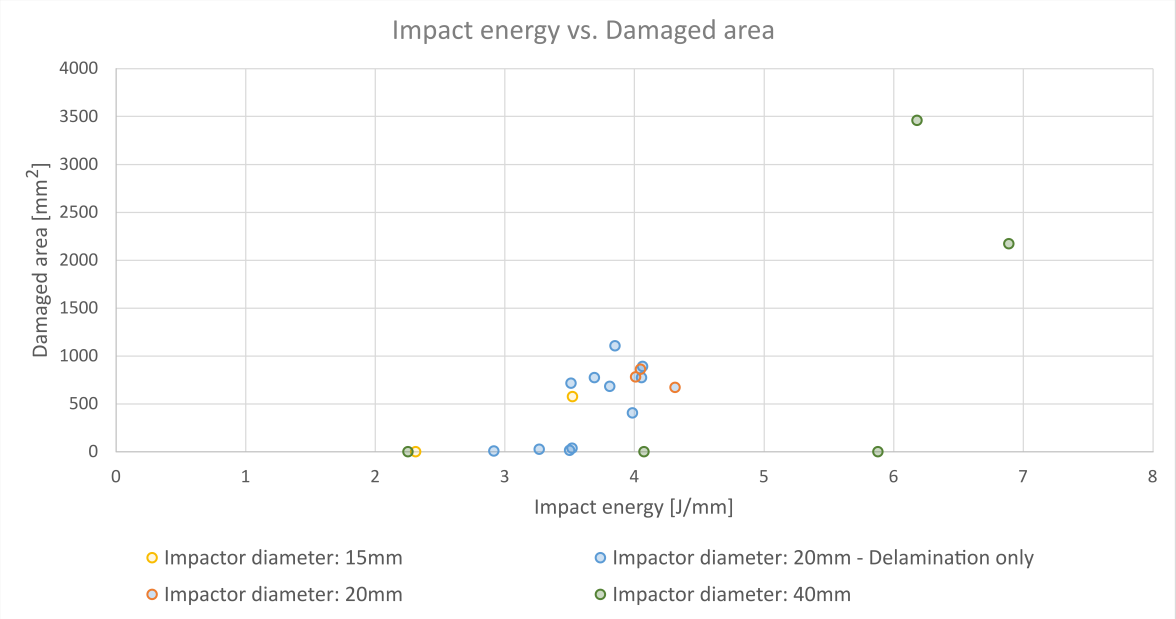


**Figure 4.1:** Diagram showing impact energy versus damaged area for different impactor shapes

The diagram, shown in figure 4.1, shows the size of the (projected) damaged area. Impacts made with an impactor with a diameter of 20mm are divided into two groups, specimens with damage only consisting of delaminations and specimens with damage consisting of delaminations and fiber damage. Impacts made with an impactor with a diameter of 15mm and 40mm are both not divided into two groups as all damaged specimens contain both delaminations and fiber damage. One exception is the specimen impacted with an impactor with a diameter of 40mm and an impact energy of 5.9 J/mm, as this specimen obtained no delaminations but did obtain fiber damage. Finally, it is important to note that all impacted specimens obtained an indent after being impacted, also the specimens that do not show delaminations or fiber damage.

For specimens with fiber damage, the fiber damage is always present on the outer-ply of the non-impacted side of the specimen. Therefore, the presence of fiber damage can always be detected by visual inspection. Depending on the extent at which fiber damage occurs, for the specimens in this research project, it is present in 1 to 5 plies starting from the outer-ply of the non-impacted side of the specimen. This can only be determined using cross-sectional microscopy. The (projected) area of fiber damage varies between approximately 1x1mm and 6x6mm. As it is difficult to determine and quantify the amount of fiber damage, it is only stated whether or not fiber damage is present.

### 4.1.3 Baseline for impact damage

As mentioned in section 3.2, only one spot weld will be used to repair the impact damage in this project. Therefore, the damaged area should, preferably, be similar to the area of the sonotrode. Looking at figure 4.1, it can be seen that impacts with a 40mm diameter impactor are not suitable as the damaged area will be too large. Looking at the figure, the impactors with a diameter of 15mm and 20mm provide a damaged area similar to a circle with a diameter

of 30mm (706.9 $mm^2$). Although this is larger than the area of the sonotrode, due to the fact that no smaller damage was obtained and the fact that the longer side of the rectangular area of the sonotrode is 30mm which means the sonotrode fits inside the damaged area, the damaged area with a diameter of 30mm is considered to be sufficient to use during the welding trials and CAI tests. For creating a baseline damage, the impactor with a diameter of 20mm is chosen as, from literature, it was expected that a larger diameter has a higher change of delamination only damage [33–36], although the impactor with a diameter of 40mm seems to disprove this statement which is discussed in section 4.2. As mentioned in section 3.1, damage is preferably only consisting of matrix damage. Therefore, for the baseline damage, an impact energy that lies just above the threshold energy (3.5 J/mm) is considered ideal as the diagram shows that specimens impacted with that energy only show delaminations. However, because of the variances of the impact tower, resulting in variances in impact energies for the same drop height, it was decided to increase the impact energy to 3.9 J/mm to ensure all specimens are damaged upon the first impact. The side effect of this increase is an increased change of fiber damage.

Figure 4.2 shows the results of the C-scan of the baseline specimen. It shows the damaged area is circular and has a diameter of around 30mm. It also shows an undamaged cone in the center of the damaged area.

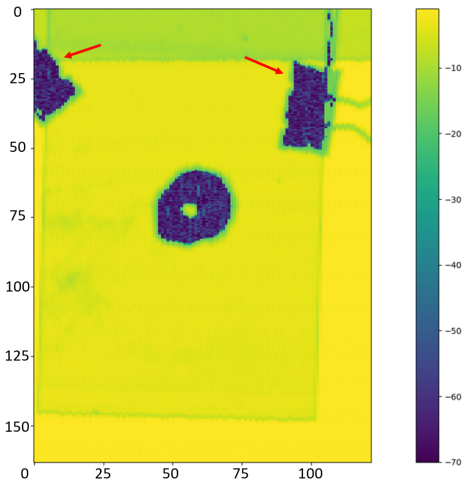


**Figure 4.2:** C-scan of the specimen used as a baseline. It shows a circular damaged area with a diameter of approximately 30mm which contains an undamaged cone in the center. The red arrows point out the clamps that hold the specimen in place during the scan and, therefore, these dark areas do not indicate damage.

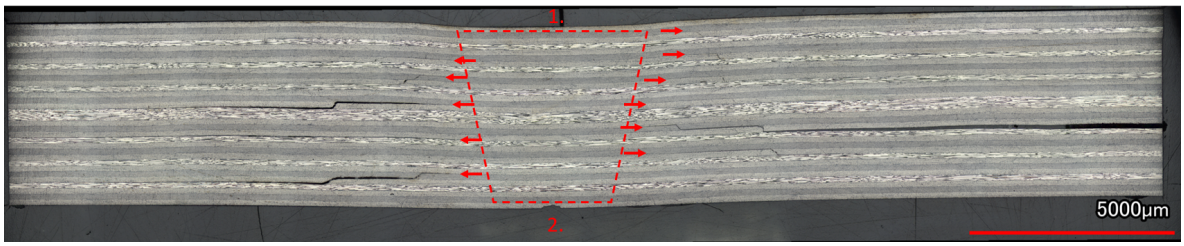


**(a)** Cross-section 1

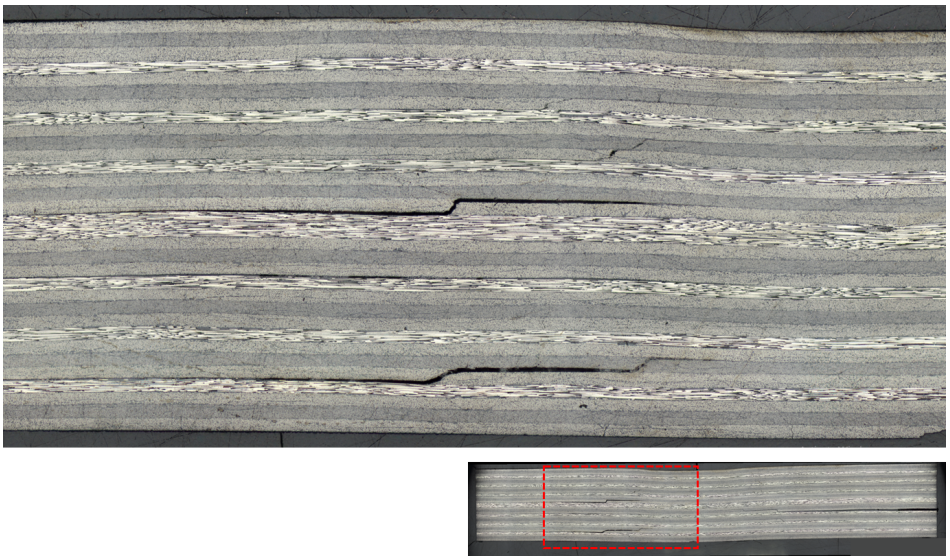

**(b)** Close-up left of undamaged cone

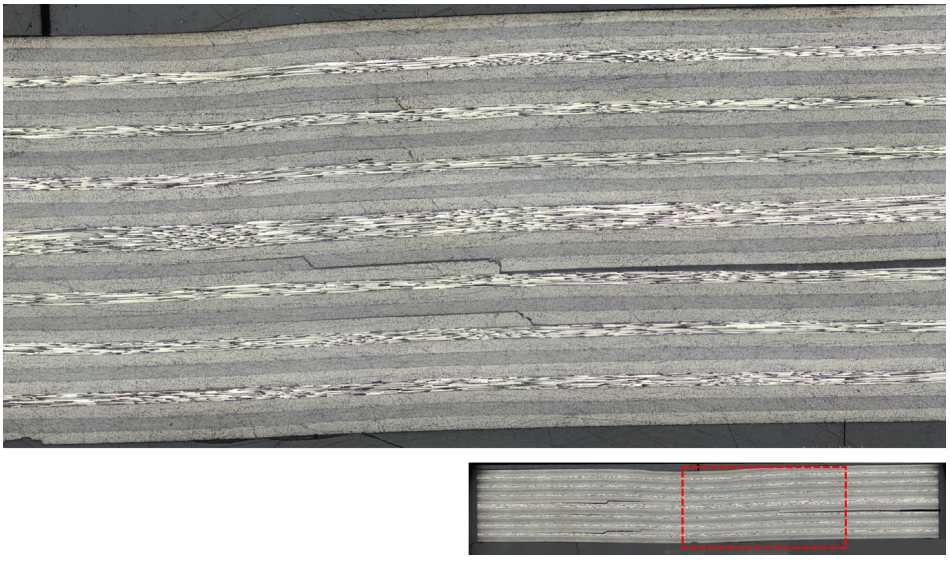

**(c)** Close-up right of undamaged cone

**Figure 4.3:** Cross-sections of the type 1 baseline specimen. 1. Indent 2. Fiber damage. Red dashed lines indicate the undamaged cone. Red arrows indicate the beginning of a delamination which continues outwards.

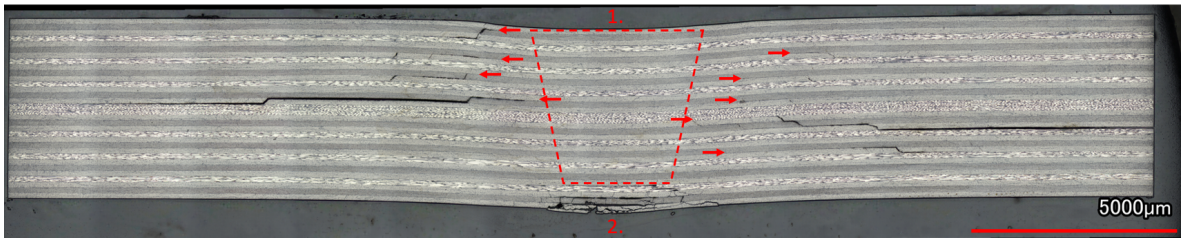


**(a)** Whole cross-section 1

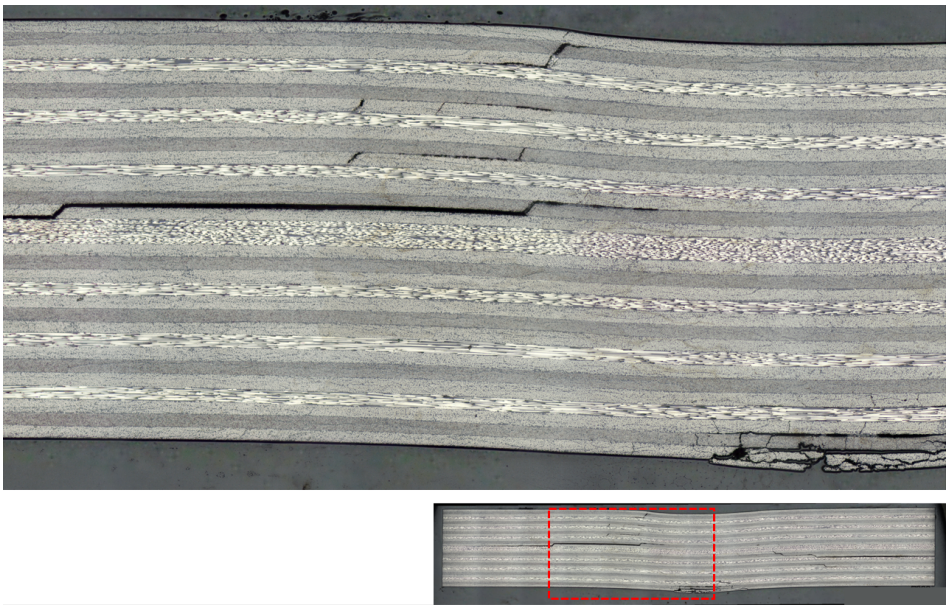

**(b)** Close-up left of undamaged cone

**(c)** Close-up right of undamaged cone

**Figure 4.4:** Cross-sections of the type 2 baseline specimen. 1. Indent 2. Fiber damage. Red dashed lines indicate the undamaged cone. Red arrows indicate the beginning of a delamination which continues outwards.

Figure 4.3 shows the cross-section of the baseline specimen obtained with cross-sectional microscopy. The cross-section shows the presence of an indent in the middle of the specimen. The indent forces the plies to curve, following the shape of the indent, which is most predominantly the case for the top plies. Beneath the indent is the undamaged cone, which does not show any delaminations, matrix cracks or fiber damage. The bottom ply, in the middle of the specimen, shows some fiber damage, in this case the presence of fiber damage is limited to only one ply. On both sides of the undamaged cone, delaminations are present between multiple plies. The delaminations located more towards the top of the specimen do not spread as wide as the delaminations that are located lower. This follows a similar pattern as the pattern described in section 2.1. For nearly all delaminations, it holds that they are present in multiple interfaces, connected by a matrix crack that travels from one interface to the neighbouring interface.

Also, a baseline specimen was made with a type 2 specimen to check whether damage in this type of specimens is similar to the damage observed in type 1 specimens. The cross-section of this specimen can be seen in figure 4.4. The specimen used for this baseline contains the largest amount of fiber damage observed by visual inspection of all type 1 and type 2 specimens. Therefore, the amount of fiber damage observed in figure 4.4, which is present in 5 plies, is considered the most extensive of all specimens used in this research project.

## 4.2 Discussion

In this section, the results of part 1 are discussed. Section 4.2.1 discusses the influence of the impact energy. Section 4.2.2 discusses the influence of the impactor shape. Finally, section 4.2.3 discusses the baseline damage which will be used for the entirety of the project.

### 4.2.1 Influence of impact energy

Figure 4.1 shows that, looking at an impactor diameter of 20mm, there is a threshold energy (approximately 3.5 J/mm) below which no damage is inflicted. However, every impact does leave an indent on each specimen, but this is not considered damage in this research project. For impact energies higher than this threshold energy, delaminations start to occur. The graph shows that, when delaminations occur, the area of the delaminations does not gradually increase with increasing impact energies, but instead makes an immediate jump to a certain size, in this case approximately 710 $mm^2$. Looking at the data for an impactor diameter of 20mm, no clear relationship can be established between the impact energy and the size of the damaged area. However, it must be noticed that the number of data points and the impact energy range is limited, therefore, it is difficult to determine whether the area will or will not increase when further increasing the impact energy. The graph shows that, when increasing impact energies past the threshold, first damage occurs which only consists of delaminations. Increasing the impact energy to 4.0 J/mm and above, also fiber damage starts to occur, which indicates the presence of a threshold energy for fiber damage around 4.0 J/mm. The graph also shows the presence of a delamination threshold energy for an impactor diameter of 40mm at around 6.0 J/mm. However, in case of this impactor shape, the threshold for fiber damage appears to be lower than for delamination as it shows a specimen only containing fiber

damage. Both threshold energies are also expected to be present for an impactor diameter of 15mm, however, not enough data points are present to conclude this.

As mentioned in section 2.1.2, there are conflicting conclusions about the impact behaviour of thermoplastic composites. However, these results show that, at least for the lay-up and material used in this project, it is possible for thermoplastic composites to obtain impact damage which only consists of matrix damage. Additionally, they show similar behaviour as thermoset composites when considering the concept of delamination and fiber damage threshold energies. However, contrary to thermosets, the data does not show a clear linear increase of damaged area with increasing impact energy after the threshold energy for delaminations. To conclude this with more certainty, more data points are needed.

### 4.2.2 Influence of impactor shape

Figure 4.1 shows that, for different impactor shapes, there are different threshold energies. In the case of this study, increasing the impactor diameter from 20mm to 40mm, the threshold energy of delaminations increases from approximately 3.5 J/mm to 6.0 J/mm. Also, the size of the damage that occurs when the specimen is impacted with an energy just above the threshold energy increases when the impactor diameter is increased. Both the increase of threshold energies and initial damage size with increasing impactor diameters align with what is found in literature for thermosets [19].
Interestingly, for an impactor with a diameter of 20mm, the fiber damage threshold energy appeared to be higher than the threshold energy for delaminations. However, for an impactor with a diameter of 40mm, although the actual threshold energy cannot be established, fiber damage occurred below the threshold energy for delaminations. This observation does not align with what is observed in literature for thermosets, which shows that a larger impactor diameter results in more delamination and less fiber damage [33–36]. The reasoning of this difference is considered outside of the scope of this research project.

### 4.2.3 Baseline for impact damage

Looking at the baseline damage, it has similar characteristics to impact damage in thermoset/epoxy composites. It has an indent on the impacted side, (if present) fiber damage on the non-impacted side, an undamaged cone and delaminations in multiple interfaces following a similar pattern as described in section 2.1.1.

In contrary to what is expected from literature, it is shown that thermoplastic composites can obtain impact damage which only consists of matrix damage. Although further research on impact on thermoplastic composites is needed to better understand the conditions needed for such damage, it is promising for repair methods like the one presented in this research project, as this means that these methods can potentially fully restore the compressive strength of the impacted laminate, for these types of impacts.

The baseline damage shows a circular area with a diameter of approximately 30mm. Unfortunately, during the impact trials a smaller damaged area could not be achieved. A circular area with a diameter of approximately 30mm means that, during the welding process, the damaged area is not completely covered by the sonotrode. Therefore, it is expected that not

the entire damaged area will be repaired. This will be taken into account during the welding trials.

Although, the damage characteristics are similar between impacts, meaning all impacts contain an indent, delaminations, matrix cracks and (if present) fiber damage at similar locations, the size of the damaged area and the extent of fiber damage will vary for each impacted specimen. This is the case even when each specimen is impacted using the same settings on the impact tower. These variations between all specimens used for the welding trial and CAI tests, must be taken into account when reviewing the results. Although the effect of these variations on the welding process are yet to be known, for CAI testing, it is known that increasing the damaged area or the extent of fiber damage will have a negative influence on the compressive strength.

Looking at the two cross-sections with different amounts of fiber damage, it can be observed that, besides the fiber damage, the specimens show similar damage. Figure 4.4 shows that, even for the most severe case of fiber damage, it does not seem to have had a considerable effect on the surrounding damage. Therefore, if fiber damage itself does not seem to affect the welding process, it is expected that, when comparing welding results, no special distinction has to be made between specimens with or without fiber damage.

## 4.3 Conclusion

In order to conclude part 1 of this research project, the following sub research questions will be answered:

- What are the damage characteristics of impacted thermoplastic composites?
  - What is the influence of impact energy on the impact damage characteristics?
  - What is the influence of the impactor shape on the impact damage characteristics?

**What are the damage characteristics of impacted thermoplastic composites?**

All impacts resulted in an indent on the impacted side of the specimen. Depending on the impact energy, delaminations occur. If present, delaminations are located in multiple interfaces. Most of the time, the delaminations closest to the non-impacted side extents over the whole diameter of the damaged area, while others extent to no more than half the diameter of the damaged area. For each specimen containing delaminations, an undamaged cone is present. Fiber damage, if present, only occurred on the non-impacted side of the specimen, limited to the 1 to 5 outermost plies. In contrary to what was expected from literature, for certain impact parameters, impact damage was obtained only consisting of matrix damage. This shows that a repair method based on US welding, only capable of repairing matrix damage, has the potential to fully repair the impact damage, in those cases.

**What is the influence of impact energy on the impact damage characteristics?**

Two energy thresholds were observed, one for delamination damage and one for fiber damage. Below these threshold energies, besides an indent, no damage was observed. Above these thresholds, depending on the type of threshold, delaminations and/or fiber damage was

observed. However, for the range of energies used, no clear relation was found between the impact energy and the area of delaminations.

**What is the influence of the impactor shape on the impact damage characteristics?**

Increasing the impactor radius resulted in an increase of both the threshold energy for delaminations as well as for fiber damage. However, it was observed that the increase of the delamination threshold was higher than the fiber damage threshold. Therefore, where it was possible to create delamination only damage with an impactor diameter of 20mm, this was not possible using a diameter of 40mm.

# Chapter 5

# Part 2 - Ultrasonic welding

In this chapter, the results of part 2 are shown and discussed. Section 5.1.1 shows the results of the welding trials to characterize heating inside undamaged and damaged specimens. These results will be discussed in section 5.2.1. Section 5.1.2 shows the results of the welding trials to determine the influence of the welding parameters on the welding process. These results will be discussed in section 5.2.2. Finally, section 5.1.3 shows the results of the final repairs. These results will be discussed in section 5.2.3. For this report, the resolution of the cross-sectional microscopy images had to be lowered, high resolution images can be found in the database through this link: https://dataverse.nl/dataverse/TPCWeldingRepair

## 5.1 Results

### 5.1.1 Characterising heating in damaged composites

In this section, the results are shown of the trials for characterizing the heat generation in damaged and undamaged specimens. The results consist of welding data, temperature data and cross-sectional microscopy data. The welding parameters used for both welding trials are shown in table 5.1. To improve readability, instead of using the specimen IDs, each weld is given a name, which are also stated in table 5.1.

#### Welding data

The welding data of the welding trial with undamaged and damaged specimens is shown in figure 5.1 and 5.2, respectively. To improve the readability of the figure, only the welding power and sonotrode displacement are shown. The vibration amplitude, welding force and frequency are not shown as they can be considered constant and are shown in table 5.1.

Figure 5.1 shows the welding power and sonotrode displacement for welds performed on undamaged specimens with a duration of 5, 10, 12, 14 and 16 seconds. For all welds, the

| Name | Specimen ID | Type | $F_w$ | $A_{vibr}$ | $F_c$ | Vibration duration |
|---|---|---|---|---|---|---|
| Un-5sec | 0.0.1 | Undamaged | 300N | $70\mu m$ | 300N | 5 sec |
| Un-10sec | 0.0.2 | Undamaged | 300N | $70\mu m$ | 300N | 10 sec |
| Un-12se | 0.0.3 | Undamaged | 300N | $70\mu m$ | 300N | 12 sec |
| Un-14sec | 0.0.4 | Undamaged | 300N | $70\mu m$ | 300N | 14 sec |
| Un-16sec | 0.0.5 | Undamaged | 300N | $70\mu m$ | 300N | 16 sec |
| D-2sec | 3.2.1 | Damaged | 300N | $70\mu m$ | 300N | 2 sec |
| D-3sec | 3.2.2 | Damaged | 300N | $70\mu m$ | 300N | 3 sec |
| D-5sec | 3.2.3 | Damaged | 300N | $70\mu m$ | 300N | 5 sec |
| D-7.5sec | 3.2.4 | Damaged | 300N | $70\mu m$ | 300N | 7.5 sec |
| D-10sec | 3.2.5 | Damaged | 300N | $70\mu m$ | 300N | 10 sec |

**Table 5.1:** Welding parameters used during the welding trials for characterizing heating in damaged and undamaged specimens

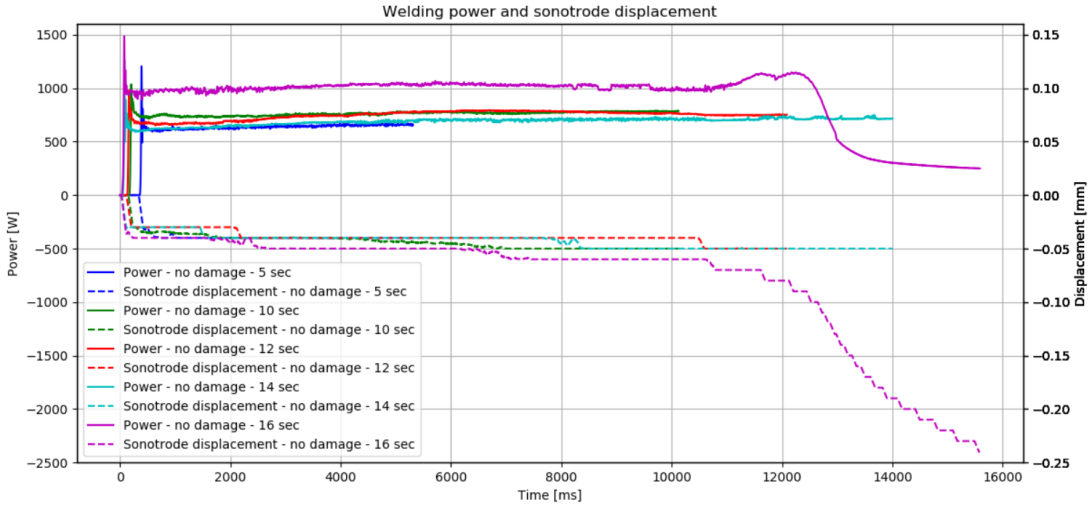


**Figure 5.1:** Power and displacement curves for welds performed on undamaged specimens

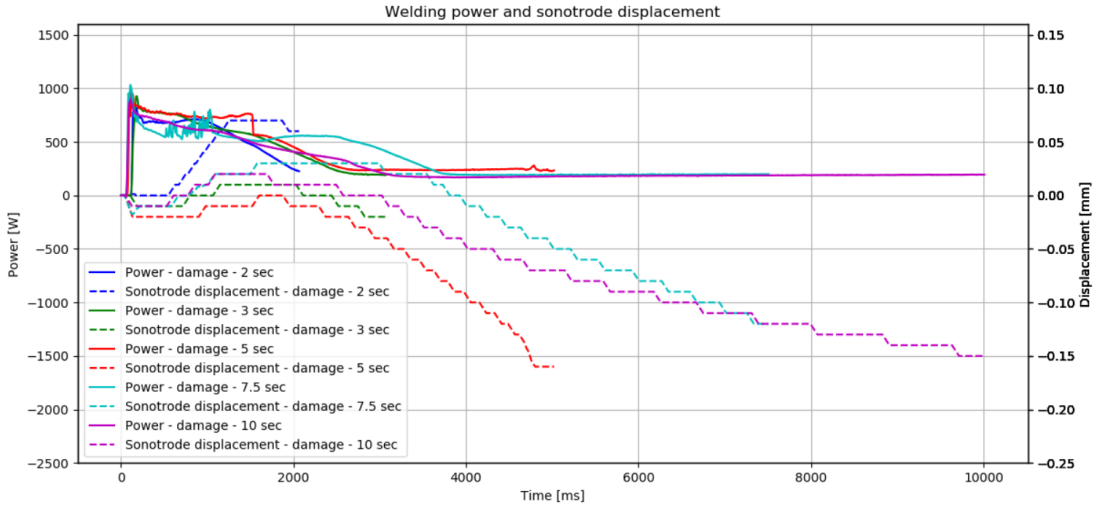


**Figure 5.2:** Power and displacement curves for welds performed on damaged specimens

power curves show an initial steep rise with a high peak, this is needed to initiate the vibration of the sonotrode. After this peak, they maintain a constant power until the vibration phase is stopped, except for the 16 second weld which shows an increase in power starting at 11 seconds and, after reaching its peak, it quickly decreases and seems to settle at a lower constant value. Looking at the displacement curves, all curves show an initial drop, which is a retraction of the sonotrode to allow it to vibrate, after which they slowly decrease until the vibration phase ends. This slow decrease is likely the result of the expanding material as it heats up. The 16 second weld shows a steeper decrease which initiates at the same time the power curve starts to increase. This decrease in displacement becomes even more steep when the power curve starts to drop.

Figure 5.2 shows the welding power and sonotrode displacement for welds performed on damaged specimens with a duration of 2, 3, 5, 7.5 and 10 seconds. Like the undamaged specimens, the power curves start with steep power rise to its peak power. The 2, 5 and 7.5 second welds settle on a constant power after which they show a small increase followed by a drop in power. After this drop, they remain constant. The 3 and 10 second welds, which immediately starts to decrease in a wavy fashion after the power peak, decrease until a lower constant power is reached.
Looking at the displacement curves, all curves have a small initial decrease. However, after a small time increment, the displacement starts to increase. At some point this increase stops and the displacement starts to decrease until to weld is stopped. The point where the displacement curve starts to decrease coincides with the increase and drop of the power curves.

Comparing the power curves of the undamaged and damaged specimens, there are similarities. For both, the power settles for a constant value after its initial peak, after which, they increase slightly which is followed by a drop to a lower constant value. However, for the damaged specimens, this happens more quickly. Where it takes more than 14 seconds for undamaged specimens, it happens in 2.5-4 seconds for damaged specimens. Also, 2 of the 5 damaged specimens showed a decreasing power (in a wavy fashion) instead of a constant power.
Comparing the displacement curves of the undamaged and damaged specimens, there is a similarity in the fact that the displacement steeply decreases at the same point the power curve starts to drop to its final constant value. However, the main difference between the two is the fact that the displacement of the undamaged specimens is very slowly decreasing/constant until this point, whereas the damaged specimens show an increase until this point.

### Temperature data

The temperature data of the welding process only consists of temperature readings after the ultrasonic vibration phase. After the vibrations are stopped, the sonotrode is lifted to ensure there is no consolidation force and that the IR-camera is able to record the whole upper surface of the specimen. Although thermocouples (TC) and an IR-camera were used to record temperature during this trial, only the IR-camera recordings are used (see the additional remarks at the end of this section).

Figure 5.3 shows the temperature curves of the undamaged and damaged specimens, which start from the moment the sonotrode is lifted, hence the end of the vibration phase. The temperature curve represents the maximum temperature of the surface at the location of the

weld. The maximum temperature is chosen over a fixed location because the temperature is not homogeneously distributed. Therefore, the curve represents the highest temperature reached independent of its location. Unfortunately, for the trial with undamaged specimens, the IR-camera used a calibration up to 160°C. This resulted in the fact that all readings above 160°C are shown as 160°C. Therefore, the 16 second weld on the undamaged specimen shows a constant 160°C for the first 12 seconds.

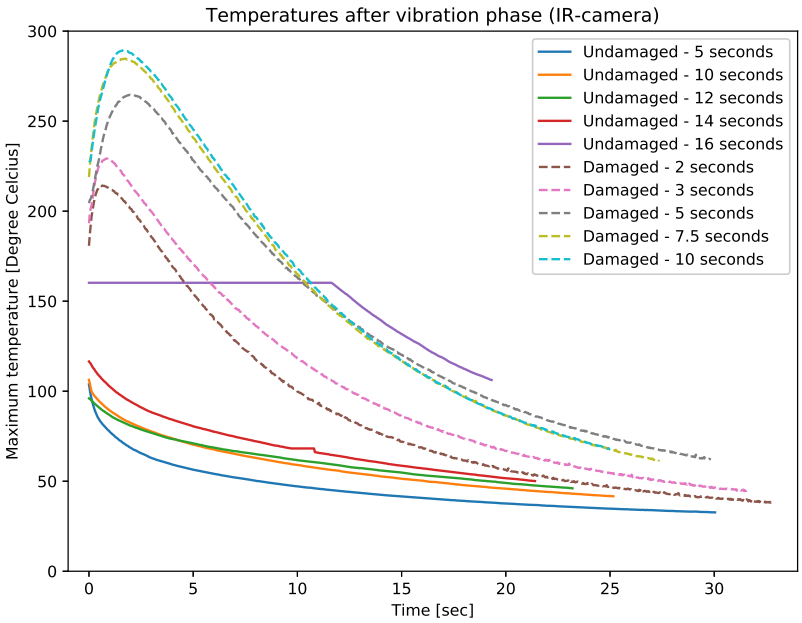


**Figure 5.3:** Maximum temperature curves of the top surfaces of the welded specimens. Measurements start directly after the vibration phase.

Looking at figure 5.3, for undamaged specimens, a distinction can be seen between the 5, 10, 12, 14 second welds and the 16 second weld. For the welds up to 14 seconds, maximum initial temperatures between 96°C and 117°C are reached after which they immediately decrease. Despite the differences in vibration duration, the initial temperatures are fairly similar. However, looking at the decay, it shows that longer duration welds hold a higher temperature for longer, indicating it is likely for the material to hold more energy in the form of bulk heat. The 16 seconds weld shows a much higher temperature. Although the first 12 seconds are compromised, it shows it is at least 160°C and, looking at the decaying part of the curve, it is expected to be much higher. This is clearly a difference compared to the welds up to 14 seconds, indicating a different aspect is contributing to this. Unfortunately, nothing can be said about the initial temperature and whether or not the temperature immediately decreases or increases after the vibration phase.

Looking at figure 5.3, for damaged specimens, all temperature curves are following the same trend. The initial temperatures range from 181°C to 227°C, where long duration welds show higher temperatures. All temperatures start to increase from the moment the vibration phase ends. The graph shows that, for welds with a longer duration, there is a larger increase in temperature. At some point, this increase stops at the peak temperature and the temperature

starts to decrease. The decaying part of the curves show that for longer duration welds (except of the weld with a duration of 5 seconds), the temperature remains higher for a longer period of time, indicating these specimens hold more energy in the form of bulk heat.

Comparing the temperature curves of the undamaged and damaged specimens, there are a few differences. The initial temperatures of all undamaged specimens are lower (although this cannot be determined for the 16 seconds weld) compared to the damaged specimens. This holds not only for welds with similar durations but even the 2 second weld on a damaged specimen shows higher temperatures than the 14 second weld on an undamaged specimen. Also, the temperature of the undamaged specimens immediately decreases when the vibration phase ends. However, for damaged specimens, the temperature increases first and, after the peak is reached, starts to decrease. Finally, after the same amount of time the remaining temperatures are higher on the damaged specimens, indicating more bulk heat energy is present.

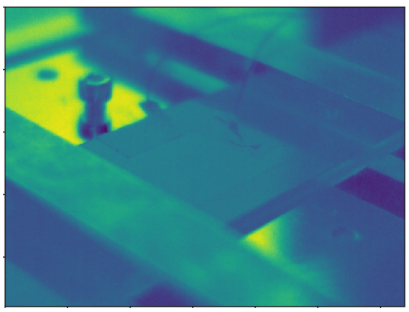

**(a)** Before welding

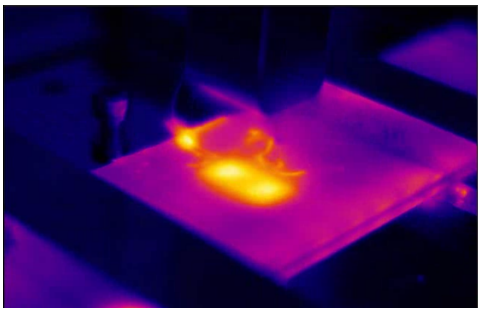

**(b)** Undamaged specimen

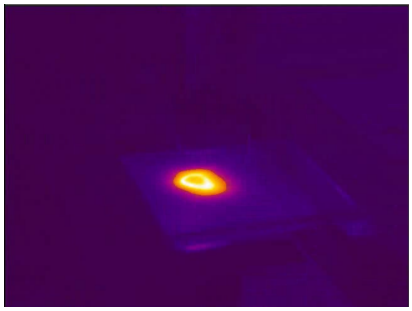

**(c)** Damaged specimen

**Figure 5.4:** Temperature distribution on the top surfaces of welded specimens directly after the vibration phase and lifting of the sonotrode. (a) Picture before welding to provide more clarity to what can be observed in (b) and (c). (b) Undamaged specimen welded for 14 seconds. (c) Damaged specimen welded for 7.5 seconds.

Figure 5.4 shows two images taken of an undamaged and damaged specimen immediately after the sonotrode is lifted, hence end of the vibration phase. Although the color scales of both figures do not match, it can be seen that the temperature distribution of each specimen is different. The temperature distribution of the undamaged specimen has a more homogeneous distribution which has the same shape as the rectangular sonotrode. Within this rectangle the largest temperature difference is 18°C. (The arbitrary looking shapes next to the rectangle

are the TC's which heat up during the vibrations phase, see the additional remarks at the end of this section). The damaged specimen shows a circular distribution pattern where the temperature of the center is lower than the circle surrounding it. The largest temperature difference between the center and its surrounding circle is 57°C. The center of the circle coincides with the center of the impact, hence the indent. For a better understanding of the IR-camera orientation and what can be observed in figure 5.4, the setup can be seen in figure 3.2.

### Cross-sectional microscopy

Figures 5.5 and 5.6 show the cross-sections of the undamaged specimens which are welded for 14 and 16 seconds, respectively. The specimens that are welded for 5, 10 and 12 seconds are not shown as they are similar to the specimen welded for 14 seconds. To determine whether the material was heated during welding, signs such as voids, heat induced delaminations, degradation of material and waviness of plies can be used as they indicate the material has reached temperatures close to the melting temperature (Tm). These signs can express themselves more easily as during this welding trial no consolidation force is used. It is important to notice that the absence of these signs cannot guarantee that there was no heating close to Tm nor can they give information about the actual temperatures.

Looking at figure 5.5, the cross-section shows no signs that indicate the material has reached Tm during welding. The cross-section does not show any differences compared to a pristine laminate that has not been welded. Therefore, it is believed that this specimen was not heated to temperatures in the range of Tm.

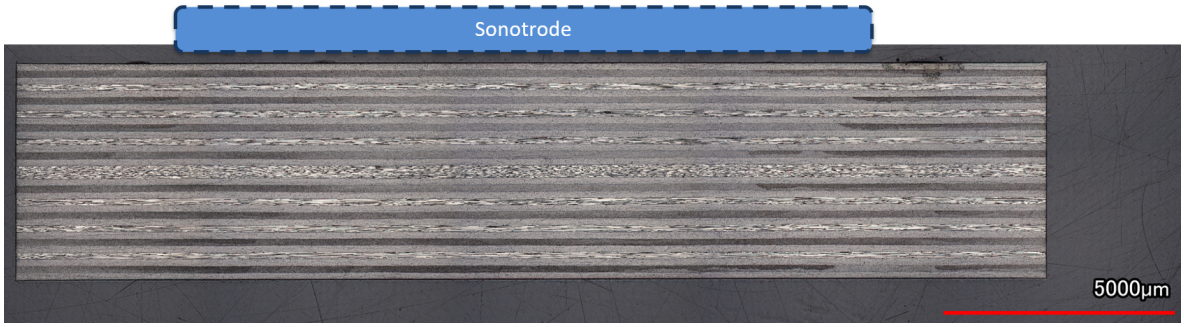


**Figure 5.5:** Cross-section 1 of an undamaged specimen welded for 14 seconds. Note: No consolidation force was applied after the vibration phase.

Looking at figure 5.6, the cross-section shows signs of heating in the upper half on the specimen. In the upper four plies, the interfaces are partially delaminated and the interface as well as the plies contain voids. Beneath these, waviness of plies can be observed. These signs indicate that, at the location of these delaminations, voids and waving plies, temperatures close to or above Tm were reached.

Figures 5.9 to 5.13 show the cross-sections of the damaged specimens which are welded for 2, 3, 5, 7.5 and 10 seconds, respectively. As these specimens contain impact damage, it can be more difficult to determine signs of melting. For example, delaminations can be induced by the impact event or by reaching Tm during the welding process. A feature that can distinguish the

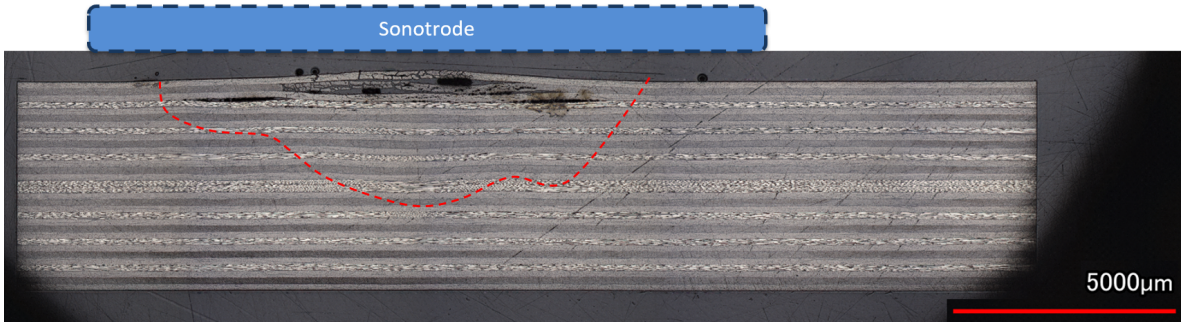


(a)

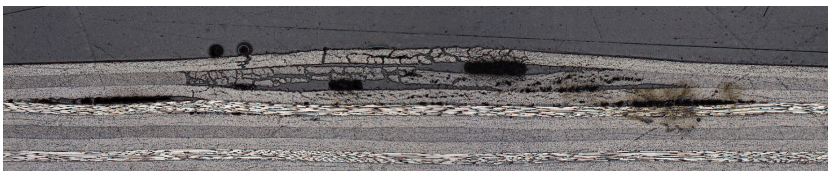

(b)

**Figure 5.6:** (a) Cross-section 1 of an undamaged specimen welded for 16 seconds. (b) Close-up of the upper plies. Red dashed line indicates the area where waviness of plies is observed. Note: No consolidation force was applied after the vibration phase.

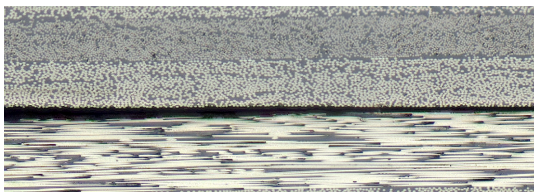

(a) Impact induced delamination

(b) Heat induced delamination

**Figure 5.7:** Figures show two types of delaminations. The difference can be seen by looking at the roughness of the edge of the ply and if there are thickness variations within the ply.

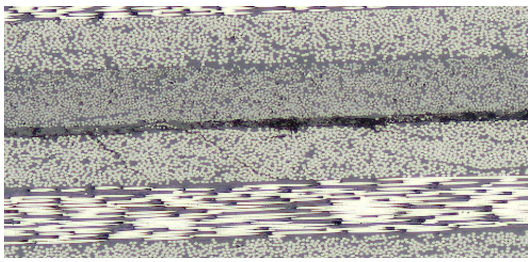

(a) Debris inside delamination

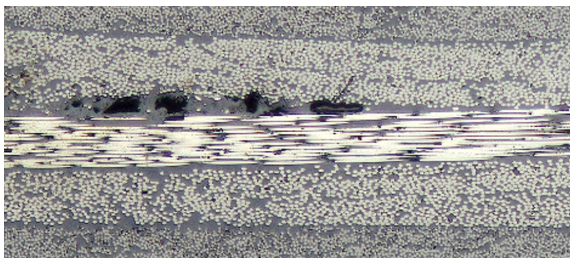

(b) Voids inside interface

**Figure 5.8:** Figures show similarities between debris inside delaminations and voids inside the interface. Both have plies that separated, but this separation is repeatedly discontinued by matrix material, connecting the plies with each other. In case of a delamination, this matrix material is debris from the impact. In case of voids, this matrix material is material which melted during the welding process.

two is variation in ply thickness around the delaminated area. If a delamination is induced by an impact event, the plies detach from one other but do not deform as the ply itself remains intact. However, when a delamination occurs due to melting of the material, the plies surrounding the delamination are also affected as they melt too. This often causes the plies to deform and vary in thickness, see figure 5.7. Additional to the previously mentioned signs, damaged specimens can also indicate melted areas when there are no delaminations present at locations where delaminations are expected as, after melting, the delaminations re-consolidate. However, after an impact event, the presence of delaminations at certain locations is never guaranteed and, therefore, the absence of delaminations cannot guarantee melting. Also, even when Tm is not reached, when above Tg, the material softens and the delamination can close without bonding together. Although the delamination is still present, it becomes increasingly difficult to detect. Finally, some plies have a smooth delamination that has the appearance of a thin crack in between the plies. However, there are also delaminations that are filled with debris from the impact event [14]. These delaminations can easily be mistaken for voids in the interface or delamination induced by the welding process, see figure 5.8.

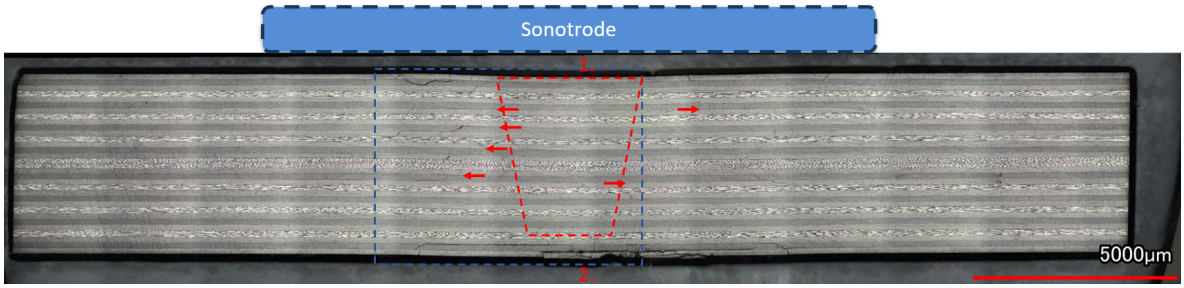


**(a)** Cross-section 1

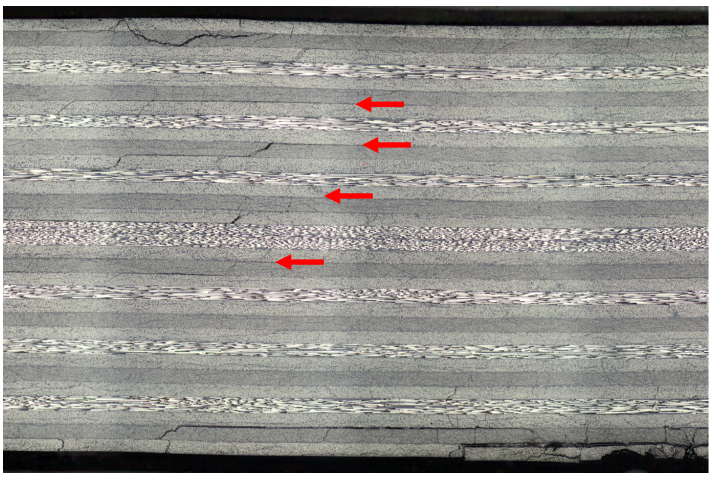

**(b)** Close-up

**Figure 5.9:** Cross-section 1 of a damaged specimen welded for 2 seconds. Two types of damage are highlighted in the image: indentation (1) and fiber damage (2). Red dashed lines indicate the undamaged cone. Red arrows indicate the beginning of a delamination which continues in the direction of the arrow, also shown in the close-up. Blue dashed lines indicate the area of the close-up. Note: No consolidation force was applied after the vibration phase.

Looking at figure 5.9, the cross-section does not show clear signs of melting. There are no voids or welding induced delaminations present. However, the right side of the cross-section shows less delaminations than is expected when looking at the left side or the baseline specimen. Comparing the indent to the baseline specimen, the indent seems to be reduced. Because of the absence of voids, it could not be guaranteed that melting has happened. Looking at figure 5.10, the cross-section of the specimen welded for 3 seconds looks similar to the cross-section of the specimens welded for two seconds. Therefore, the same can be said for this specimen.

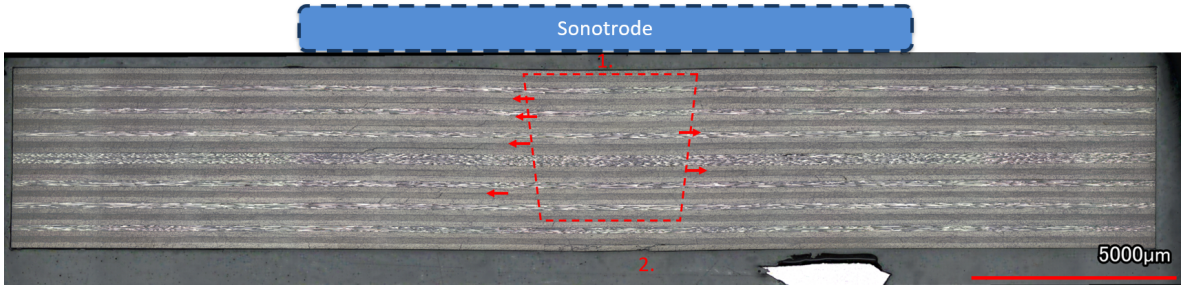


**Figure 5.10:** Cross-section 1 of a damaged specimen welded for 3 seconds. 1. Indent 2. Fiber damage. Red dashed lines indicate the undamaged cone. Red arrows indicate the beginning of a delamination which continues in the direction of the arrow. Note: No consolidation force was applied after the vibration phase.

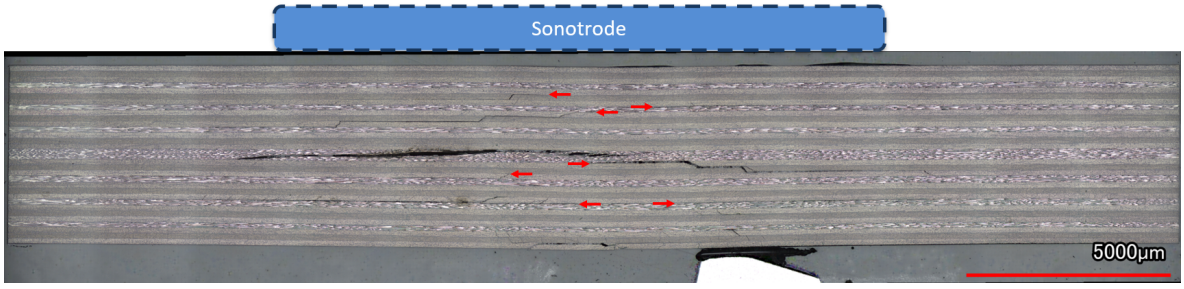


**(a)** Cross-section 1

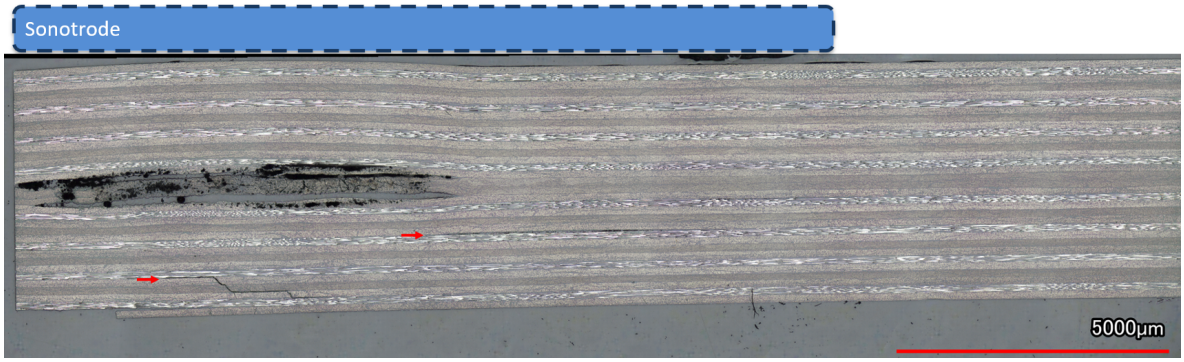


**(b)** Cross-section 2

**Figure 5.11:** Cross-section 1 and 2 of a damaged specimen welded for 5 seconds. Red arrows indicate the beginning of a delamination which continues in the direction of the arrow. Note: No consolidation force was applied after the vibration phase.

Looking at figure 5.11, the first cross-section shows a delamination induced by the welding process through the middle plies. It is determined to be caused by the welding process as delaminations due to impact only appear between plies of different orientation [17]. Also, the indent has completely disappeared. The second cross-section shows clear signs of melting. In the middle of the thickness, there is a large delaminated area which contains burned material (from here on called degraded material) (During the cutting process for preparing the specimens for cross-sectional microscopy, a distinctive burned plastic smell could be observed). Below this degraded area, waviness of the plies and a re-consolidated delamination can be observed. Furthermore, the delamination that are expected to be present above the degraded area are most likely also re-consolidated. These delaminations are believed to be able re-consolidate without the presence of the consolidation force due to the internal pressure build up due to high temperatures in the degraded area. This internal pressure also caused to formation of a bulge on the surface.

Looking at figure 5.12, the first cross-section shows two areas of welding induced delaminations and voids on the right side. These areas are offset from the center and coincide with locations where impact induced delaminations are expected. Above these areas, a bulge has formed on the surface. The second cross-section shows one impact induced delamination on the bottom. It is expected for more delaminations to be present in the middle of the laminate, because of the absence of these delaminations, it is expected that these are re-consolidated.

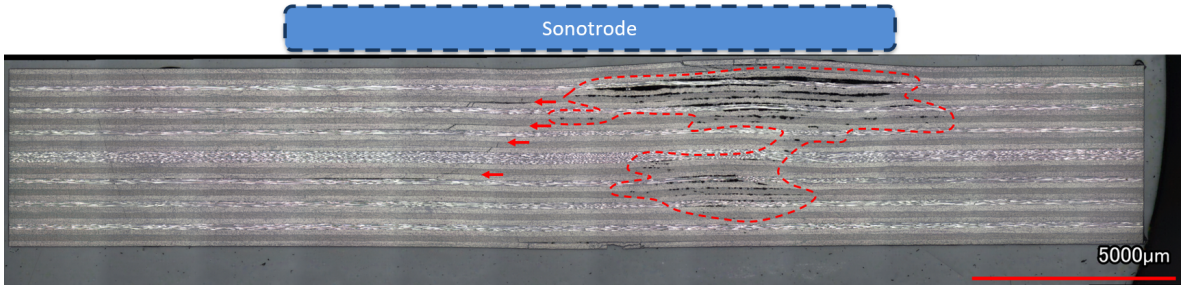


**(a)** Cross-section 1

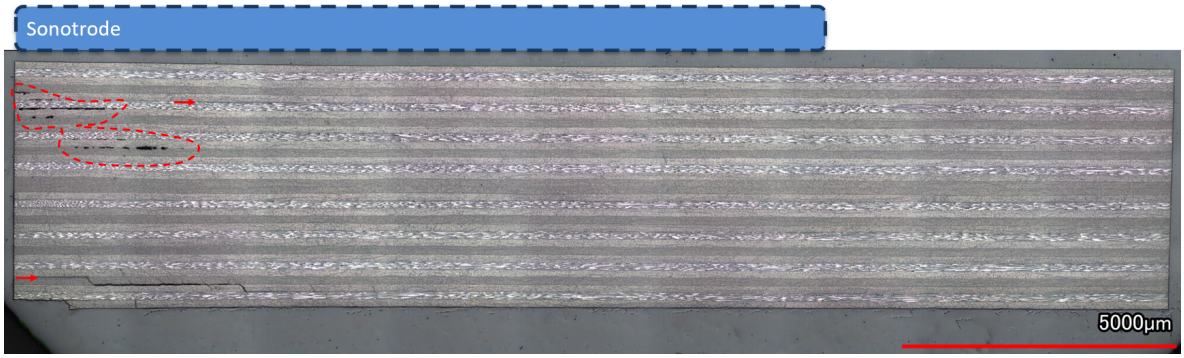


**(b)** Cross-section 2

**Figure 5.12:** Cross-section 1 and 2 of a damaged specimen welded for 7.5 seconds. Red arrows indicate the beginning of a delamination which continues in the direction of the arrow. Red dashed lines indicate areas with heat induced voids. Note: No consolidation force was applied after the vibration phase.

Looking at figure 5.13, the first cross-section shows an area with voids on the upper half of the laminate, in the middle and just left of the center, indicating melting. The second cross-section shows heat induced delaminations near the top of the laminate and areas with voids. Indicating melting throughout the thickness.

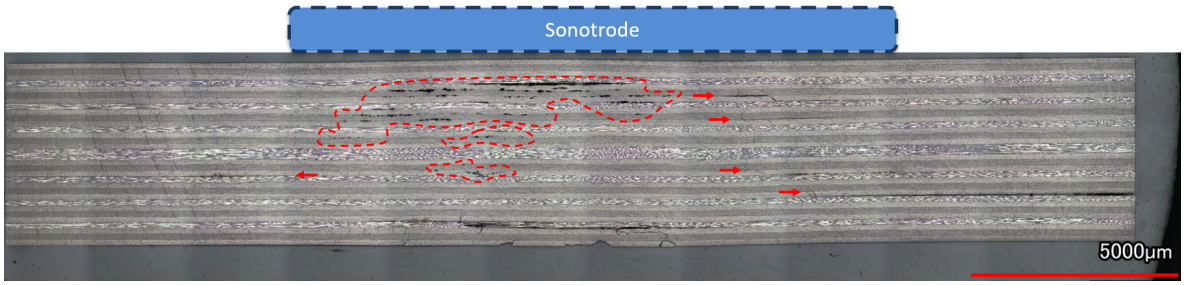


**(a)** Cross-section 1

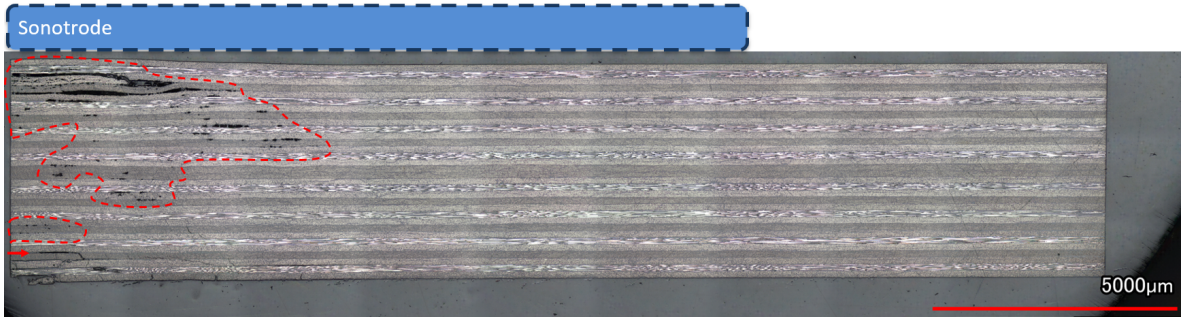


**(b)** Cross-section 2

**Figure 5.13:** Cross-section 1 and 2 of a damaged specimen welded for 10 seconds. Red arrows indicate the beginning of a delamination which continues in the direction of the arrow. Red dashed lines indicate areas with heat induced voids. Note: No consolidation force was applied after the vibration phase.

### Additional remarks

In this section, some additional remarks are pointed out. These are observations made during the welding trials. Although these do not directly affect the results, they are noteworthy.

During the welding trial of the undamaged specimens, for all specimens except the specimen welded for 16 seconds, heating was observed at a different location than under the sonotrode. This secondary heating initiated at the edge of the specimen. Secondary heating was not observed during the welding trial for damaged specimens.

During the welding trial of the undamaged specimens, thermocouples were used. The images from the IR-camera revealed local heating inside the thermocouples during and after the vibration phase, see figure 5.4. Therefore, the temperature reading from the thermocouples are considered unreliable in the case of this trial and are discarded.

### 5.1.2 Influence of welding parameters

In this section, the results will be shown from the trials that are conducted to determine the influence of the welding parameters on the welding process. The welding parameters consist of vibration duration, consolidation force, welding force and vibration amplitude. Depending on the parameter, results consist of welding data, cross-sectional microscopy images and C-scan data. For each trial, the set of welding parameters is provided in a table.

#### Vibration duration

To determine the influence of the vibration duration, the same set of welded damaged specimens will be evaluated as used in section 5.1.1. As there was no consolidation phase, it is easier to distinguish the difference in heating for each duration. The welding parameters of these welds are shown in table 5.2.

| Name | Specimen ID | $F_w$ | $A_{vibr}$ | $F_c$ | Vibration duration |
|---|---|---|---|---|---|
| D-2sec | 3.2.1 | 300N | 70$\mu m$ | 300N | 2 sec |
| D-3sec | 3.2.2 | 300N | 70$\mu m$ | 300N | 3 sec |
| D-5sec | 3.2.3 | 300N | 70$\mu m$ | 300N | 5 sec |
| D-7.5sec | 3.2.4 | 300N | 70$\mu m$ | 300N | 7.5 sec |
| D-10sec | 3.2.5 | 300N | 70$\mu m$ | 300N | 10 sec |

**Table 5.2:** Set of welding parameters used to determine the influence of vibration duration

Looking at the specimens with a vibration duration of 2 and 3 seconds, see figures 5.9 and 5.10, both specimens show no clear signs of melting. Both specimens do not contain any voids or delaminations related to melting. However, both specimens show less delaminations on the right half of the cross-section compared to the left side and to the baseline specimen. Both specimens show a reduction of the indentation.

Looking at the specimen with a vibration duration of 5 seconds, see figure 5.11, the specimen shows a large void inside of the middle two 90° plies. Furthermore, the figure shows that the indent caused by the impact event is almost completely reduced. The second cross-section shows a large area with degraded material which contains voids. Beneath this area, there is some waviness of the plies and signs of a delamination that is re-consolidated. Above the degraded area, there are no delaminations present where they are expected based on the baseline. On the top surface a bulge has formed.

Looking at the specimens with a vibration duration of 7.5 and 10 seconds, see figures 5.12 and 5.13, both specimens show clear signs of heating. Both specimens show an area with voids and delaminations caused by melting. For both specimens, this area is almost completely located on either the left side (specimen with duration of 10 sec) or the right side (specimen with duration of 7.5 seconds) of the undamaged cone. For both specimens, the indent is removed and a bulge has formed on the top surface. On the second cross-sections, both specimens show only one delamination, which is less than is expected from the baseline. Also, on these cross-sections, both specimens contain voids.

Looking at the welding graphs, see figure 5.2, all power curves show that, after 3-4 seconds, the welding power remains almost constant. Therefore, for these welding parameters, by

varying the duration, for durations longer than 3-4 seconds, only the period of this constant power is changed. Looking at the displacement curves, it shows that, from the moment the power curves become constant, the displacement curves keep decreasing. This means that, for these welding parameters, for durations longer than 3-4 seconds, increasing the duration will decrease the displacement.

Looking at figure 5.3, the temperature curves show that, for welds with a longer duration, higher (surface) temperatures are reached at the end of the vibration phase. Also, for welds with a longer duration, the temperature increase after the vibrations phase ended is higher, resulting in higher peak temperatures. Finally, for welds with a longer duration, it takes more time for the (surface) temperature to go down.

### Consolidation force

To determine the influence of the consolidation force, a welding trial was performed where all the welding parameters were kept the same except for the consolidation force which was varied. The welding parameters of these welds are shown in table 5.3.

| Name | Specimen ID | $F_w$ | $A_{vibr}$ | $F_c$ | Vibration duration |
|---|---|---|---|---|---|
| Con-300N | 3.4.1 | 300N | $70\mu m$ | 300N | 10 sec |
| Con-600N | 3.4.2 | 300N | $70\mu m$ | 600N | 10 sec |
| Con-900N | 3.4.3 | 300N | $70\mu m$ | 900N | 10 sec |

**Table 5.3:** Set of welding parameters used to determine the influence of consolidation force

Unfortunately, for this trial, the welding graphs are not usable. For the welds with a consolidation force of 600N and 900N, after the vibration phase, the force is increased from 300N which is used during the welding phase. This increase in force happens almost instantaneously. This increase in force not only has an effect on the specimen but also on the welding machine itself. When the welding and consolidation force are equal, there is no difference in force exerted on the welding machine, hence there is no change in deflection of the machine. Therefore, the measured displacement of the sonotrode is solely caused by the specimen. An increase in force after the welding phase causes a deflection of the machine itself, which is also measured as a displacement of the sonotrode. Therefore, the readings of the displacement are a combination of machine deflection and changes of the specimen. For this reason, the readings cannot be used to determine displacements only related to the specimens.
As the consolidation force only affects the consolidation phase, the power and displacement curves during the vibration phase are not affected and are therefore not discussed.

Figures 5.14 to 5.16 show the cross-sections of the specimens used during this trial. Figure 5.14 shows a large delamination in the middle of the cross-section, that travels from the left, through the middle, all the way to the right. The upper half of the plies are all slightly curved, which results in the specimen having a curved top surface. Looking at the second cross-section, it shows a degraded area with large delaminations and voids. Comparing the degraded area to the right side of the cross-section, it shows that the degraded area has expanded. Similar to the cross-section in figure 5.11 which had a consolidation force of 0N, a bulge can be seen on the top surface of the specimen. However, in this case the bulge is flattened on the top with a kink on the right side of the bulge.

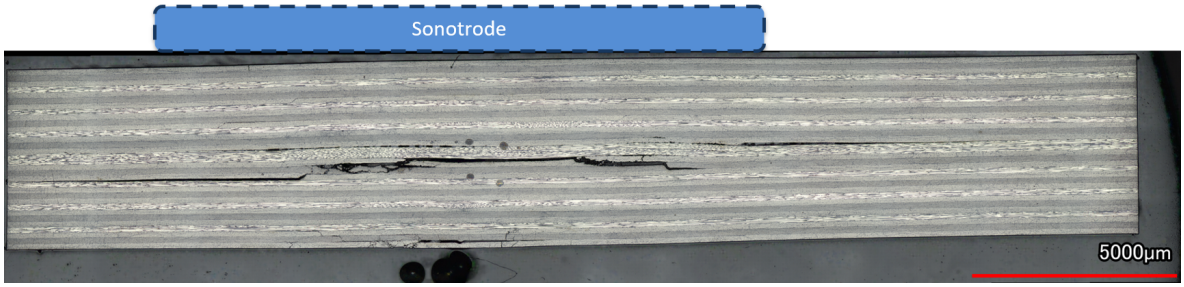


**(a)** Cross-section 1

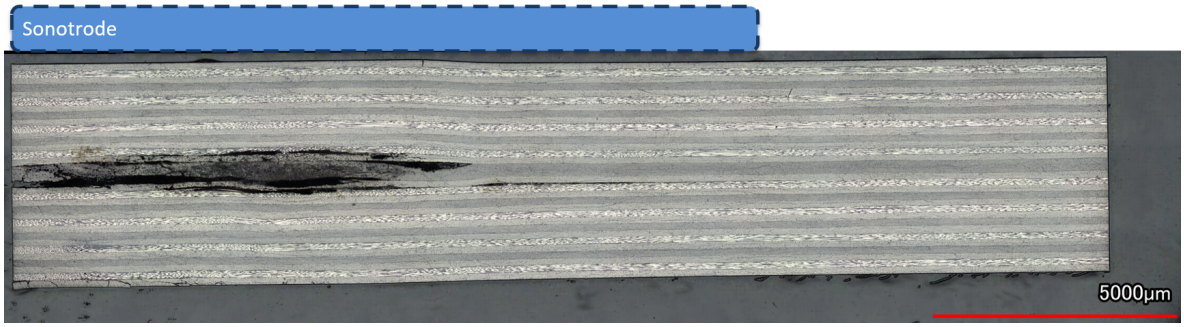


**(b)** Cross-section 2

**Figure 5.14:** Cross-section 1 and 2 of the specimen consolidated with a consolidation force of 300N

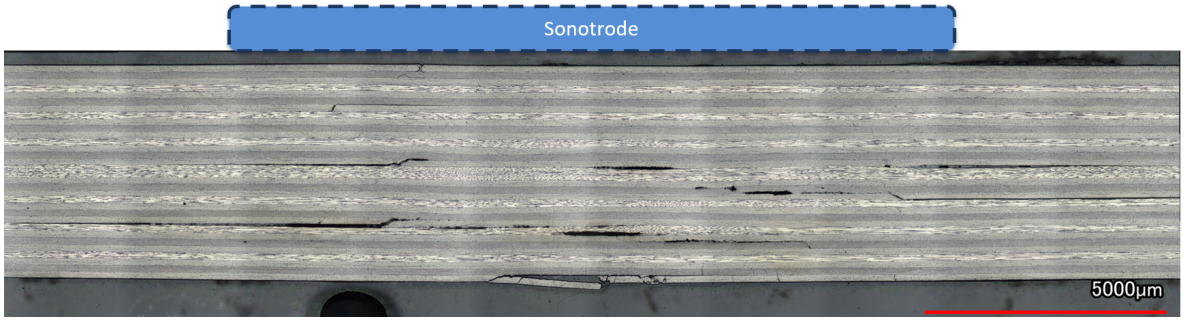


**(a)** Cross-section 1

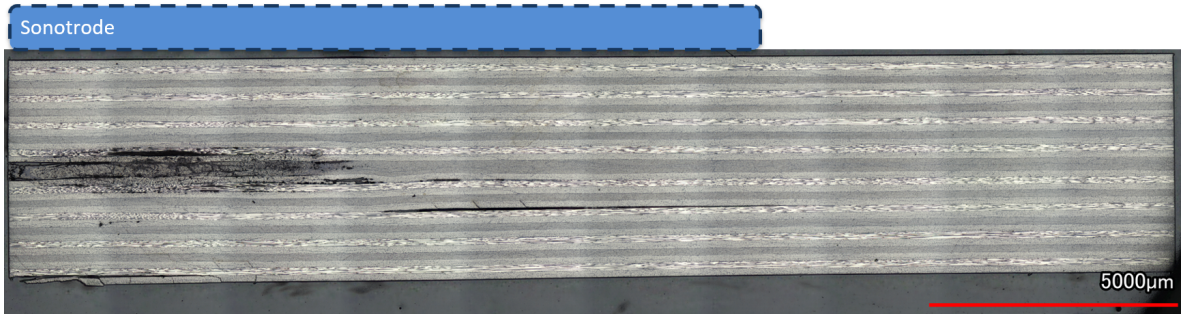


**(b)** Cross-section 2

**Figure 5.15:** Cross-section 1 and 2 of the specimen consolidated with a consolidation force of 600N

For the specimens which had a consolidation force of 600N and 900N, the cross-sections look similar to each other, see figures 5.15 and 5.16. The first cross-sections of both specimens show voids and delaminations induced by melting. However, compared to the specimen with a consolidation force of 300N, these specimens do not have a curved top surface and curved plies, instead these are straight. Looking at the second cross-sections of both specimens, they show that both have a degraded area. However, these areas did not expand. Also, there is no bulge present of the top surface and the plies between the degraded area and the top surface are straight.

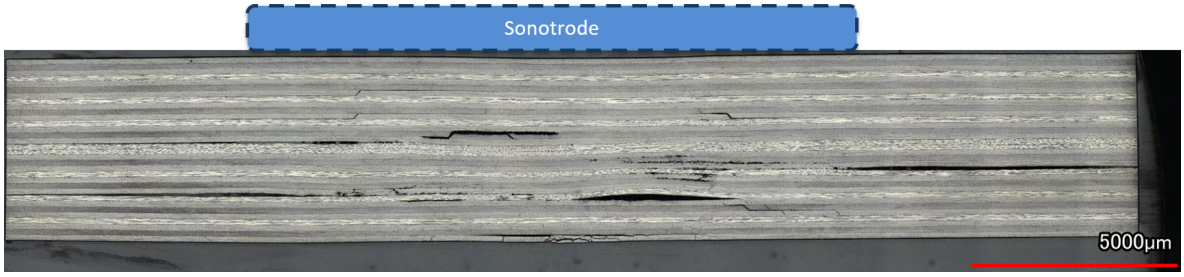


**(a)** Cross-section 1

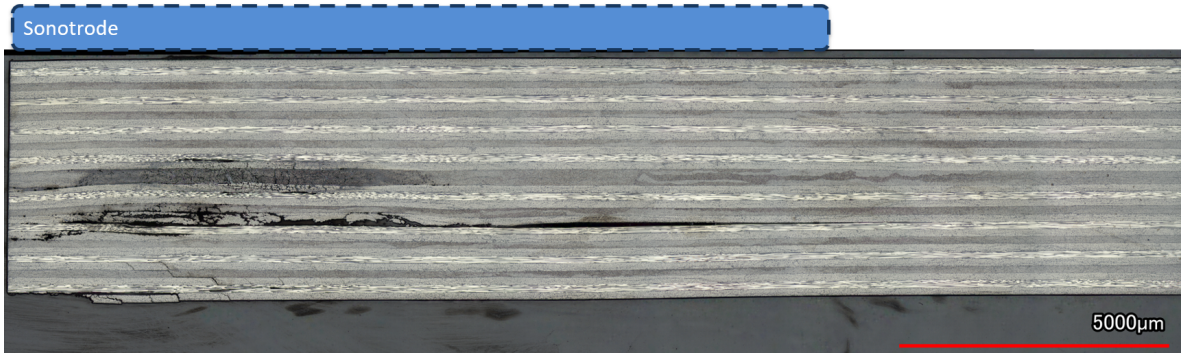


**(b)** Cross-section 2

**Figure 5.16:** Cross-section 1 and 2 of the specimen consolidated with a consolidation force of 900N

### Welding force

To determine the influence of the welding force, a welding trial was performed where all the welding parameters were kept the same except for the welding force which was changed. Additionally, an extra weld was performed with 300N and a longer vibration duration. The welding parameters of these welds are shown in table 5.4. The welding forces of 300N and 600N were chosen as a force lower than 300N will most likely be too low for the welding process work as it can lead to excessive hammering and insufficient frictional heating. If the force is higher than 600N, the welding machine is not able to initiate the ultrasonic vibrations.

Figure 5.17 shows the power curves of 17 welds with a welding force of 600N and 8 welds with a welding force of 300N, all with a vibration amplitude of $70\mu m$. These are all the welds performed with these two different welding forces and an amplitude of $70\mu m$. The figure clearly shows the welding force has an effect on the power curves. The welds with a welding

| Name | Specimen ID | $F_w$ | $A_{vibr}$ | $F_c$ | Vibration duration |
|---|---|---|---|---|---|
| WF-300N-3.5sec | 3.5.3 | 300N | $70\mu m$ | 600N | 3.5 sec |
| WF-600N-3.5sec | 3.5.4 | 600N | $70\mu m$ | 600N | 3.5 sec |
| WF-300N-4.25sec | 3.5.5 | 300N | $70\mu m$ | 600N | 4.25 sec |

**Table 5.4:** Set of welding parameters used to determine the influence of welding force

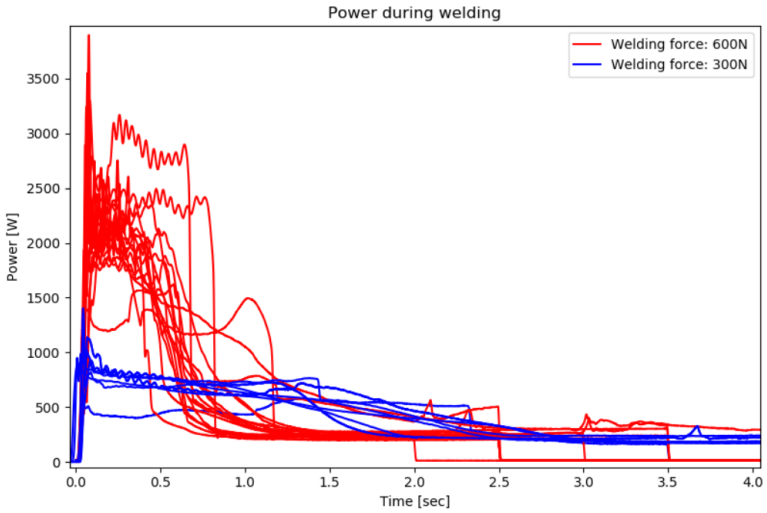


**Figure 5.17:** Power curves of specimens welded with a welding force of 300N and 600N. All welds high a vibration amplitude of $70\mu m$.

force of 600N have a higher peak power at the beginning of the weld and a higher power at the following power plateau. It also has a shorter power plateau and a steeper drop in power compared to the welds with a welding force of 300N. This results in the fact that the welds with a welding force of 600N reach the final state, where the power remains constant, quicker.

Figure 5.18 and 5.19 show cross-sections of two welds with a duration of 3.5 seconds, amplitude of $70\mu m$ and consolidation force of 600N. However, one has a welding force of 300N and the other 600N. The first cross-section of the weld with a welding force of 300N, see figure 5.18, shows some signs of melting. On the right side, there is a little waviness in the plies and in the same area few delaminations are present. Additionally, the indent is not completely removed. The second cross-section does not show any signs of melting. The first cross-section of the weld with a welding force of 600N, see figure 5.19, shows clear signs of melting. There is an area with waviness of plies and voids. Few delaminations are present in the middle of the cross-section. Additionally, the indent is removed. The second cross-section has similar signs. On the left side of the cross-section, an area with waviness of plies and voids is present.

Figure 5.20 shows the cross-section of a specimen welded with a welding force of 300N, amplitude of $70\mu m$, consolidation force of 600N and a duration of 4.25 seconds. Due to the longer duration compared to the 3.5 second welded specimen, melting has happened. Looking closer at the delaminations in this cross-section, some of the delaminations show partially re-consolidated areas, see figure 5.21. These partially re-consolidated delaminations are not seen in any of the welded specimens that are welded with a welding force of 600N and amplitude of $70\mu m$.

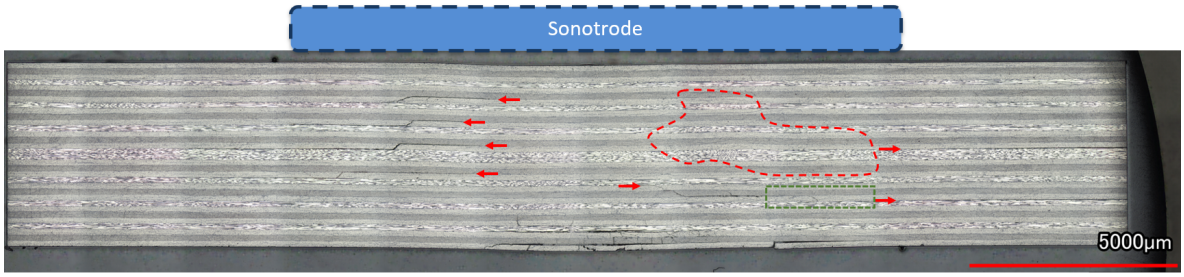


(a) Cross-section 1

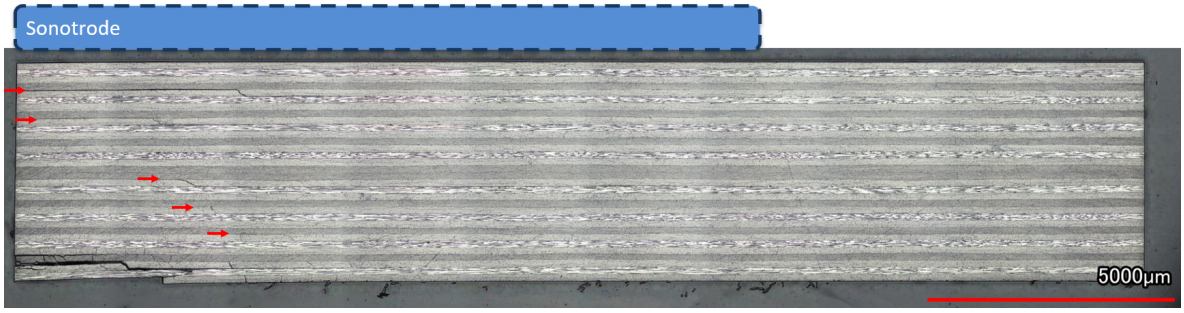


(b) Cross-section 2

**Figure 5.18:** Cross-section 1 and 2 of specimen WF-300N-3.5sec. Red arrows indicate the beginning of a delamination which continues in the direction of the arrow. Red dashed lines indicate areas with waviness of plies, indicating melting. Green dashed lines indicate an area where the delamination re-consolidated, creating two separate delaminations.

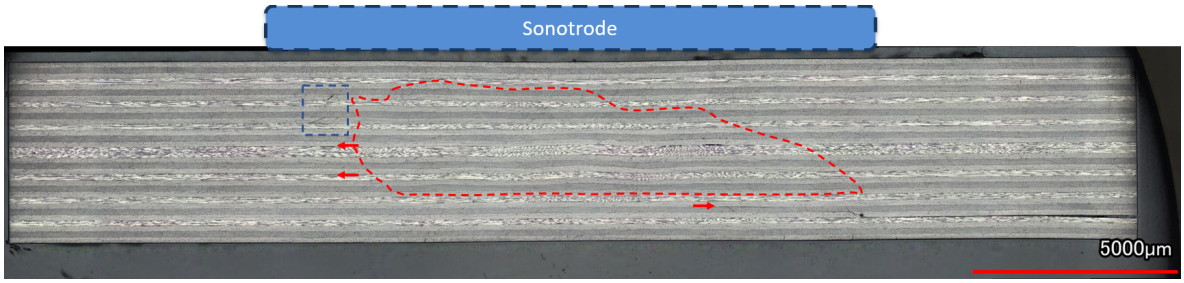


(a) Cross-section 1

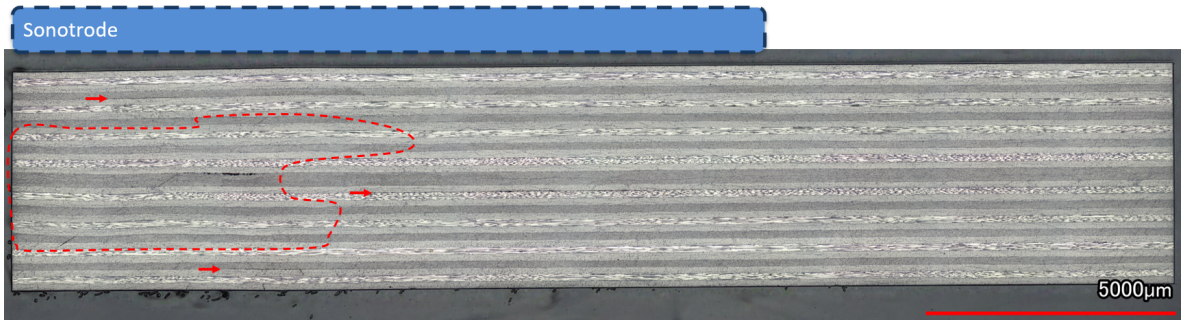


(b) Cross-section 2

**Figure 5.19:** Cross-section 1 and 2 of specimen WF-600N-3.5sec. Red arrows indicate the beginning of a delamination which continues in the direction of the arrow. Red dashed lines indicate areas with waviness of plies, indicating melting.

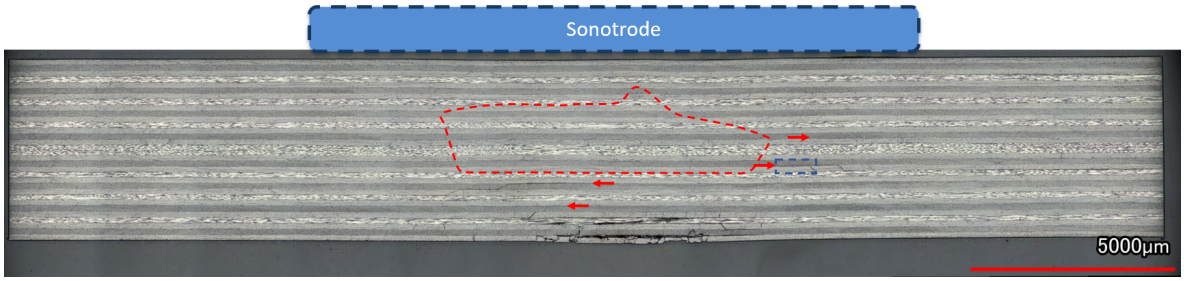


**(a)** Cross-section 1

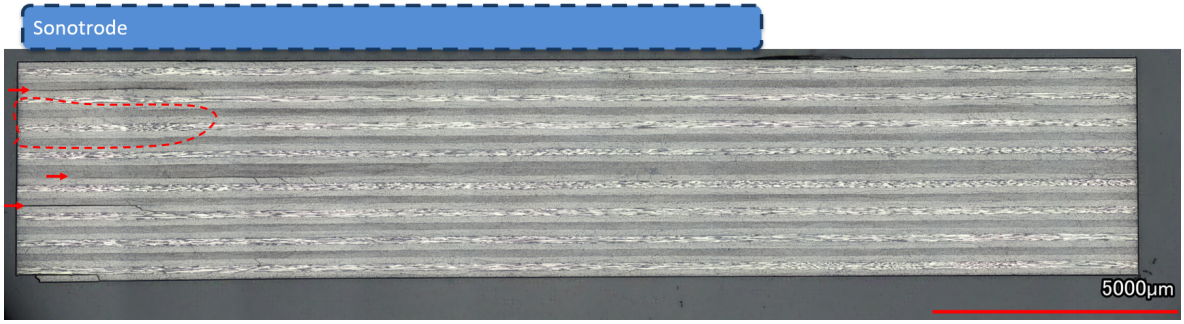


**(b)** Cross-section 2

**Figure 5.20:** Cross-section 1 and 2 of specimen WF-300N-4.25sec. Red arrows indicate the beginning of a delamination which continues in the direction of the arrow. Red dashed lines indicate areas with waviness of plies, indicating melting. Blue dashed lines indicate the area of the close-up, shown in figure 5.21.

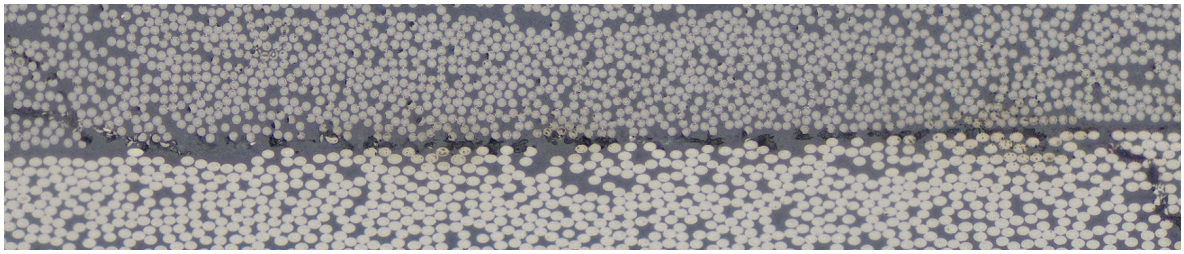

**Figure 5.21:** Close-up of a delamination that is partially re-consolidated. The location of this close-up is shown in figure 5.20.

Figures 5.22 and 5.23 show the C-scans of both specimens, welded with a welding force of 300N/600N, amplitude of 70$\mu m$, consolidation force of 600N and duration of 3.5 seconds, before and after welding. Looking at figure 5.22, little of the damaged area has changed. Looking at the total area encapsulated by the outer perimeter of the damaged area, this area increased by 1.7% after welding.
Looking at figure 5.23, the damaged area clearly changed after welding. The undamaged cone, which can be seen before welding, increased in size after welding. The outer shape of the damaged area shows changes, especially the lower left side of the damaged area. The total area encapsulated by the outer perimeter of the damaged area increased by 9.7% after welding. This indicates that the delaminations, on the outer edge of the damaged area, grew to the outside.

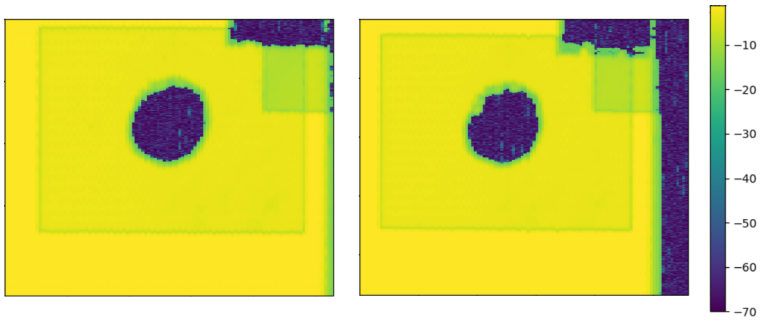


**Figure 5.22:** C-scans of specimen WF-300N-3.5sec. Left: before welding. Right: after welding

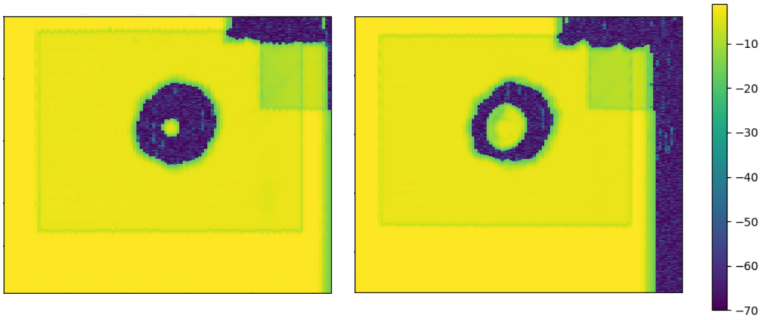


**Figure 5.23:** C-scans of specimen WF-600N-3.5sec. Left: before welding. Right: after welding

### Vibration amplitude

To determine the influence of the vibration amplitude, a welding trial was performed where the vibration amplitude was lowered to $40\mu m$. Welds were performed with a welding force of 300N and 600N. The welding parameters of these welds are shown in table 5.5.

| Name | Specimen ID | $F_w$ | $A_{vibr}$ | $F_c$ | Vibration duration |
|---|---|---|---|---|---|
| AMP-300N-10sec | 3.5.1 | 300N | $40\mu m$ | 600N | 10 sec |
| AMP-600N-10sec | 3.5.2 | 600N | $40\mu m$ | 600N | 10 sec |
| AMP-600N-16sec | 3.3.1 | 600N | $40\mu m$ | 600N | 16 sec |

**Table 5.5:** Set of welding parameters used to determine the influence of vibration amplitude

Figure 5.24 shows that, for welds with a welding force of 300N and 600N and an amplitude of $70\mu m$, the power curve has a higher power peak and plateau at the beginning of the weld compared to the welds with the same welding force and an amplitude of $40\mu m$. Furthermore, the plateau is shorter and the power drop after the plateau is steeper. For both welds with a welding force of 300N, the constant power and the end of the weld seems to be the same. For the 600N welds, the weld with an amplitude of $70\mu m$ seems to have a higher constant power.

Figures 5.25, 5.26 and 5.27 show the cross-sections of specimens welded with an amplitude of $40\mu m$. For all three specimens, only cross-section 1 is shown as, for all specimens, cross-section 2 does not show any noteworthy differences compared to the baseline damage.

Figure 5.25 shows the cross-section of a specimen welded with a welding force of 300N and an amplitude of $40\mu m$. Although there are no clear signs of melting and the indent is not

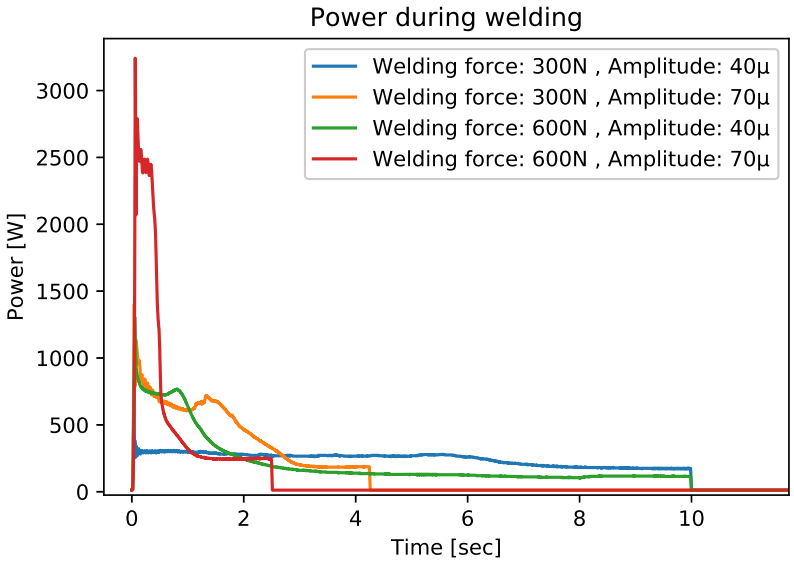


**Figure 5.24:** Power curves of welded specimens that show the difference between welds with an amplitude of 40$\mu m$ and 70$\mu m$ for welding forces of 300N and 600N.

completely reduced, it is interesting that the right side of the cross-section only contains one small delamination. The left side only shows two delaminations of which one seems partially re-consolidated as this delamination is discontinued by a section of re-consolidated material, see figure 5.25. One of the delaminations on the left side seems to extent into the, normally undamaged, cone.

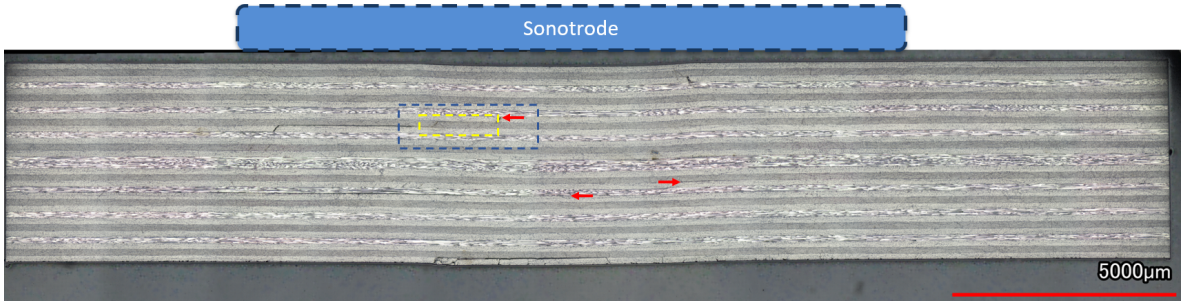


**(a)** Cross-section 1

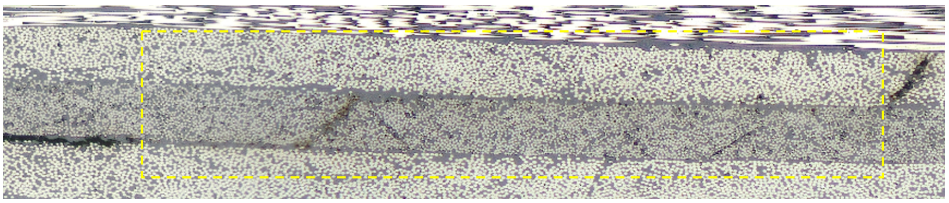

**(b)** Close-up

**Figure 5.25:** Cross-section 1 of specimen AMP-300N-10sec. Red arrows indicate the beginning of a delamination which continues in the direction of the arrow. Yellow dashed lines indicate the area of the delamination which re-consolidated, also shown in the close-up.

Looking at the specimens welded with a welding force of 600N, see figures 5.26 and 5.27, both show a reduction of the indent, although it is not completely eliminated. Both specimens show no clear signs of melting, but do show some delaminations that seem to be partially re-consolidated. An example of such a delamination is shown in figure 5.27. Interestingly, the specimen that was welded for 16 seconds shows a delamination present inside the, normally undamaged, cone.

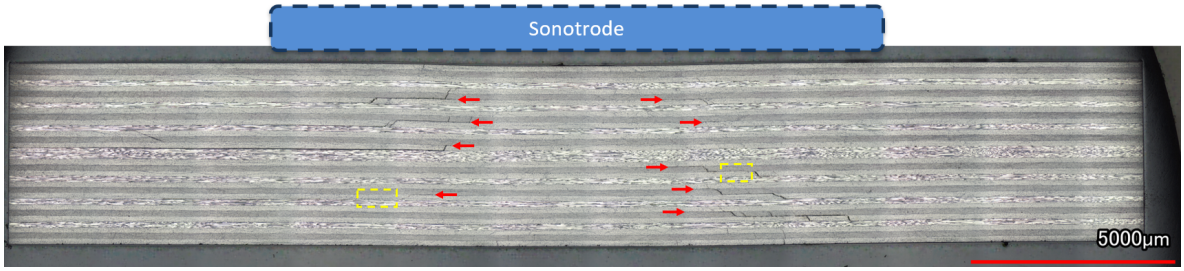


**Figure 5.26:** Cross-section 1 of specimen AMP-600N-10sec. Red arrows indicate the beginning of a delamination which continues in the direction of the arrow. Yellow dashed lines indicate areas of the delamination which re-consolidated.

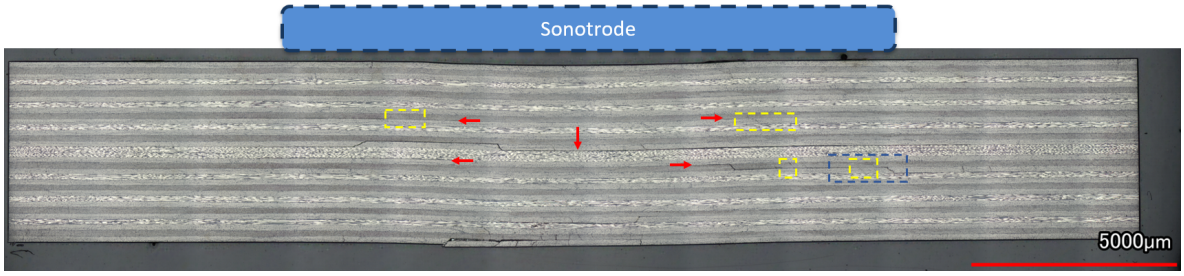


**(a)** Cross-section 1

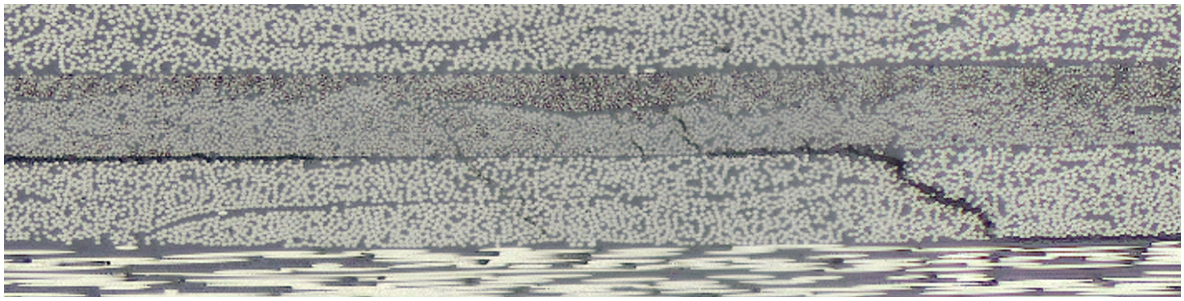

**(b)** Close-up of cross-section 1, showing a partially re-consolidated delamination.

**Figure 5.27:** Cross-section 1 of specimen AMP-600N-16sec. Red arrows indicate the beginning of a delamination which continues in the direction of the arrow (vertical arrow indicates delamination that runs through the undamaged cone). Yellow dashed lines indicate areas of the delamination which re-consolidated. Blue dashed lines indicate the area of the close-up.

Figure 5.28 shows a C-scan of the specimen welded with a welding force of 300N and an amplitude of $40\mu m$. The C-scan shows that the undamaged cone is changed in location and shape which coincides with the observation that a delamination grew into the undamaged cone. Also, the edge of the damaged area is slightly altered. An increase of the total area

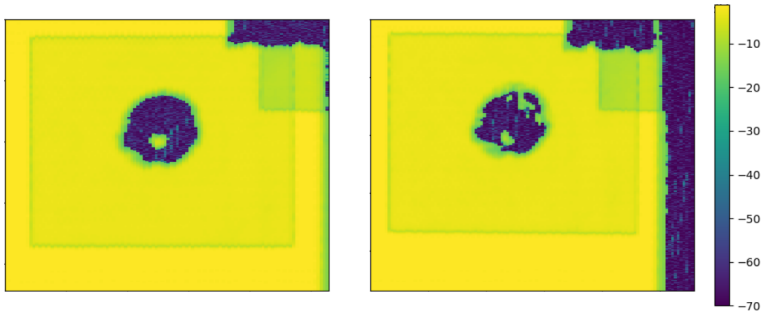


**Figure 5.28:** C-scan of specimen AMP-300N-10sec. Left: before welding. Right: after welding.

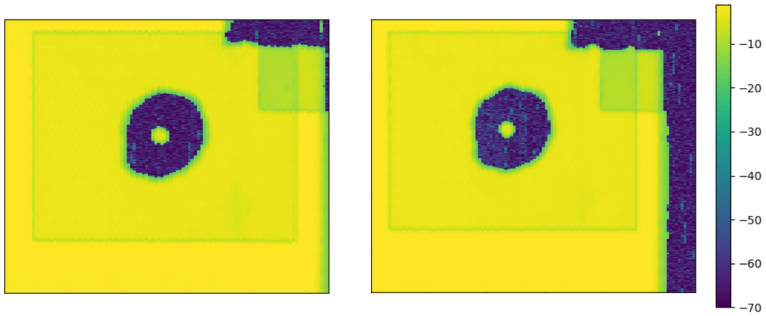


**Figure 5.29:** C-scan of specimen AMP-600N-10sec. Left: before welding. Right: after welding.

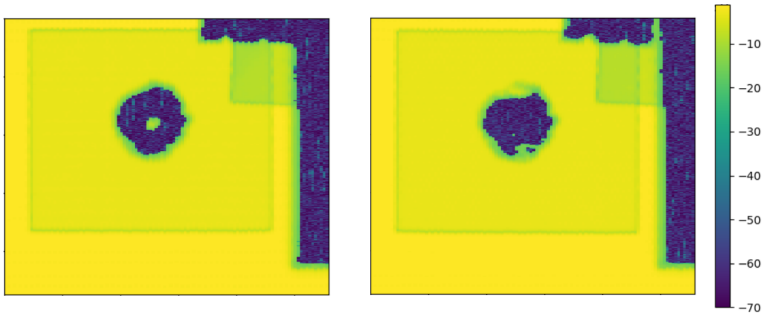


**Figure 5.30:** C-scan of specimen AMP-600N-16sec. Left: before welding. Right: after welding.

encapsulated by the outer perimeter of the damaged area indicates delamination growth at the outer edge of the damaged area. For the specimen shown in figure 5.28, this is less than 1% which, taking into account possible measurement uncertainty, is considered negligible. Therefore, it is believed that no delamination growth occurred at the outer edge of the damaged area. Finally, at the top right of the damaged area, near the edge, some spots have appeared in an arbitrary fashion.
Figure 5.29 shows a C-scan of the specimen welded with a welding force of 600N, an amplitude of $40\mu m$ and a duration of 10 seconds. The C-scan shows little changes to the damaged area. The undamaged cone is unaltered. Only the outer edge of the damaged area shows minor changes. The total area encapsulated by the outer perimeter of the damaged area increased with 1.1%, indicating marginal delaminations growth at the outer edge of the damaged area.

Figure 5.30 shows a C-scan of the specimen welded with a welding force of 600N, an amplitude of $40\mu m$ and a duration of 16 seconds. The C-scan shows that, after welding, the undamaged cone has completely disappeared, which coincides with the observations from figure 5.27. The outer edge of the damaged area shows that, at the top and bottom, same changes have occurred. The total area encapsulated by the outer perimeter of the damaged area changed with less than 1% which is considered negligible. Therefore, it is believed that no delaminations growth occurred at the outer edge of the damaged area.

#### Additional remarks

This section will elaborate on additional remarks and observations obtained during the welding trial. These will be summed up in an arbitrary order.

During the welding trial, it was observed that for welding forces higher than 600N, and in some cases equal to 600N, the welding machine was not capable of initiating an ultrasonic vibration. Therefore, it is considered not possible to use welding forces higher than 600N with this welding machine and sonotrode. For this reason, higher welding forces were not considered during this research project. However, it was found out that, in case the machine was not able to initiate an ultrasonic vibration when the welding force was 600N, it is possible to initiate vibrations by using a two phase weld. Here, the first phase has a welding force of 300N and the second phase a welding force of 600N. By reducing the duration of the first phase to 0.05 seconds, this results in the ultrasonic vibration being initiated with a welding force of 300N and immediately being increased up to 600N. With this particular welding machine this increase happens almost instantaneous (less than 0.07 seconds). However, for researching practices, this method is considered unpractical as doing this can have an unknown effect on the welding process. Additionally, as mentioned before, changing the welding force during the welding process will have an effect on the displacement data, making the displacement data unusable.

Analyzing the welding data, which is obtained with the external data acquisition unit, it shows that, for all welds, the sonotrode displacement is never negative, hence upwards (zero displacement being the sonotrode position at the beginning of the vibration phase with the welding force already applied). Investigation shows that the external data acquisition unit is unable to record negative sonotrode displacements and records all negative displacements as zero displacement. This means that, when a displacement curve shows zero displacement, it is either indeed zero or any amount of negative displacement. Unfortunately, it is not possible to determine this afterwards and therefore these segments of the displacement curve are indecisive and cannot be used. Although the internal data acquisition unit of the welding machine overwrites itself after 16 seconds, it does save the sonotrode position at the beginning and end of the vibration phase. Using this, the relative sonotrode displacement at the end of the vibration phase can be determined. This shows that almost all welds have a negative sonotrode displacement at the end of the welding phase, confirming the zero displacement readings of the external data acquisition unit, at the end of the vibration phase, are incorrect.

Investigation of the specimens containing degraded material shows that, for all such specimens, at some point during the last section where the power curve is constant, a spike is present, see figure 5.31. This type of spike is not seen in any of the other specimens which do not contain degraded areas. The cause of this spike in power has not been determined. A

possible explanation is that, at the moment of this spike, the material degrades and produces gasses which expand the material. This causes a momentary higher force on the sonotrode which causes a power spike as welding force and welding power are related.

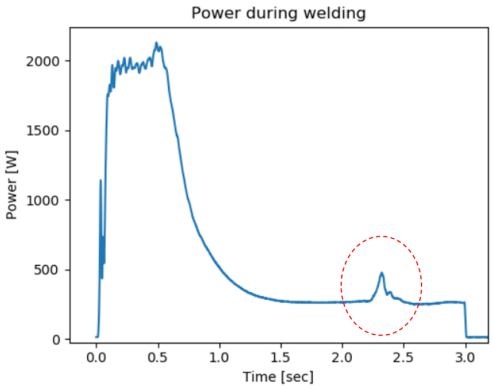


**Figure 5.31:** Power curve of a specimen containing degraded material

### 5.1.3 Final repairs

This section shows the results of the repairs of the impacted specimens that will be used for the compression after impact tests. The welding parameters that are used for the repairs are listed below, see table 5.6. These welding parameters were chosen as these resulted in the largest re-consolidated area, which is expected to have a positive influence on the CAI strength. Before the welding settings were finalized, a sequence of welds was performed with these welding settings but with varying durations. The aim was to find a suitable duration that will ensure re-consolidation of the damaged area but minimize the chance of degradation of the material, resulting in a duration of 2.5 seconds. The results of this sequence can be found in appendix B. All 9 specimens are repaired using the same welding parameters. However, the last 4 specimens are clamped slightly different. The first 5 specimens were clamped with a distance of approximately 31mm (called clamping A from here on) between the clamp and the sonotrode. For the last 4 specimens, this distance was 22mm (called clamping B from here on). Clamping B has the same clamping distance as used for all specimens during the welding trials. Clamping A was used because with this clamping distance, like during the welding trails, the clamps were located near the edges of the specimen. After evaluating the results of the first five repairs using clamping A, it was observed that there was a clear difference with respect to the results obtained during the welding trail. Therefore, as the main difference was the clamping distance, it was decided to change to clamping B where the clamping distance is the same as used during the welding trails. Because the specimens are used for CAI testing, there is no cross-sectional microscopy data. The welding and C-scan data are shown below.

| Welding force | Amplitude | Consolidation force | Vibration duration | Consolidation Duration |
|---|---|---|---|---|
| 600N | $70\mu m$ | 600N | 2.5 sec | 60 sec |

**Table 5.6:** Set of welding parameters used to repair the damaged specimens for CAI testing

Figure 5.32 shows all the power curves of the repaired specimens. As the only difference between all specimens is the different in clamping, two colors are used to indicate the different

specimens with different clamping. The figure shows a clear difference between the specimens with different clamping. Clamping A specimens behave similar to each other, an initial power plateau and a power drop at around 0.5 seconds. Clamping B specimens not only differ from the clamping A specimens but also from themselves. Two curves show an initial power plateau, followed by an almost vertical drop, after which they remain constant. The other two curves are different from the curves usually observed. One shows a steady decrease till the end. The other starts with a power plateau, followed by a step-wise decrease, after which it remains constant till the end.

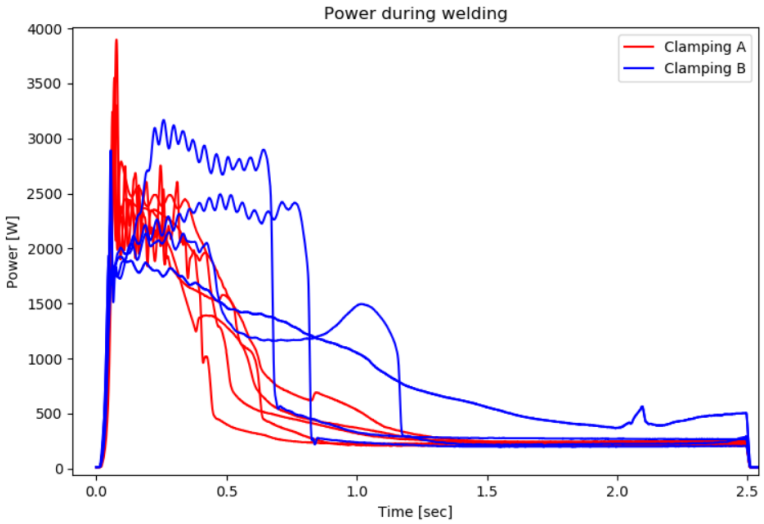


**Figure 5.32:** Power curves of specimens welded with the welding parameters stated in table 5.6, using clamping A and clamping B.

Table 5.7 shows the welding energies for all the repaired specimens that will be used for CAI testing. The table shows that the five specimens with clamping A have a welding energy between 1348J and 1825J and the four specimens with clamping B have a welding energy between 2062J and 2280J. It can clearly be observed that the welding energies for specimens with clamping B are higher than those for specimens with clamping A.

| Specimen ID | Clamping | Welding energy [J] |
|---|---|---|
| 1.6 | A | 1546 |
| 1.8 | A | 1481 |
| 1.11 | A | 1825 |
| 2.3 | A | 1348 |
| 2.5 | A | 1652 |
| 2.1 | B | 2280 |
| 2.4 | B | 2062 |
| 2.6 | B | 2263 |
| 1.10 | B | 2119 |

**Table 5.7:** Welding energies for all the repaired specimens that will be used for CAI testing

Figures 5.33 and 5.34 show the C-scan data for all repaired specimens. The five specimens with clamping A all show areas where material is re-consolidated. After the repair, three specimens show a single re-consolidated spot near the middle of the specimen. The two other specimens show multiple re-consolidated spots and their undamaged cones have (partially) disappeared. The four specimens with clamping B all show some re-consolidated areas. However, two show a re-consolidated spot near the middle of the damaged area at the location where the undamaged cone was located. The other two specimens show two re-consolidated spots. Further investigation, after the CAI tests, shows that these two specimens contain degraded material. It should be noted that, for all repaired specimens, not the entire damaged area has re-consolidated. Also, the total area encapsulated by the outer perimeter of the damaged area increased between 3.9% and 9.9%, depending on the specimen.

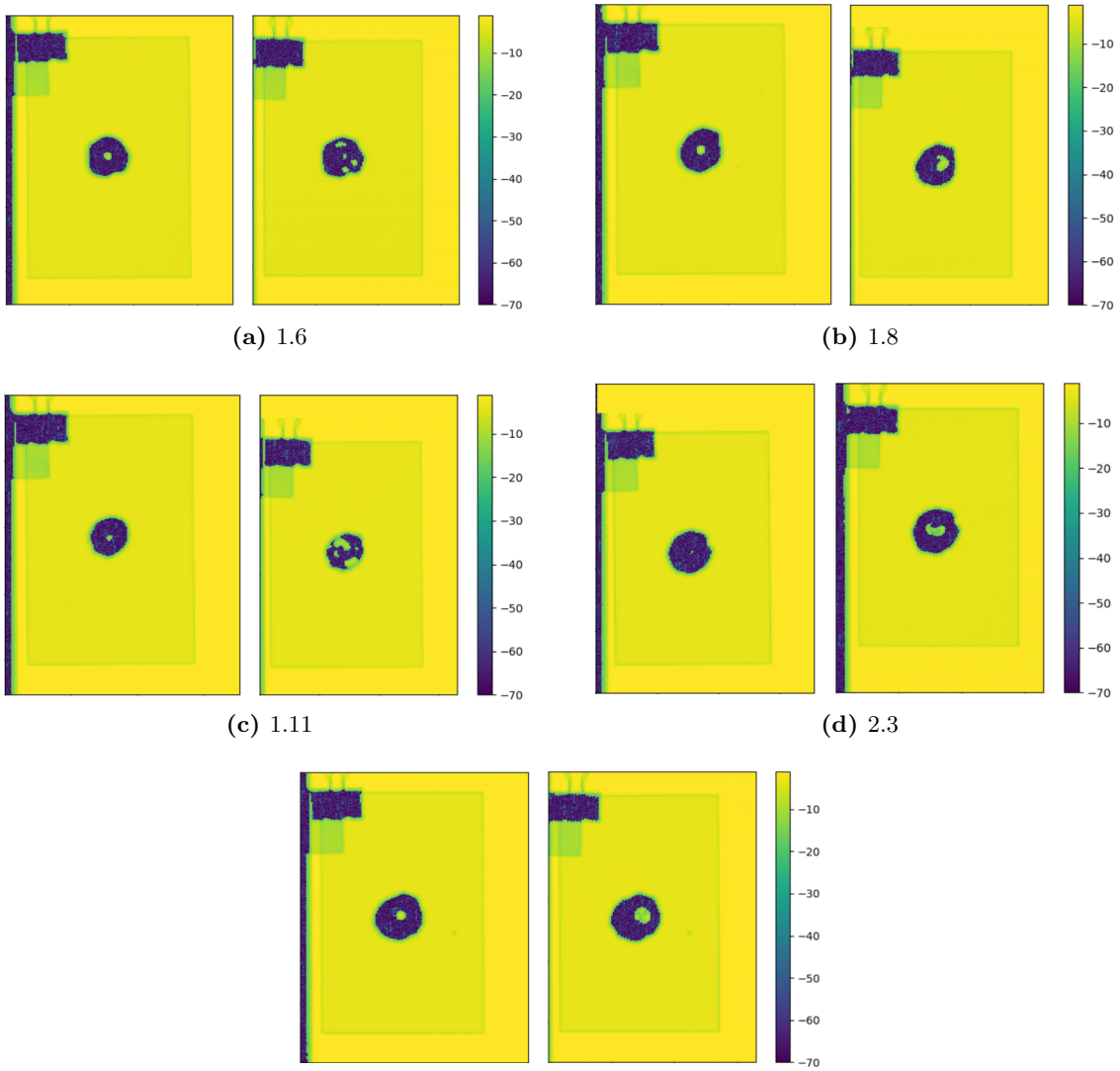


**(a)** 1.6 **(b)** 1.8

**(c)** 1.11 **(d)** 2.3

**(e)** 2.5

**Figure 5.33:** C-scans of all repaired specimens with clamping A. Left: before welding. Right: after welding.

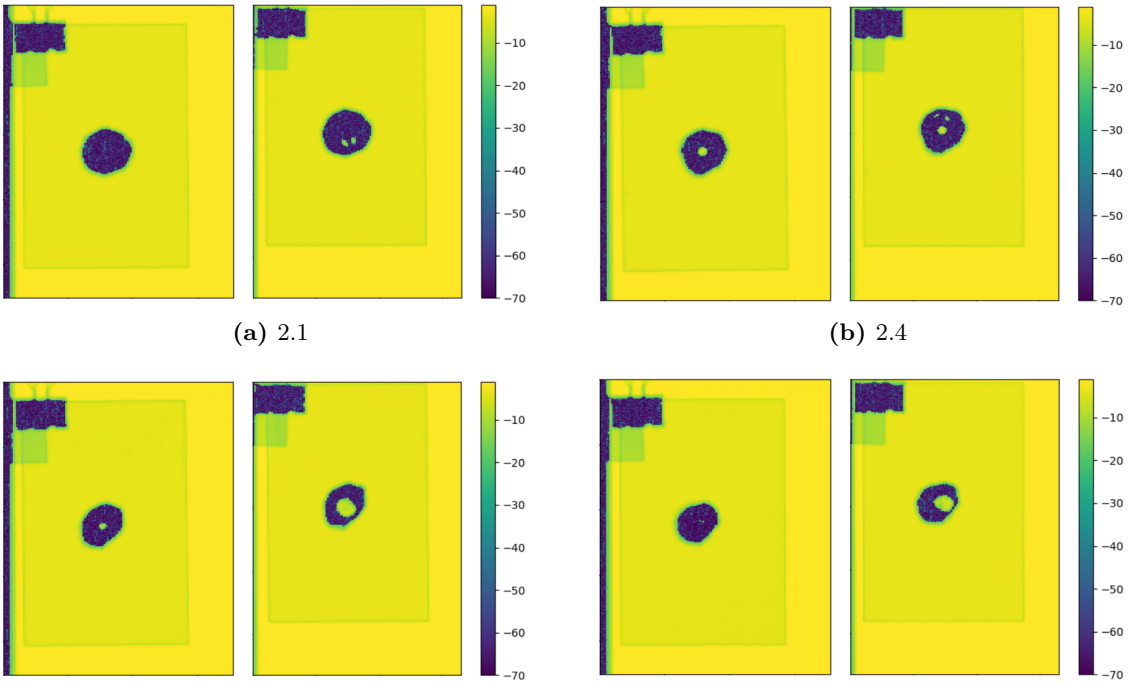


**(a)** 2.1 **(b)** 2.4

**(c)** 2.6 **(d)** 1.10

**Figure 5.34:** C-scans of all repaired specimens with clamping B. Left: before welding. Right: after welding.

## 5.2 Discussion

### 5.2.1 Characterising heating in damaged composites

As mentioned in section 2.3, for ultrasonic welding, there are two heating mechanisms, which are frictional heating and viscoelastic heating [49]. Generally, it is believed that frictional heating is responsible for heating up to the Tg, after which viscoelastic heating becomes the dominant heating mechanism. In case of the undamaged specimens, it is expected that frictional heating is located between the sonotrode and the specimen. This is the case as this is the only location where relative movement could be present during the welding process (A second location could be between the specimen and the base plate. However, due to the clamping of the specimen and the relatively large contact area compared to the area of the sonotrode, this is assumed to be negligibly small compared to the frictional heating between the sonotrode and the specimen). Viscoelastic heating happens due to introduction of mechanical vibrations when the material is above Tg and therefore is assumed that it could be present throughout the whole thickness of the specimen, at locations where the material is above Tg, in area of the specimen under the sonotrode. Looking at the temperature data of the undamaged specimens, see figure 5.3, it shows that all specimens have a surface temperature below the Tg (143°C), except for the specimen which was welded for 16 seconds which has a higher temperature (160+°C). This means that for all specimens, except for the one which was welded for 16 seconds, most likely only frictional heating happened at the surface of the

specimen. As, for these specimens, the temperature of the surface decreased immediately, it is likely that the inside of the specimen did not have a higher temperature, as this would have increased the temperature of the surface of the material due to heat dissipation. As the inside of the specimens has not reached a temperature above the Tg, no viscoelastic heating is expected to have happened. As, for these specimens, this means that the entire specimen remained below Tg, it is expected that none of the material has changed inside the specimen after the welding procedure. This is confirmed by the cross-section shown in figure 5.5, which shows no differences compared to a pristine laminate. From literature it is known that the power and displacement curve can be used to indicate certain stages of the welding process [8], hence changes inside the welded material. Looking at the power and displacement curves of all the undamaged specimens, except for the specimen which was welded for 16 seconds, the power and displacement remains almost constant, indicating little material changes inside the specimen. This coincides with the statement that the entire specimen remained below Tg and that little changes can be found in the cross-sections.
Figure 5.3 shows the temperature data of the specimen which was welded for 16 seconds, it can be observed that the surface of the specimen was at least 160°C after the vibration phase. This means that the temperature was above Tg and it is likely that viscoelastic heating has happened at the surface. Although the actual temperature after welding cannot be determined, looking at the decaying section of the temperature curve, it is expected that the temperature could have been in the same range as the damaged specimens, also shown in figure 5.3. Looking at figure 5.6, which shows the cross-section of the specimen which was welded for 16 seconds, it shows the upper five plies contain voids and heat induced delaminations. Below these plies, there is an area that contains some waviness of the plies. This indicates melting has happened, meaning the temperature must have reached at least Tm (343°C). The large difference in temperature between the specimen which was welded for 16 seconds and the other specimens is believed to be caused by viscoelastic heating, which started when the surface reached temperatures above Tg. As mentioned before, the power and displacement curves can indicate different stages of the welding process. As the specimen reached Tg and Tm, the material properties changed which would have had an effect on the power and displacement curves. Looking at the power curve of the specimen which was welded for 16 seconds, instead of being constant, the power curve changes after about 11 seconds. It increases slightly after which it drops down to around 280 Watt. At the same time, after around 11 seconds, the displacement starts to decrease. It is believed that, around 11 seconds, Tg was reached changing the material properties and therefore the power curve. As viscoelastic heating is faster than frictional heating, Tm is reached quickly, resulting in a drop in power as the material becomes fluid and the sonotrode requires less power to vibrate. It is believed that localized melting is already enough for the power to drop [8]. The decrease in displacement is believed to be caused by the build up of internal pressure due to the increasing temperatures, forming a bulge and pushing the sonotrode upwards, especially when temperatures reach Tm. For this reason, the steep decrease in displacement coincides with the beginning of the power drop. This is in contrary to what happens for lap joint welding, as with a lap joint there is less internal pressure building up as it can escape more easily and, due to the possibility for molten material to get squeezed out, there is an increase in sonotrode displacement. It is expected that, when welding undamaged material, due to the fact that under the sonotrode there are still areas with solid material and that material squeeze out is not possible inside the specimen, it is not possible for the sonotrode displacement to increase.

Looking at the temperature data of the damaged specimens, see figure 5.3, all surface temperatures are above Tg after the vibration phase ended, which means that viscoelastic heating has happened at the surface of the specimens. Interestingly, all temperatures increase after the vibration phase has ended, until they reach their highest temperature about 2-3 seconds later. As the vibrations, hence power input, has already ended, the only explanation for the increasing surface temperature is that the inside of the material has a higher temperature than the surface. Dissipation of the heat inside the specimen causes the surface to heat up. This means that the inside of the specimen had a higher temperature, after the vibration phase ended, than the peak temperature shown in figure 5.3. A higher temperature inside the specimen is an indication that heat is not only generated at the surface, hence fictional heating between the specimen and the sonotrode, but also inside the material due to the presence of damage inside the specimen. This could be explained by the fact that each delamination could act similar to the interface of a lap joint. Due to the vibrations, there is relative motion between the delaminated plies, causing frictional heating. After this frictional heating causes the material to reach Tg, viscoelastic heating causes the material to heat up further in this area. Interestingly, looking at figure 5.4, figure (b) shows the heat distribution from an undamaged specimen, showing a heated surface with the same shape as the sonotrode due to frictional heating. Figure (c) shows the heat distribution of a damaged specimen, which includes a circular shape with a higher temperature. This circle has the same shape as the delaminations surrounding the undamaged cone. As the circle has a diameter of roughly 12-15mm, it is confined within the contact area of the sonotrode. The difference between the center of the heated area and the circle surrounding it is 57°C. This indicates that heat is likely to be generated inside the delaminations. This would be beneficial as, ideally, only the delaminations are heated, so they can re-consolidate, hence be repaired, without the surrounding area being affected.
The cross-sections of the damaged specimens confirm that heat is generated inside the specimens, more specifically inside the damaged area. Looking at the second cross-section of figure 5.11, the middle of the specimens shows an area of degraded material. This indicates that the middle of the specimen reached the highest temperature, showing that heat was generated here. Looking at figures 5.12 and 5.13, it is noticed that the areas with voids coincide with the areas were delaminations are expected to be present due to the impact, confirming heat was generated inside the delaminations.

Looking at the power and displacement curves of the damaged specimens, it shows similarities with the curves of the undamaged specimens, especially the specimen which was welded for 16 seconds. As the power and displacement curves of the damaged specimens show similar trends as the undamaged specimen which was welded for 16 seconds, it is assumed that the same features of the curves indicate the same stages of the welding process. Which means the power plateau indicates the material is below Tg, the increase and following drop in power indicates the material reached Tg and heats up to Tm and after the the power drop the material remains molten. The main differences between the curves are the downward movement of the sonotrode for damaged specimens at the beginning of the vibration phase and the duration of the power plateau. The increase of displacement is believed to be caused by the elimination of the indentation as the specimen heats up and softens. The duration of the power plateau of the damaged specimens is around 1 second, compared to 11 seconds for undamaged specimens, which means the damaged specimens heat up to Tg faster. This large difference is believed to be one of the reasons why the damaged specimens show higher temperatures in figure

5.3, even for shorter vibration durations. There are three possible explanations why the damaged specimens reach Tg faster. Firstly, because there are multiple delaminations present throughout the thickness, fictional heat is generated in multiple interfaces, speeding up the heating process. Secondly, contrary to the sonotrode and the surface of the specimen, the surface of the delaminated plies is rough which could increase the heating rate of the frictional heating process. Thirdly, for undamaged specimens, the sonotrode could act as a heat sink which lowers the heating rate of frictional heating between the sonotrode and the surface of the specimen.

### 5.2.2 Influence of welding parameters

#### Duration

Section 5.2.1 already discusses the heating characteristics during the welding process of a damaged specimen, indicating that, more heat is generated when increasing the vibration duration. However, during the welding trials, it is discovered that heating can vary between different welds. From the power and displacement curves shown in figure 5.2, it can be seen that, although the curves show similar trends, they do vary with time. For these five welds, it takes between approximately 1.5 and 3.25 seconds for the power curve to initiate the drop to the final constant value, hence for the specimen to start melting locally. This means that, between the different welds, there is variation in the time it takes for the material to reach Tm. Looking at the cross-sections of specimens welded for 5, 7.5 and 10 seconds, see figures 5.11 to 5.13, only the specimen which was welded for 5 seconds reached high enough temperatures for the material to degrade, even though the other specimens had a longer vibration duration and likely more generated heat. It must be noted that, reaching the highest temperature at a certain location and having the highest amount of heat energy are two separate things. If a certain amount of heat is generated inside a small volume, this volume reaches a certain temperature. If the same amount of heat is generated evenly inside a large volume, the temperature reached inside this volume will be lower than the temperature reached inside the small volume. This means that, when a certain amount of heat is generated unevenly inside the damaged area, higher temperatures can be reached compared to when this amount of heat is generated evenly over the damaged area. Therefore, it is possible that uneven heat generation inside the specimen welded for 5 seconds caused the material to locally reach temperatures high enough for the material to degrade. While more even heat generation inside the specimens welded for 7.5 and 10 seconds caused the material not to reach high enough temperatures for the material to degrade, even when the total amount of heat generated during the welding process was likely higher.

Figure 5.2 shows that the displacement curve also decreased with time after the drop of power is initiated. Like temperature, the rate at which this decreases also varies for the different welds, hence the time it takes for a certain displacement to be reached varies.

#### Consolidation force

Looking at the cross-section in figure 5.14, it shows that using a 300N consolidation force is not sufficient to compress the material which was expanded at the end of the vibration

phase. Compared to the specimen that did not have a consolidation phase, see figure 5.11, the consolidation force of 300N is able to flatten the bulge that is caused by the expanding degrading area. However, it is not able to completely eliminate this expansion. As a result, the area containing degraded material remains expanded and full of large voids as the material cools down and re-consolidates. Due to the still expanded area, the material above this area remains lifted and causes the plies to kink at the edge of the flatted bulge. Also, the delamination halfway through the thickness, that grew into the undamaged cone as the degraded material expanded during the welding phase, has not been able to close and remains present after consolidation.
Looking at the cross-sections in figures 5.15 and 5.16, it shows that both a consolidation force of 600N and 900N will produce similar results. Compared to a consolidation force of 300N, both are able to eliminate the expanded material. As a result, there is no bulge present, no kinked plies and the degraded area is not full of voids. Both specimens show no delamination through the undamaged cone, however, they do still show voids in this region but these are believed to be caused by the large amount of heat due to the long vibration durations.
Due to the long vibration durations that cause the material inside the damaged area to degrade, it is assumed that these welding settings produce higher internal pressures inside the damaged material than welding settings suitable for repairing specimens. These higher internal pressures are the result of the expansion of material due to the high temperatures and the possible build up of gasses produced by the degrading material. Therefore, as a consolidation force of 600N and 900N is able to eliminate any expansion of material caused by these pressures, both consolidation forces are considered suitable for the welding settings that will be used for repairing damaged specimens.
Although both consolidation forces are considered suitable, both forces have their own advantages and disadvantages. Using 900N will most likely make the consolidation phase more robust as it is able to cope with higher internal pressures in case they do occur. However, from a practical aspect a force of 600N is more beneficial. When using a welding force of 600N, the welding force and the consolidation force match, as mentioned before, this will make sure the displacement data will not be compromised during the consolidation phase which might contain useful information. Also, considering this is a repair technique, lower forces on the sonotrode will enable the machine to be lighter which is beneficial for practical applications.

### Welding force

The power curves in figure 5.17 show a clear difference between a welding force of 300N and 600N. Using a welding force of 600N, compared to using 300N, the initial power plateau is higher and shorter, the power drop following the power plateau is steeper. As mentioned before, it is believed that the power drop indicates melting of the material, therefore, using a higher welding force reduces the time it takes for the material to reach Tm. Looking at the cross-sections in figures 5.18 and 5.19, it can be seen that, although the duration of both welds was the same, the weld with a welding force of 600N has a larger heat affected area, indicating that more heat was generated. Similarly, this can be observed when looking at the C-scan data of these specimens, see figures 5.22 and 5.23. Here, the weld with a welding force of 600N shows a large re-consolidated area in the middle of the damaged area, while for a welding force of 300N few changes can be observed.

Interestingly, the cross-section in figure 5.20 shows delaminations that appear to be only partially re-consolidated. As this is not seen in any of the specimens welded with a welding force of 600N and similar amplitude of $70\mu m$, this is believed to be caused by the lower welding force. A possible explanation is that not all locations in the delamination are heating at the same rate, therefore some locations start to melt earlier than others. As the heating process for welding with a lower welding force is slower, it is possible that when the vibration phase is over, some delaminations are at an intermediate phase where the delamination is only partially re-consolidated. It is also possible that the same happens with a welding force of 600N, but because here the heating process is faster, this intermediate state between not re-consolidated and completely re-consolidated is less likely to be present when the vibration phase is over. This highlights that a higher welding force increases the heating rate. Another possibility is that an increased welding force results in a more even distribution of pressure inside the interfaces of the delaminations and a bigger intimate contact area. A more even pressure and bigger intimate contact area could result in more even distribution of frictional heating, viscoelastic heating and melting.

When decreasing the welding force, it will not only decrease the welding power which reduces the heating rate, but because the heating rate is reduced, it will also allow more heat dissipation which decreases the heating rate further. For this reason, for lower welding forces, higher welding energies are required for the material to reach Tm.

#### Vibration amplitude

Figure 5.24 shows that, for both a welding force of 300N and 600N, when the amplitude is decreased from $70\mu m$ to $40\mu m$, the power curves show a similar trend but with a lower and longer power plateau and less steep power drop. As mentioned before, it is believed that the power drop indicates melting of the material, therefore, using a lower amplitude increases the time it takes for the material to reach Tm.

Looking at the cross-sections in figures 5.26 and 5.25, specimens welded with an amplitude of $40\mu m$ show no eliminated indent, no voids, no heat induced delaminations and no degraded area. This indicates that lower temperatures were reached inside these specimens, hence lower heating rates. The cross-sections also show partially re-consolidated delaminations which, like for lower welding forces, are possibly caused by the lower heating rates.

As for the welding force, decreasing the amplitude will not only decrease the welding power which reduces the heating rate, but, because the heating rate is reduced, it will also allow more heat dissipation which decreases the heating rate further. For this reason, for lower amplitudes, higher welding energies are required for the material to reach Tm. The cross-sections in figures 5.19 and 5.30 are a good example of this. Although the welding energy of the specimen welded with an amplitude of $40\mu m$ (3391J) is 56% higher compared to the welding energy of the specimen welded with an amplitude of $70\mu m$ (2170J), the cross-section of the specimen welded with an amplitude of $70\mu m$ clearly shows that higher temperatures are generated inside this specimen.

### 5.2.3 Final repairs

Although the fact that two slightly different clamping distances are used is not ideal from a research perspective as it divides the welded specimens into two different subsets, it does show that clamping has a noticeable effect on the outcome of the welding process. As shown in section 5.1.3, the power curves, welding energies and C-scan data all show differences between the two groups of specimens. Although, at this point, it is not possible to determine the exact effect of the clamping distance and is out of the scope of this research project, it is important to notice the importance of consistent clamping when further researching this topic.

The welding setting used for the repairs was chosen as, during the welding trials, this resulted in a large re-consolidated spot in the middle of the damaged area, see figure 5.23. However, the welding sequence shown in appendix B shows that, when using these settings with a duration of 3.0 seconds, there is a possibility that the material degrades. Therefore, a shorter duration of 2.5 seconds was chosen as this duration already shows a large re-consolidated area and reduces the chance the material will degrade. Looking at the C-scan data of the resulting repairs, five specimens show such re-consolidated spots and two specimens show signs of degraded material which was confirmed after CAI testing. Additionally, two specimens show multiple randomly located spots. From the results of the nine repairs, it becomes evident that there is a noticeable variation between the repaired specimens. This confirms the need for a better method to control the welding process, for example, through closed-loop control using welding power or sonotrode displacement data as it is observed that this data is related to what happens inside the material during welding, or the need for different welding settings to ensure more consistent results.
However, the difference in clamping is believed to be one of the reasons why there is variation between the two subsets of repaired specimens. Looking at the welding energies, specimens welded with clamping A show lower welding energies (1348J - 1825J) compared to specimens welded with clamping B (2062J - 2280J). The difference in welding energy itself, together with the fact that a difference in boundary conditions can change the energy required for a successful spot weld [55], is believed to cause the difference in the degree of melting inside the specimens. It is believed that, for this reason, two specimens welded with clamping B have larger re-consolidated spots in the middle of the damaged area and two specimens have degraded material, indicating a higher degree of melting.
Besides differences between the specimens with different clamping distances, for the same clamping distance, also variations between specimens can be observed, especially when looking at the specimens welded with clamping B. When looking at figure 5.35, the two specimens with a re-consolidated spot show a higher and longer power plateau with an almost vertical power drop, while the two specimens with degraded material show a lower and shorter power plateau with a more gradual and step-like drop in power. Normally, the decrease of power is attributed to the progressive reduction in area of the solid material under the sonotrode [8]. The step-like shape decrease of the power curve is ascribed to localised melting and re-consolidation of the material as generated heat dissipates to the colder surrounding material [8]. More intimate contact, normally obtained with higher welding forces, increases the amount of initiations sites where melting occurs, which causes the power to drop continuously instead of in a step-like fashion [8]. This could explain the power curves of the four specimens, welded with clamping B, in figure 5.32. For the two specimens with a re-consolidated spot, a possible explanation for the longer power plateau and vertical drop is that, in these specimens, a more intimate

contact is present between the delaminations inside the damaged area. This causes a more even distribution of frictional heating, followed by viscoelastic heating, in a larger area, which takes more time than when this only happens locally. As a result of the even heating, the delaminations reach Tm almost at the same time, hence a large, almost instant, reduction on solid material under the sonotrode occurs. As the decrease of power is attributed to the reduction of solid material, this means the power makes a large, almost instant, drop. The result of heating the delaminations evenly is the large re-consolidated spot, showing a large area reached similar temperatures during the welding process. On the contrary, the two specimens with degraded material have a shorter power plateau and more gradual step-like drop in power. The shorter power plateau could be caused by uneven less intimate contact inside the delaminations which promotes uneven, hence local, heating. The uneven heating causes some areas to heat up faster and some to heat up slower, therefore, local melting will happen faster. As mentioned before, local melting is enough to decrease the power [8], therefore, the power plateau is shorter. The local melting is also responsible for the gradual step-like decrease of power [8]. The result of heating the delaminations unevenly is that some areas do not reach Tm, while, locally, areas can surpass Tm and even reach temperatures where degradation starts to occur. As degradation of material is not beneficial and is an irreversible process, this should be avoided, therefore, uneven heating should be avoided.
If a difference in intimate contact is responsible for uneven heating, because for all four welds the same clamping and welding settings are used, the difference must be caused by a difference in the specimens themselves. For example, the indent of a specimen can cause differences in the pressure distribution inside the damaged area, when the specimen is clamped and the welding force applied, resulting in uneven heating. It is expected that eliminating influences of factors like the indent will improve the consistency of the welding process. This can possibly be achieved by performing two welds instead of one, using two different sets of welding parameters. The purpose of the first weld is to (partially) eliminate the indentation. The purpose of the second weld is to re-consolidate the damaged area. The welding parameters of the first weld should consist of a short vibration duration in combination with a lower welding force or vibration amplitude (compared to the welding parameters used for re-consolidating the damaged area) as it is shown that these welding parameters can (partially) eliminate the indentation with no/little melting of the damaged material.

Looking at the final repairs as well as all other welded specimens, it can be observed that none of the welded specimens achieved full re-consolidation of the damaged area. One possible explanation is the fact that the sonotrode did not cover the entire damaged area. As the average area of a damaged specimen was around $700mm^2$ and the sonotrode has an area of $450mm^2$, this means that around 65% of the damaged area was covered. As discussed in section 5.2.2, the heating rate during the welding process is influenced by the welding force. Although it is expected that the welding force applied by the sonotrode will also provide some pressure, and some intimate contact, inside the material/delaminations surrounding the sonotrode, this will be lower than is the case inside the material/delaminations directly under the sonotrode. Therefore, the heating rate inside the material surrounding the sonotrode is also expected to be lower, resulting in lower temperatures. This means that, when the vibration phase is stopped at the moment the material under the sonotrode starts to melt, it is likely that the material surrounding the sonotrode did not reach Tm and did not re-consolidate. Looking at the C-scan of the largest achieved re-consolidated area, see figure 5.36, it shows that the re-consolidated area did not become wider than the sonotrode. If melting would have hap-

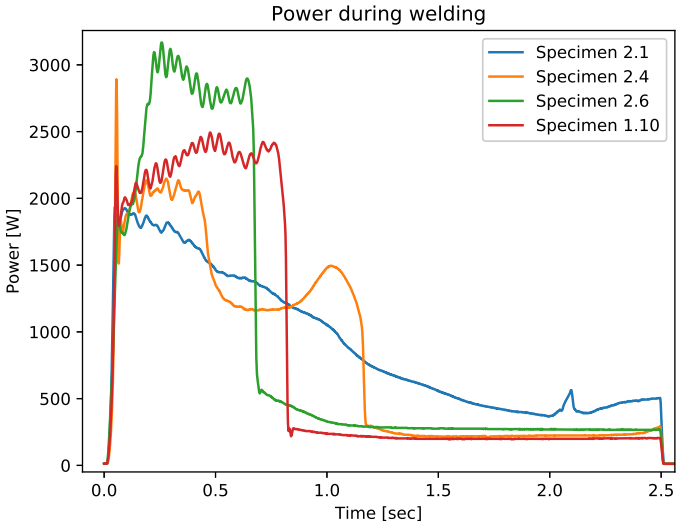


**Figure 5.35:** Power curves of specimens welded with clamping B

pened inside the surrounding material, due to the lack of a sufficient consolidation pressure, it is likely that voids and heat induced delaminations would have formed which cannot be distinguished from impact induced damage inside the C-scan image. However, figure 5.19 confirms that melting only happened inside the material directly under the sonotrode and excludes the possibility that melting happened inside the material surrounding the sonotrode as no signs of melting such as voids are observed in this area. The situation were melting only happens directly under the sonotrode would be ideal as it is likely that only directly under the sonotrode sufficient consolidation pressures can be achieved to ensure proper material quality without the use of additional consolidators.

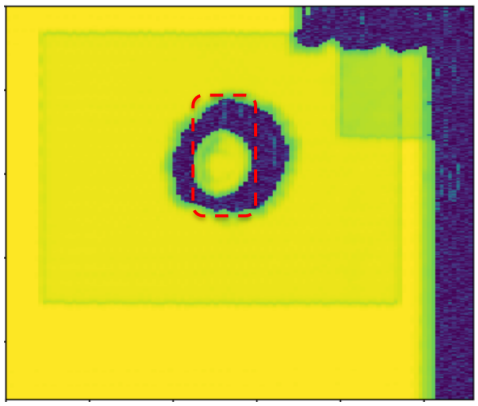

**Figure 5.36:** C-scan of specimen WF-600N-3.5sec, the specimen with the largest achieved re-consolidated area. The red rectangle represents the location and size of the sonotrode during welding.

Another possible explanation on why melting only happens directly under the sonotrode is related to the damage characteristics of the damaged area. Figure 5.37 shows the baseline damage were the delaminations are highlighted with red lines. It can be observed that most of the delaminations are located inside the material directly under the sonotrode. Therefore, it is expected that most of the heat is generated in this location and this area melts before the surrounding areas. This would also explain why the re-consolidated area in figure 5.36 is still circular while the area covered by the sonotrode is rectangular.

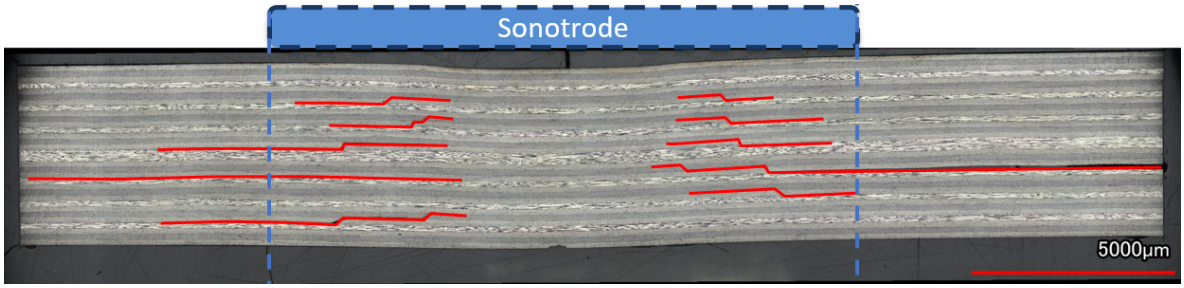


**Figure 5.37:** Cross-section 1 of the baseline specimen. Red lines highlight the delaminations. Blue rectangle represents the size and location of the sonotrode during welding. Blue vertical lines indicate the material directly under the sonotrode.

## 5.3 Conclusion

In order to conclude part 2 of this research project, the following sub research questions will be answered:

- To what extent can US welding re-consolidate impact damage in thermoplastic composites?
  - What are the heating characteristics of US welding impact damage?
  - What is the influence of US welding parameters on the ability to re-consolidate the impact damage?

**To what extent can US welding re-consolidate impact damage in thermoplastic composites?**

Depending on the welding parameters, as well as the success of the repair, a maximum of approximately 25% of the projected damaged area could be re-consolidated. Often, the re-consolidated area was the area around the undamaged cone. This area does contain the highest amount of delaminations, when looking through the thickness. Therefore, in that case, the extent of re-consolidation of damage could be considered higher than 25%.

**What are the heating characteristics of impact damage during US welding?**

At the start of the vibration phase, frictional heating is present between the sonotrode and the surface of the specimen, as well as inside the delaminations of the damaged area. However, the heating rate of the frictional heating inside the delaminations is much higher, therefore,

frictional heating between the sonotrode and the surface of the specimen can be considered negligible. When frictional heating heats up the material to Tg, viscoelastic heating starts, which becomes dominant. As not all areas heat up at the same rate, due to variation in the amount of intimate contact within the damaged area, some areas reach/surpass Tm while others do not.

**What is the influence of US welding parameters on the ability to re-consolidate the impact damage?**

Increasing the vibration duration will increase the amount of heating that takes place inside the specimen. Increasing the amount of heating will increase the amount of melting but does allow certain areas to potentially overheat, resulting in degradation. It is shown that, for the same duration, there is a lot of variation between the welded specimens. The welding force has an influence on the heating rate. Decreasing the welding force will decrease the heating rate inside the specimen. Also, by decreasing the welding force, there is less intimate contact which, together with the lower heating rate, is believed to be responsible for the presence of partially re-consolidated delaminations. The vibration amplitude also has an influence on the heating rate. Increasing the vibration amplitude will increase the heating rate inside the specimen. Welds with a long duration and with a low amplitude showed that, although no clear signs of melting can be observed, it can be observed that delaminations have grown inside the undamaged cone during the welding phase. A sufficient consolidation force is needed to compress the material which expands during the vibration phase. When the consolidation force is not sufficiently high, voids and misalignment of plies can remain after the material cooled down.

# Chapter 6

# Part 3 - Compression after impact

In this chapter, the results of part 3 are shown and discussed. Section 6.1.1 shows the results of the reference repair process. These results will be discussed in section 6.2.1. Section 6.1.2 shows the results of the reference repairs themselves. These results will be discussed in section 6.2.2. Finally, section 6.1.3 shows the results of the compression after impact tests. These results will be discussed in section 6.2.3.

## 6.1 Results

### 6.1.1 Reference repair process using a hot-press

For the reference repair using a hot-press, two different strategies were considered. The first strategy consisted of using a vacuum bag to provide support and limit the amount of squeeze out during the pressing process. The second strategy consisted of using a steel mold to provide support. After testing, the strategy using a vacuum bag proved to be unable to provide any support or to limit any squeeze out. However, a steel mold proved to be capable in providing support and limiting squeeze out, therefore, this strategy was used for the reference repair process. Limiting squeeze out during the pressing process is of utmost importance as squeeze out will have a negative effect on the consolidation pressure near the edges of the specimen, resulting in poor material quality, as well as on the dimensional quality of the repaired specimen. As the repaired specimen will be tested for their CAI strength, the dimensions of the specimens are dictated in the ASTM D7137 test standard [5]. As these dimensions are the same as the impacted specimens which needs to be repaired, this means that the entire specimen, including the edges, needs to be of proper quality. In case of squeeze out, this can be trimmed off. However, if poorly consolidated material exists within the boundaries of the specimen dimensions, these areas cannot be trimmed off and these areas can become an issue during CAI testing. Especially the top and bottom edge are sensitive to defects as the compression forces are introduced here.

The process of repairing the impacted specimens using the hot-press consists of five steps. The first step is designing and manufacturing the steel mold. Secondly, the mold is prepared

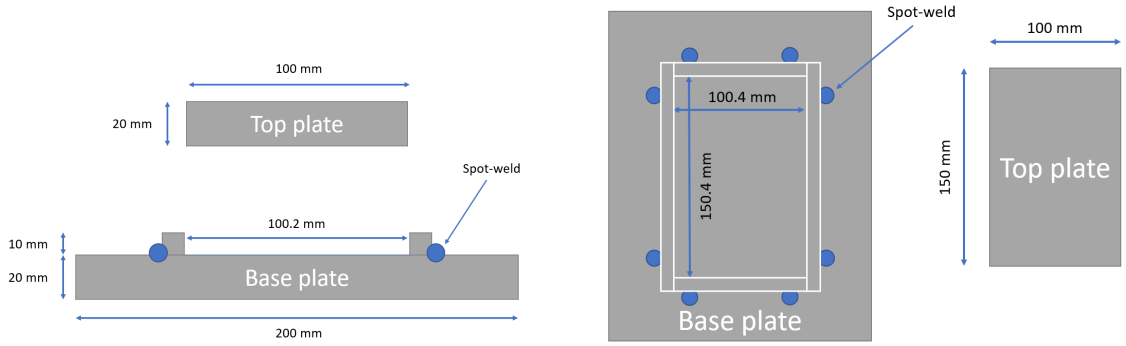


**(a)** Front view **(b)** Top view

**Figure 6.1:** Design of the mold used to repair the impacted specimens

for pressing and the specimen is inserted. Thirdly, the mold is placed inside the hot-press and the pressing cycle is run. Fourthly, the mold is removed from the press and the specimen is released from the mold. Finally, if applicable, any squeeze-out material is trimmed off.

As the geometry of the specimen consists of a rectangular flat shape, the geometry of the mold is simple. The mold consists of a 200mm by 250mm rectangular flat steel base plate with a thickness of 20mm. The thickness of the base plate ensures the temperature inside the mold is more evenly distributed. Also, it ensures structural rigidity to prevent possible warpage of the mold, hence also the specimen. On top of the base plate, four sections of square steel bar are placed as is shown in figure 6.1. These four sections form the vertical walls of the mold. They are welded onto the base plate using two spot welds for each section. These spot welds make it easier for the steel sections to be removed in case the specimen is stuck inside the mold after pressing. The four sections are placed in such a way that there is a slight gap between the walls and the specimen to allow for Kapton foil to be used as a release film and a film that seals the gap between the top and base plate. The final part of the mold is the top plate. This plate has the same dimensions as the specimen (100mm by 150mm) and has a thickness of 20mm. As for the thickness, like the base plate, it helps distributing the heat equally over the specimens and prevents warpage. Additionally, the thickness is needed as the top plate will be pressed down in between the vertical walls. The thickness of the top plate will prevent the press from pressing against the vertical walls instead of the top plate.

The mold is prepared for pressing by applying a release-agent on the base plate, vertical sections, the top plate and the Kapton foil. Furthermore, two pieces of Kapton foil are cut to fit inside the base plate and to cover the top plate. The Kapton foil acts as a release-film but also to fill the gap between the vertical sections and the top plate to ensure there is limited squeeze out, hence sufficient pressure on the entire specimen. Additionally, the Kapton foil can absorb some of the shrinkage of the mold during the cooling phase of the pressing process, and reduce some of the compression loads that the vertical walls of the mold apply onto the specimen, as it is expected that the mold shrinks more than the specimen. After the release-agent and Kapton foil are applied, the specimen is placed inside the mold, see figure 6.2.

After the mold is prepared and the specimen is inserted, the mold is placed inside the hot-press. The cycle that is used for the repair is the same as for consolidating the laminates

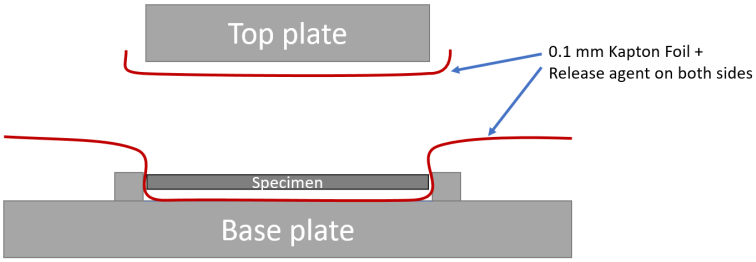


**Figure 6.2:** Figure shows how the specimen is placed inside the mold

which the specimens are made off. This means an initial pressure of 4 bars and temperature ramp of 5°C per minute to 385°C and hold for 30 minutes. Increase the pressure to 10 bars and hold for 45 minutes. Finally, it is cooled down to room temperature with 5°C per minute and a pressure of 10 bars.

After the mold and specimen are cooled down, the specimen is released by grinding away the spot welds on two of the four vertical sections. After the specimen is released the Kapton foil can be removed. Finally, the excess material can be trimmed off.

### 6.1.2 Reference repair data

After the repairing process, the specimens are measured for their dimensions and C-scanned.

As expected, the repaired specimens have a decreased thickness and an increased height and width compared to the specimens before repairing, see table 6.1. The increased width and height is due to the fact that the mold had a small gap in between the vertical walls and the specimen. The decreased thickness is caused by the increase in width and height and due to some material squeeze out. As the change in width and height is limited and the specimen fits inside the fixture used for CAI testing, it was decided not to cut the specimen to the original size and only to trim off the squeezed out material.

| Specimen ID | Before/after hot-press | Height [mm] | Width [mm] | Thickness [mm] |
|---|---|---|---|---|
| 1.4 | Before | 150.15 | 100.15 | 4.47 |
| 1.4 | After | 151.55 | 101.32 | 4.28 |
| 1.5 | Before | 150.15 | 100.15 | 4.48 |
| 1.5 | After | 151.64 | 101.70 | 4.25 |

**Table 6.1:** Dimensions of the specimens which are repaired using a hot-press

Figure 6.3 shows the C-scan data for the repaired specimens. For both specimens, the entire damaged area in the middle of the specimen has re-consolidated and there is no indication of any residual damage. The C-scan shows that, except for the right top corner, the whole specimen, including the edges, is properly re-consolidated. The reason for the large initial damage inside the specimens, used for the reference repair, is due to the fact that these specimens originate from the impact trials before the correct baseline damage was obtained. These specimens were supposed to be used to test the reference repair process before applying

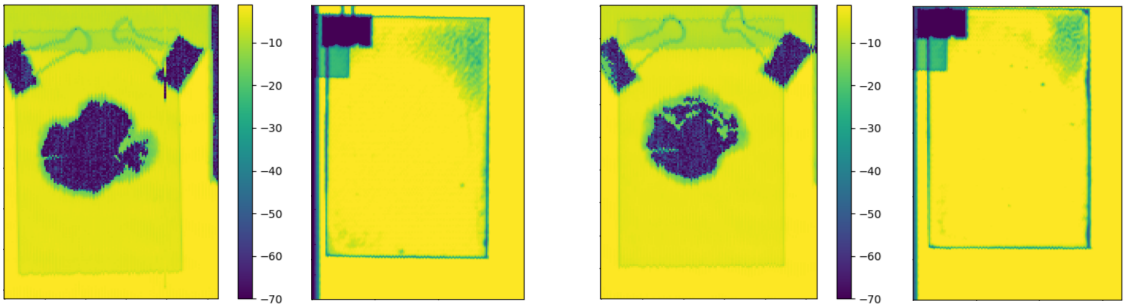


**(a)** 1.4 **(b)** 1.5

**Figure 6.3:** C-scans of the specimens which are repaired using a hot-press. Left: before the repair. Right: after the repair.

the process to specimens which did contain the correct baseline damage. However, after these two test specimens, due to the occurrence of an area with poor material quality at the top right of both specimens and the expectancy that this will occur for every new repaired specimen, it was decided not to continue using this repair process with specimens that did contain the correct baseline damage. As will be discussed in section 6.2.3, even with such large initial damage, it is believed the area with poor material quality on the top right of the specimen is responsible for the premature failure of the specimen. As the specimens containing baseline damage have an even smaller damaged area, the same results are expected and it was deemed unnecessary to use any of the specimens containing the correct baseline damage.

### 6.1.3 Compression after impact testing

This section shows the results from the CAI tests. The results consist of force and displacement data from the compression load frame, DIC data and visual observations. CAI test results are summarized in table 6.2

Figure 6.4 shows the force versus displacement curves for all successfully tested specimens. The shown graph is corrected with the compliant displacement of the compression load frame itself which is responsible for the odd beginning of each curve. The tests of specimen 1.8 and 2.5 are discarded as one of the vertical supports inside the fixture came lose, allowing it to buckle and fail prematurely. Specimen 2.2 is not shown inside the graph as, during the test, it was the first time the compression load frame with the fixture was fully loaded. Therefore, the displacement data of this test includes settling of the compression load frame and fixture as well as the displacement of the specimen itself, which does not provide a fair comparison to the other specimens. However, the CAI strength of this specimen is included in the results as this has not been affected. All shown specimen show a settling phase up to a displacement of approximately 0.2mm, where the lines are curved. After a displacement of 0.2mm, all lines, except for the two reference repairs, become linear with a certain gradient. This settling phase varies between the specimens and is responsible for the offsets in displacement from the beginning of the tests. Three of the four highest achieved loads are from the pristine specimens, which is to be expected as these are in optimal condition. Interestingly, the highest force achieved by a welded specimen, is higher than the force of one of the pristine specimens. The graph does not show a clear difference between the damaged and the welded specimens.

However, from all welded and damaged specimens, the welded specimens are accountable for the highest and lowest performing specimens. The average forces of the welded and damaged specimens are 149.0 kN and 149.5 kN for average damaged areas of 711.3 $mm^2$ and 714.5 $mm^2$, respectively. The two reference repaired specimens account for the two lowest achieved forces. Both specimens show a different behaviour compared to the rest as they show a less linear behaviour and have a lower gradient.

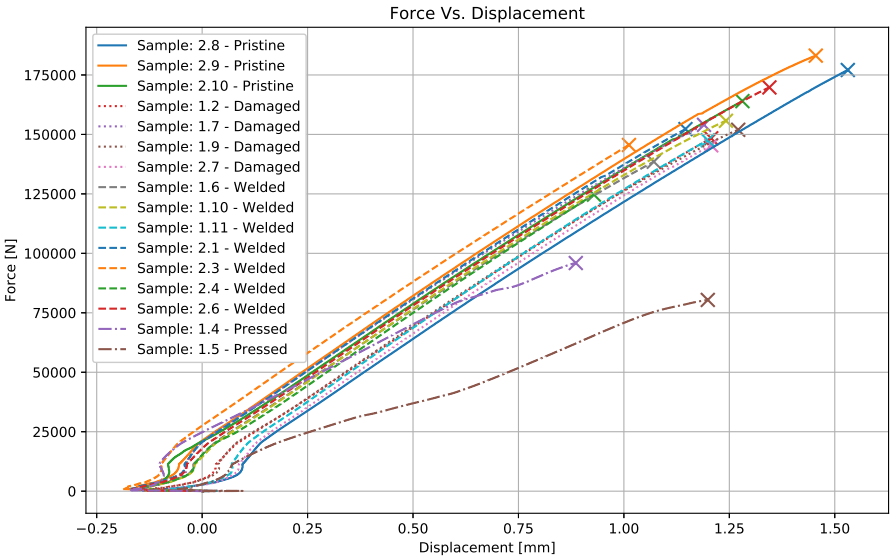


**Figure 6.4:** Force versus displacement curves of the successfully tested specimens

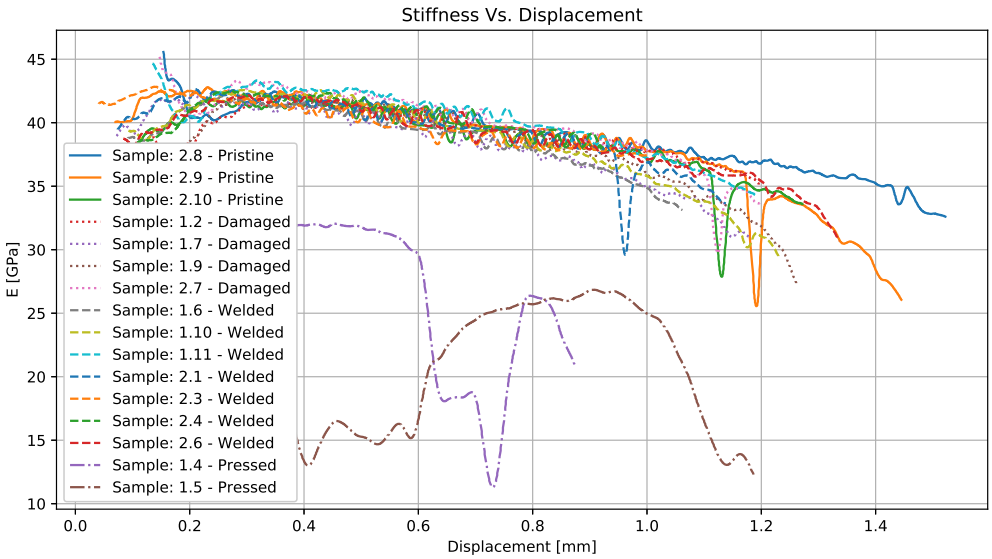


**Figure 6.5:** Stiffness versus displacement curves of the successfully tested specimens. Obtained by converting the corrected force versus displacement data from the compression load frame.

| Specimen ID | Type | Failure location | Damaged area | $F_{max}$ | Displacement at $F_{max}$ |
|---|---|---|---|---|---|
| 2.8 | Pristine | Top | - | 177937 N | 1.53 mm |
| 2.9 | Pristine | Top | - | 186611 N | 1.46 mm |
| 2.10 | Pristine | Top | - | 164904 N | 1.28 mm |
| | | | | | |
| 1.2 | Damaged | Middle | 702 $mm^2$ | 149184 N | 1.21 mm |
| 1.7 | Damaged | Top | 713 $mm^2$ | 154754 N | 1.19 mm |
| 1.9 | Damaged | Middle | 610 $mm^2$ | 152630 N | 1.27 mm |
| 2.2 | Damaged | Middle | 405 $mm^2$ | 159649 N | - |
| 2.7 | Damaged | Middle | 1104 $mm^2$ | 146369 N | 1.21 mm |
| | | | | | |
| 1.6 | Welded | Middle | 671 $mm^2$ | 139349 N | 1.07 mm |
| 1.10 | Welded | Top | 646 $mm^2$ | 156533 N | 1.24 mm |
| 1.11 | Welded | Middle | 572 $mm^2$ | 148536 N | 1.2 mm |
| 2.1 | Welded | Middle | 860 $mm^2$ | 153220 N | 1.2 mm |
| 2.3 | Welded | Middle | 778 $mm^2$ | 146567 N | 1.01 mm |
| 2.4 | Welded | Middle | 770 $mm^2$ | 128296 N | 0.93 mm |
| 2.6 | Welded | Top | 682 $mm^2$ | 170510 N | 1.35 mm |
| | | | | | |
| 1.4 | Hot-pressed | Top | 3456 $mm^2$ | 96298 N | 0.89 mm |
| 1.5 | Hot-pressed | Top | 2851$mm^2$ | 80622 N | 1.2 mm |

**Table 6.2:** Compression after impact test results

Figure 6.5 shows the stiffness versus displacement diagram which is derived from the force and displacement data. The diagram shows that all specimens, except for the reference repairs, show a similar stiffness behaviour. After the settling phase (displacement of 0.3mm), the stiffness is approximately 42 GPa. This slowly decreases to a stiffness of approximately 39 GPa at a displacement of around 0.8mm. From this point, the stiffness of the specimens start to deviate from one another. Generally, they start to slowly decrease and decreases more quickly towards failure of the specimen. Although the four specimens with the highest CAI strength also maintain the highest stiffness while undergoing the largest displacements, between the rest of the specimens, no further trends were discovered.
The two reference repaired specimens clearly deviate from the rest of the specimens, the stiffness is not only lower compared to the rest, it also shows large fluctuations.

Figure 6.6 shows the relationship between the damaged area and the CAI strength. The damaged area that is used for the repaired (welded and pressed) specimens is the damaged area before repairing. This way, the graph shows the difference in performance of the repaired specimens with respect to the initial damaged state. From literature, it is known that the CAI strength is linear with the damaged area [23]. Therefore, to better distinguish differences between damaged and welded specimens, a linear trend line is plotted for the data points of the pristine and damaged specimens. The welded specimens deviate more from the trend line than the damaged specimens. However, there are two points that deviate more than others. One of these specimens is specimen 2.6 which performs better, the other is specimen 2.4 which under performs, compared to specimens with similar damage.

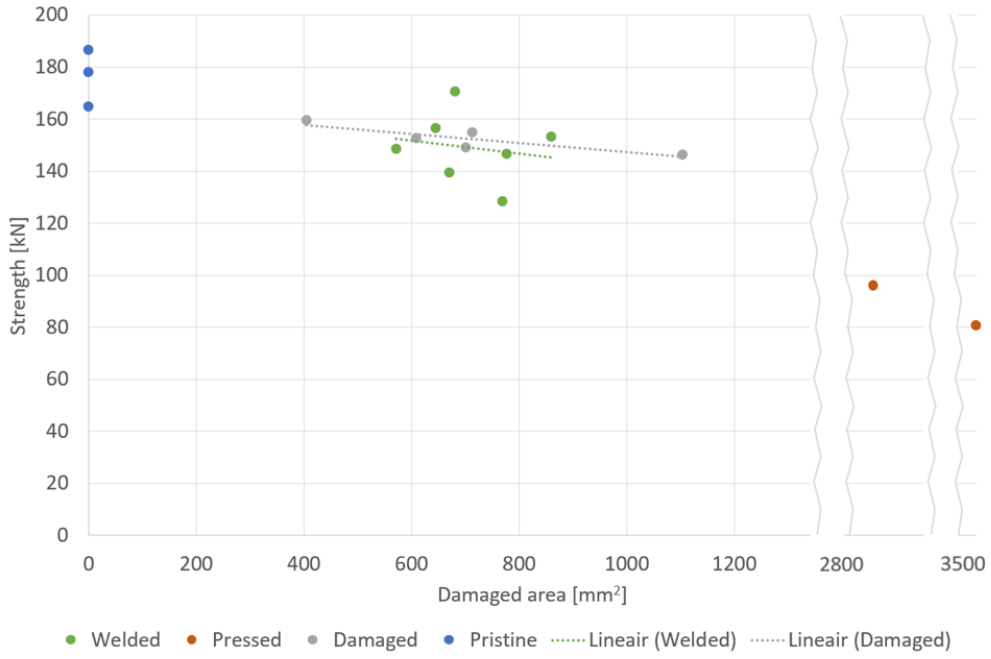


**Figure 6.6:** Damaged area versus CAI strength

Figures 6.8 to 6.11 show the DIC data of the CAI tests. In this section, the most relevant specimens are shown. DIC data of all specimens is shown in appendix C. The DIC data consists of strain (yy) and displacement (z) distributions of the moment just before failure. As this will illustrate the situation which has led to failure. Additionally, displacement (z) data is shown that represents the displacement of the vertical middle line of the specimen during the entire CAI test. This will show the buckling behaviour of the specimen during the compression loading.

Looking at the DIC data, the pristine only shows global buckling. Two specimens show mode 2 buckling and one shows mode 1 buckling. The different strain distributions are caused by the global buckling of the specimens. The strain distribution shows less compressive strain at locations where the specimens buckle towards the observer and more compressive strain at locations where the specimen buckles away from the observer.

Looking at the damaged specimens, all specimens show global and local buckling, except for one (2.7) which only shows local buckling. This local buckling is characterized by a specific strain distribution located at the same location as the damage. The pattern consists of a horizontal area with a high compressive strain which is caused by the local buckling of plies at this location. Above and below this area are two areas with lower compressive strains. This is caused by the fact that the locally buckled area cannot be loaded as high as the surrounding area, therefore less compressive stresses, hence strains, can build up in these areas. The displacement data indicates local buckling by large fluctuations in the middle of the specimen, hence location of the damage.
Except for three specimens (1.6 , 2.1 and 2.4), the welded specimens only show global buckling. Of these three specimens which, besides global buckling, also show local buckling, it seems that two (1.6 and 2.1) show less severe local buckling compared to the damaged specimens, the other specimen (2.4) seems to show similar local buckling.

Both pressed specimens only show global buckling. However, it must be noted that both specimens show higher strains in the right top corner of the specimen, compared to the rest of the specimens. This location coincides with the area where C-scan data revealed a section of poor material quality. However, the middle of the specimens show no deviations in strain or displacement, hence no signs of local buckling.

During the CAI tests, specimens failed either in the middle of the specimen at the same height as the damaged area or at the top of the specimen next to the clamping, see figure 6.7. The location of failure for each specimen is summarized in table 6.2. All pristine specimens failed at the top of the specimen. Interestingly, also one damaged and two welded specimens failed at the top. Important to note is the fact that according to the test standard, when a specimen fails at the top, the test is not valid. It is deemed invalid as the damaged area did not fail, therefore the maximum strength before failure is not the maximum strength of the damaged area. However, this does conclude that the damaged area is stronger than the maximum strength determined for those specimens. Therefore, the damaged area of the damaged specimen and the two welded specimens, that failed at the top, have a higher strength than the results indicate.

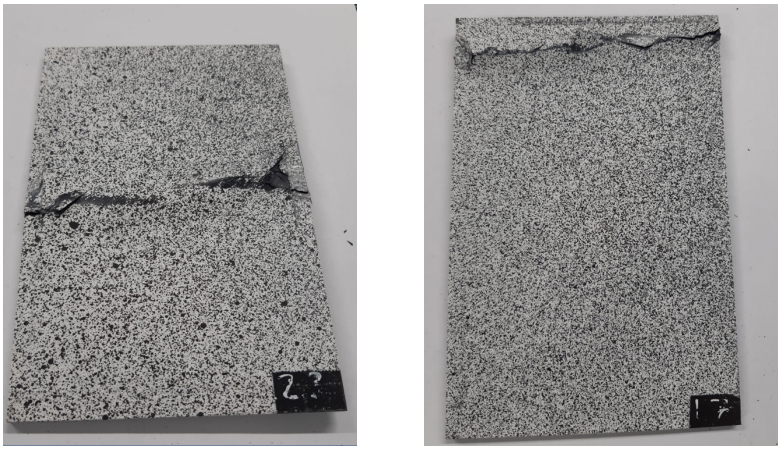

**(a)** **(b)**

**Figure 6.7:** Specimens failed during CAI testing. Left: failure in the middle section of the specimen. Right: failure at the top of the specimen.

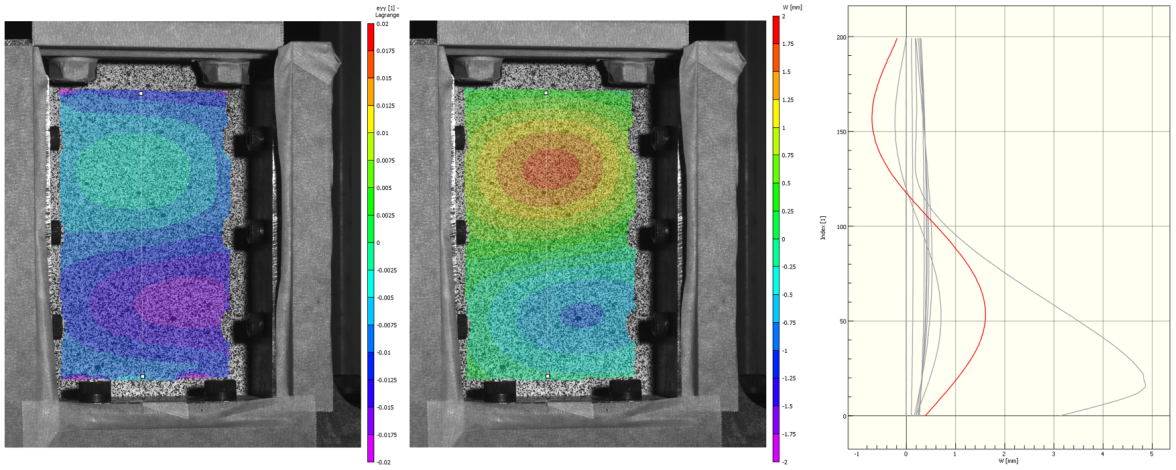

**Figure 6.8:** DIC data of pristine specimen 2.9. Left: Distribution of strain in y-direction just before failure , Middle: distribution of displacement in z-direction just before failure , Right: displacement in z-direction over the line that runs vertically through the middle of the specimen, progressing throughout the whole test.

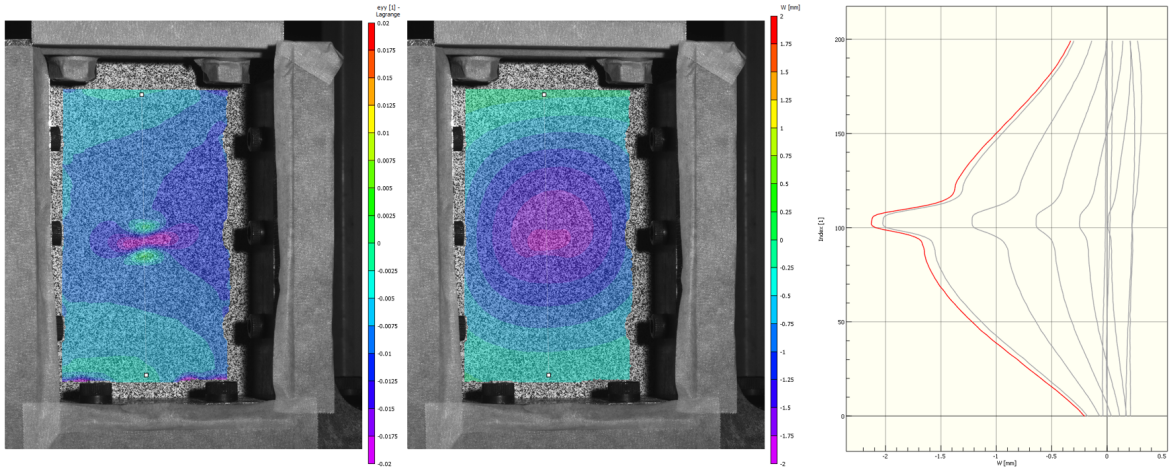

**Figure 6.9:** DIC data of damaged specimen 1.7. Left: Distribution of strain in y-direction just before failure , Middle: distribution of displacement in z-direction just before failure , Right: displacement in z-direction over the line that runs vertically through the middle of the specimen, progressing throughout the whole test.

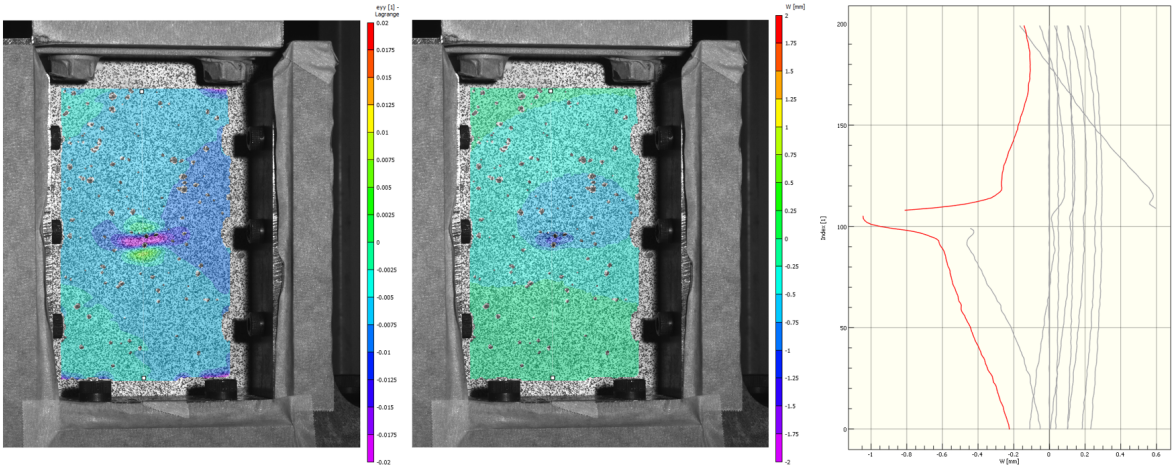

(a) 2.4

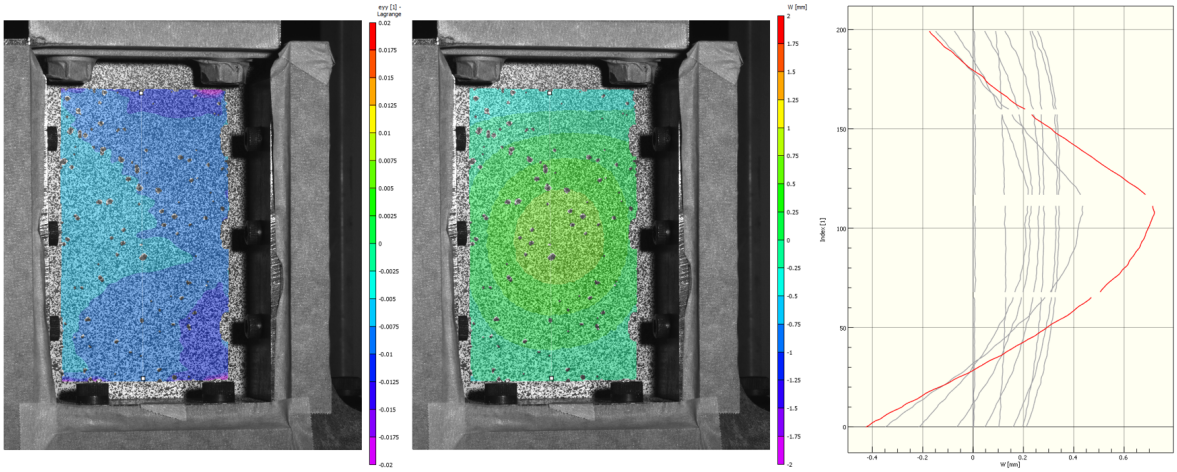

(b) 2.6

**Figure 6.10:** DIC data of welded specimens 2.4 and 2.6. Left: Distribution of strain in y-direction just before failure , Middle: distribution of displacement in z-direction just before failure , Right: displacement in z-direction over the line that runs vertically through the middle of the specimen, progressing throughout the whole test.

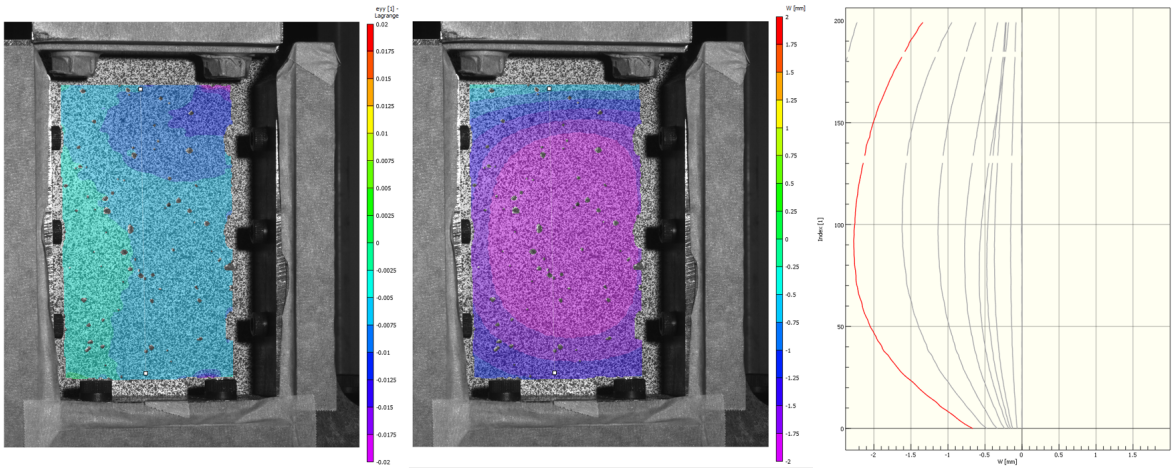

**Figure 6.11:** DIC data of pressed specimen 1.5. Left: Distribution of strain in y-direction just before failure , Middle: distribution of displacement in z-direction just before failure , Right: displacement in z-direction over the line that runs vertically through the middle of the specimen, progressing throughout the whole test.

## 6.2 Discussion

### 6.2.1 Reference repair process using a hot-press

The reference repair process, except for designing and manufacturing the mold, is similar to the process of manufacturing a composite laminate. Designing and manufacturing a mold for the damaged specimens, used in this research project, has not been a complex task, as the specimens are flat and rectangular. Yet, the first design was not capable of successfully repairing the entire specimens. However, it is believed that, with minor changes, it would be capable of a successful repair. However, designing and manufacturing a mold is expected to be become significantly more complex if specimens have a more complex geometry, for example a curved surface. Also, as the whole specimen needs to be re-consolidated, molds will increase in size with larger specimens. It must be noted that, with increased mold complexity and size, the repair process will become more cost and time intensive as well as more difficult to successfully execute.

### 6.2.2 Reference repair data

Although the dimensions of the specimen changed after the repair, it is expected that this could be reduced close to zero after improving the design of the mold. However, iterating the design of the mold is considered outside the scope of this research project. Also, it is expected that changes in dimensions will be reduced for larger specimens as the effect of material squeeze out and the small gap between the mold and specimen will decrease.

The C-scan data shows that the reference repairing process is able to completely re-consolidate the damaged area. This means that, in case the specimen only contains matrix damage and no fiber damage, it is completely restored to its original state before impact. However, although

the damaged area is re-consolidated, the process did create a spot with poor material quality in the upper right corner of both specimens. This shows that this process can, besides repairing damage, also create damage. As this process consists of re-consolidating the entire specimen, this damage can occur at every location on the specimen. When the damaged area is relatively small compared to the size of the component, this is something to consider. However, further iterations of the design of he mold should be able to eliminate this damaged area, in this case the area in the right upper corner, but this is considered outside of the scope of the project. However, it does show that mold design, especially the design of the mold concerning re-consolidation of the edge, is a critical point to the success of the repair. Normally, to ensure proper material quality at the edges of a component, the component that is pressed is made larger. This way, it allows the edges to be of improper material quality, as this material is trimmed off to the final dimensions. Unfortunately, as the component that needs to be repaired is already trimmed to the final dimensions, and no material can be added, this means that the entire component, including the edges, needs to be properly re-consolidated to obtain the desired material quality.

### 6.2.3 Compression after impact testing

During CAI testing, the specimens failed in one of two ways. The first, the specimens failed in the middle of the specimen with failure in a horizontal line which runs trough the damaged area. The second, the specimen failed at the top of the specimen with failure in a horizontal line close to the clamping. The specimens that failed at the top consist of 3 pristine specimens, 2 reference repaired specimens, 1 damaged specimen and 2 welded specimens. This means that, for these specimens, the CAI strength of the specimen, more specifically, the middle section of the specimen, is stronger than indicated. Although, it is not possible to determine the actual strength of the middle sections of these specimens, DIC data can be used to estimate whether the middle of the specimen was close to failure before it failed at the top. Due to the fact that the damaged area causes a specimen to fail in the middle and the damaged area will create specific strain patterns which are captured by the DIC system, determining this is only possible for damaged and welded specimens and not for pristine specimens.

#### Pristine specimens

As mentioned before, all pristine specimens failed at the top of the specimen. This is to be expected as the absence of a damaged area means the whole specimen has the same strength, therefore fails at the location where load is introduced. Because the strength, determined by the CAI test, is not the maximum strength of the middle of the specimen, it is not possible to determine the strength reduction of the middle section of the specimen due to the presence of damage. Instead, the difference between the strength of a pristine and damaged specimen is a minimum strength reduction. In this research project, the compression after impact strength achieved by the pristine specimens is used as a reference. When a welded or pressed specimen matches this strength, this specimen is considered successfully repaired.

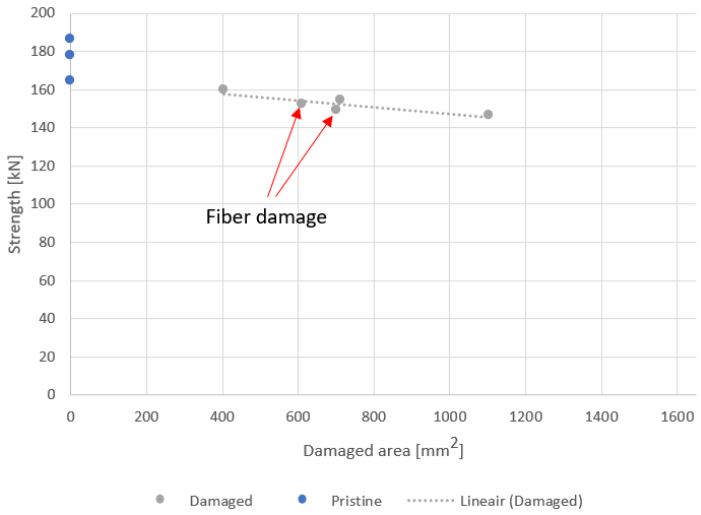


**Figure 6.12:** Damaged area versus CAI strength graph, only containing the damaged and pristine specimens, showing which specimens have fiber damage.

### Damaged specimens

The damaged specimens all show local and global buckling, except for one specimen which only shows local buckling, which is in contrast to the pristine specimens which only show global buckling. This indicates that the damaged area is causing local buckling in the middle of the specimen, from which it is known to be a key aspect that initiates the failure process of a specimen [38]. As mentioned before, the damaged specimens follow a linear relationship between CAI strength and damaged area.
Figure 6.12 shows all damaged specimens that are tested for their CAI strength. Two of the five specimens contain fiber damage (specimen 1.2 and 1.9). The extent of fiber damage of these specimens is shown in appendix C. These two specimens have the largest amount of fiber damage of all tested (included US welded and hot-pressed) specimens. Although these two specimens are below the trend line, considering how close the CAI strength is to the other specimens and the fact that these have the largest amount of fiber damage, the effect of fiber damage on the other specimens is considered to be negligible, especially comparing this effect to the variation caused by the welding process, see figure 6.6.
It must be noted that one of the damaged specimens (specimen 2.6) failed at the top of the specimen, indicating the middle section of the specimen would have a higher strength than the maximum strength shown by the CAI test. However, looking at the DIC data of this specimen, more specifically the strain distribution, just before failure, it shows a similar state as the specimens that did fail in the middle section. Therefore, it is expected that the strength of the middle section of the specimen is close to the maximum strength indicated by the CAI test.

### Reference repair specimens

The reference repaired specimens had a lower strength and stiffness compared to all other specimens. However, the specimens failed at the top, therefore the strength indicated does

not represent the strength of the middle section of the specimens. Looking at the DIC data, high strains are located at the top right of the specimens which coincides with the bad area which is observed by the C-scan. Therefore, the lower strength and stiffness is believed to be caused by this area. Although this does indicate a critical aspect of the process, the fact that re-consolidating the entire specimen can cause a damaged area at any location on the specimen, further investigating this is considered outside of the scope of this project. Looking at the DIC data, the strain distribution in the middle of the specimen shows no local deviations, indicating there was no local buckling or damage. Because of this, together with the fact that the C-scan did not show any remaining damage, it is expected that the strength and stiffness of the middle section of the specimens is completely recovered.

#### Welded specimens

Looking at the welded specimens, it can be seen that there is a larger variation between the specimens compared to the damaged specimens. This indicates that, even though the welding parameters are the same for all welded specimens, the welding process can have varying effects. As some welded specimens perform better than the damaged specimens and some worse, it shows the welding process introduces positive as well as negative aspects to the damaged area. These aspects include damage growth, size and location of re-consolidated areas and degradation of material. As these aspects vary between all welded specimens, it is important to look at each individual welded specimen separately.

Looking at the total area encapsulated by the outer perimeter of the damaged area, all welded specimens show a growth of 6.4% to 8.3%. Although this growth is expected to have a negative influence on the compressive strength, because it is similar for all welded specimens, this is not an aspect that determines whether a welded specimen performs better or worse than their damaged counterpart. In contrary to the damaged specimens, only 3 out of 7 welded specimens (1.6 , 2.1 and 2.4) show local buckling before failure. Of these three, two (1.6 and 2.4) have the lowest strength of all the welded specimens. The C-scan data of these two specimens shows that a limited amount of material has re-consolidated and the re-consolidated area consist of small separate dots. The lack of re-consolidated material most likely contributed to the local buckling of the damaged area and the lower strength compared to the other specimens. One of these two specimens (2.4), the one with more severe local buckling and the lowest CAI strength, also contains degraded material (which was determined directly after the CAI test as a burned smell could be perceived which could only originate from the welding process), which is believed to be the reason why this specimen performed the worst of the two.

Interestingly, the second specimen (2.1) that contains degraded material performed noticeably better than the other specimen containing degraded material (2.4). This specimen (2.1), besides only containing small re-consolidated spots, also had an undamaged cone which disappeared during the welding process. However, this specimen did perform well with a CAI strength above the trend line. A possible explanation can be found in figure 5.15, here it shows that although the middle of the cross-section is degraded, the delaminations above and below the degraded material are re-consolidated. These are likely re-consolidated due to the internal pressure caused by the degrading material, the same internal pressure which likely caused the delaminations to grow inside the undamaged cone, making it disappear. These

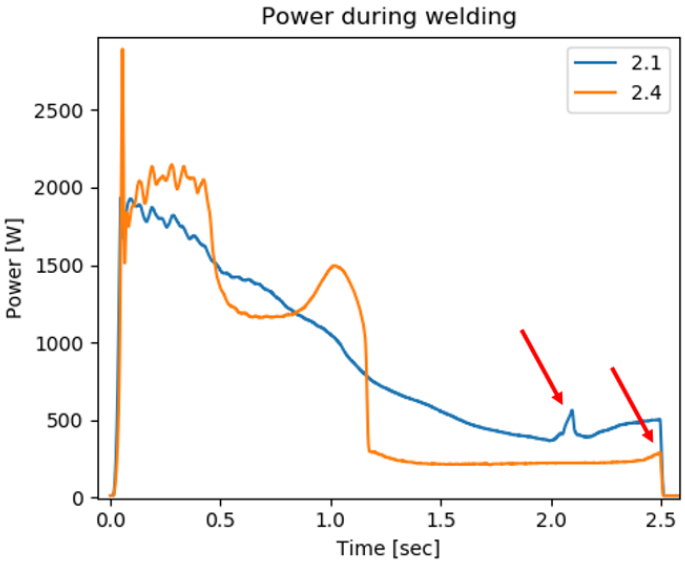


**Figure 6.13:** Power curves of specimen 2.1 and 2.4 which show the (beginning of the) power spikes, indicated by the red arrows, that are believed to indicate degradation of material

re-consolidated delaminations are not noticed on the C-scan as the signal of the C-scan is still blocked by the degraded area. Although the degraded material is still present and has a negative influence on the local buckling load, due to the fact that the surrounding delaminations are re-consolidated which has a positive influence on the local buckling load, the local buckling load of the damaged area as a whole has still increased. Therefore, specimen 2.1 has a higher strength than the other specimen containing degraded material which, due to the fact that the undamaged cone is still present, is believed not to have had sufficient internal pressure to re-consolidate the delaminations. Another reason why it is expected that this specimen did not have sufficient pressure can be seen in the power curve of this specimen, see figure 6.13. As mentioned before, it is believed that a spike in the power curve, during the last phase where the power is normally constant, indicates that the material inside the specimen is degrading. The spike is believed to be caused by the internal pressures that temporarily increase the welding force, hence the welding power. This particular specimen shows the beginning of a spike just before the vibration phase ended, possibly indicating pressure was just about to start building up but did not because the vibration phase ended which stopped the degradation process.

Between the four specimens (1.10, 1.11, 2.3 and 2.6) that did not show local buckling, there are two specimens that have the highest strength of all welded specimens (1.10 and 2.6) and failed at the top and two specimens that failed in the middle section (1.11 and 2.3). Looking at the C-scan data of these four specimens, between the four different specimens, there is a difference is the size and location of the re-consolidated area. It is believed that these two aspects contribute to the higher strength of the specimens that failed at the top. The location is believed to be important for two reasons. Firstly, from literature it is known that the undamaged cone has a positive contribution to the CAI strength of a specimen because it can increase the local buckling load of the damaged area by locally decreasing the buckling length [4]. A re-consolidated area will do the same and, like the undamaged cone, is most

effective in the center of the damaged area. Not only is the local buckling length the highest in the middle (on the in-plane axis perpendicular to the loading direction) of the damage area, therefore reducing this section will be more effective. Also, having a re-consolidated area in the middle (on the in-plane axis parallel to the loading direction) of the damaged area reduce the buckling length of the damaged area by a factor of 2, which will be less than 2 at any other location. Secondly, looking at the characteristics of the impact damage for thermoplastics, it can be seen that the area in the middle of the damaged area contains the most delaminations when looking through the thickness. Therefore, this area is more prone to local buckling and re-consolidation of this area is more effective than re-consolidating the areas further away from the middle. The size of the re-consolidated area is believed to be important for two reasons. Firstly, increasing the re-consolidated area will further decrease the before mentioned buckling length, which will increase the load at which local buckling occurs. Secondly, from literature it is know that, during loading, delaminations can grow which can eliminate the undamaged cone [4], similarly, this can happen with the re-consolidated area. Increasing the re-consolidated area is expected to suppress/delay this process, increasing the load at which this will happen.

The process of delamination growth, eliminating the re-consolidated area, is believed to be the reason why specimen 1.11 and 2.3, although failing in the middle section, did not show local buckling in the DIC data. The specimens that did show local buckling in the DIC data were gradually loaded, therefore, local buckling happened gradually and was captured by the DIC system. In contrast, the re-consolidated area of specimen 1.11 and 2.3 suppressed local buckling, achieving higher loads without indications of local buckling. At some point the delaminations growth eliminates the re-consolidated area and the local buckling is not suppressed anymore. As the load is already above the normal local buckling load, the damaged area will immediately buckle locally, followed by total failure of the specimen. As this happens very quickly and the frame rate of the DIC system is only 1 frame per second, this is not captured by the DIC system.

After the CAI test of specimen 1.10, it was observed that the top clamp has moved open slightly. This would have had a negative effect on the failure load of the top section of the specimen, where it ultimately failed. As the initial damage, welding parameters, welding curves, welding energy, C-scan data and DIC data are similar to specimen 2.6, it is believed that this specimen could possibly have reached similar strength levels as specimen 2.6, if the clamp had not opened slightly.

Although the CAI strength of specimen 2.6, and possibly specimen 1.10, is similar to the strength of the pristine specimens, this does not conclude that the repaired damaged area has the same strength as the pristine material. That is the case because all specimens failed at the top, therefore, no specific strength for the middle section of the specimens was determined. To the author's knowledge, there is no specific method or test procedure that is able to completely isolate this area from external influences such as global buckling and load introduction, therefore, the true strength of the middle section cannot be determined. However, it is important to realise that, knowing how much higher the ultimate strength of this section is compared to the strength obtained by the CAI test might not be important in practical applications as here, like in the CAI test, this will never be reached due to the inevitable buckling and load introductions.

## 6.3 Conclusion

In order to conclude part 3 of this research project, the following sub research questions will be answered:

- How much strength does hot-pressing restore in case of matrix damage only?
- Which aspects influence the amount of compressive strength restored by hot-pressing?
- How much strength does US welding restore in case of matrix damage only?
- Which aspects influence the amount of compressive strength restored by hot-pressing?

**How much compressive strength and stiffness does hot-pressing restore in case of matrix damage only?**

Due to failure of the top section of the hot-pressed specimens, the true strength of the repaired middle section could not be determined. However, due to the fact that the whole damaged area has re-consolidated, it is expected that the compressive strength of this section was fully restored. As for the strength and stiffness of the specimen as a whole, these were both greatly reduced after the repair process.

**Which aspects influence the amount of compressive strength restored by hot-pressing?**

The repair process with a hot-press has shown that, although being able to fully repair the damaged section, it is sensitive for occurrence of damage on the edges of the repaired specimen, when not correctly designing the mold. In the case of this research project, this has had a catastrophic effect of the CAI strength of the specimen as a whole.

**How much compressive strength and stiffness does US welding restore in case of matrix damage only?**

The repair process using US welding has shown, although using the same welding parameters, to have varying results. The process has shown to be able to fully restore the CAI strength and stiffness of a specimen, but also to decrease the CAI strength and stiffness with respect to damaged specimens which were not repaired.

**Which aspects influence the amount of compressive strength restored by US welding?**

One aspect, which has a positive influence on the CAI strength of welded specimens, is the re-consolidation of delaminations inside the damaged area. The re-consolidation of delaminations, especially in the center of the damaged area, will suppress local buckling during compressive loading. As local buckling is responsible for premature failure, suppressing this will increase the CAI strength. One aspect, which has a negative influence on the CAI strength, is overheating of the material inside the specimen. This could cause voids, heat induced delaminations, degradation of material and misalignment of plies, which cannot always be fully suppressed after the consolidation phase. Each of these elements are believed to decrease the local buckling load of the damaged area, which promotes premature failure.

# Chapter 7

# Conclusion

This research project aimed to investigate the use of ultrasonic welding to repair impacted thermoplastic composites with the objective to evaluate the use of ultrasonic welding as an alternative to hot-pressing. This was done by first determining the damage characteristics of impacted thermoplastics and how they are influenced by the impact energy and impactor shape. This was followed by an investigation on the heating behaviour of impact damage inside thermoplastic composites during the US welding process and the influence of welding parameters on this heating behaviour. The knowledge gained from this investigation was then used to set up the welding parameters for repairing the specimens that were tested for their compression after impact strength. Besides repairing specimens using US welding, hot-pressing was used as a reference repair method. In each part of the report, the relevant sub research questions, stated in chapter 1, have already been answered, however, to conclude the entirety of this research project, the main research question will be answered here. The main research question is stated below:

*How does ultrasonic spot welding compare to hot-pressing to repair impacted CFRP composites and restore the compressive strength and stiffness?*

Answering this question is not as straightforward as comparing the restored CAI strength and stiffness of both repair methods. During this research project, it become evident that both methods have a completely different approach to re-consolidating impact damage, both with its advantages and disadvantages. Hot-pressing has shown that it is capable of fully re-consolidating the impact damage which in theory should fully restore the CAI strength of the specimen. However, this methods relies on the fact that the whole specimen has to be melted and re-consolidated. This has proven to be the downfall of this repair method as improper re-consolidation of the edges of the specimen has shown to be catastrophic, lowering the CAI strength with respect to its original damaged state. Although it is expected that hot-pressing should be able to fully restore the compressive strength of the specimens, for the repair to be successful, each repair will require properly designed dedicated tooling.
In contrary to hot-pressing, repairing using ultrasonic welding is a local process, only locally

melting and re-consolidating the damaged area. It was shown that, using the same welding parameters with duration control, the repair process has varying results, something that should be addressed for this process to become a usable repair method. Depending on the outcome of the welding process, the CAI strength either increased or decreased. As one specimen restored its CAI strength and stiffness within the range of the pristine specimens, it was shown that the welding process is capable of fully restoring the CAI strength and stiffness. Compared to hot-pressing, the welds that were not successful were less detrimental to the CAI strength and stiffness as the welding process had a more local, hence less severe, (negative) effect. Importantly, it was shown that, in order to fully restore the CAI strength and stiffness, it is sufficient to partially re-consolidate the damaged area as this is enough to suppress local buckling. Although it is not necessary to re-consolidate the entire damaged area to restore the compressive strength, something that was achieved with hot-pressing but not with US welding during this research project, it is still desirable as it is expected this will improve other important characteristics such as fatigue and damage propagation characteristics of the repaired area.

In summary, ultrasonic welding has proven to be capable of fully restoring the compressive strength and the local nature of the process has shown to be beneficial as it does not affect undamaged material. However, the consistency of the process needs to be improved in order to be used as a repair method.

# Chapter 8

# Recommendations

This chapter provides recommendations based on the results and observations obtained during this research project. The recommendations are split into two groups, recommendations for further research and practical recommendations.

**Recommendations for further research:**

- Additional research is required on gaining a better understanding of the heating behaviour of impact damage during US welding. This knowledge is needed to identify key aspects contributing to the large variation in welding results.
- Additional research is required to get a better understanding of the relationship between the welding power/sonotrode displacement and what happens inside the damaged area during welding. Not only can this be used as a tool to directly determine the success of a weld, before the use of additional inspection methods, also, this can be used to investigate the possibility of using power and displacement data to control the welding process in a closed-loop.

**Practical recommendations:**

- Specification changes to the welding machine, in case of the welding machine used in this research project. As the specifications of the welding machine are not tailored towards using the machine for repairing thermoplastic composites, some specifications fell short. Recommended updates would be:
  - Extending the maximum duration during which the welding machine can record the welding data to at least 60 seconds, as the vibration and consolidation phase are considerably longer compared to normal spot welding.
  - The ability to record negative sonotrode displacements as these are observed for all welds were material was re-consolidated.

  - Depending on how power and displacement data can be used for closed-loop control, additional options inside the welding machine to incorporate this, such as allowing for a negative target displacement or minimum welding power at which the vibration phase is stopped.

- Investigate the use of quasi-static impacts instead of using an impact tower. It is expected this will decrease the variation between damage inside the specimens, increasing consistency in welding results during further research.

- Investigate the use of alternative non-destructive inspection techniques such as improved C-scanning including depth information or the use of micro-CT scanning. This will provide a more complete picture of the state of the damaged/repaired area compared to the C-scans used in this research project.

# References


[1] T.W. Shyr and Y.H. Pan. Impact resistance and damage characteristics of composite laminates. *Composite Structures*, 62(2):193–203, 2003.

[2] T. Ishikawa, S. Sugimoto, M. Matsushima, and Y. Hayashi. Some experimental findings in compression-after-impact (cai) tests of cf/peek (apc-2) and conventional cf/epoxy flat plates. *Composites Science and Technology*, 55(4):349–363, 1995.

[3] S. Abrate. Impact on laminated composite materials. *Applied Mechanics Reviews*, 44(4):155–190, 1991.

[4] D.J. Bull, S.M. Spearing, and I. Sinclair. Observations of damage development from compression-after-impact experiments using ex situ micro-focus computed tomography. *Composites Science and Technology*, 97(1):106–114, 2014.

[5] ASTM International. Standard test method for compressive residual strength properties of damaged polymer matrix composite plates. 2017.

[6] H. Tuo, Z. Lu, X. Ma, J. Xing, and C. Zhang. Damage and failure mechanism of thin composite laminates under low-velocity impact and compression-after-impact loading conditions. *Composites Part B: Engineering*, 163(1):642–654, 2019.

[7] S.K. Bhudolia, G. Gohel, K.F. Leong, and A. Islam. Advances in ultrasonicwelding of thermoplastic composites: A review. *Materials*, 13(6):1284, 2020.

[8] I.F. Villegas. In situ monitoring of ultrasonic welding of thermoplastic composites through power and displacement data. *Journal of Thermoplastic Composite Materials*, 28(1):66–85, 2015.

[9] R. Heuss, N. Müller, N. Van Sintern, A. Starke, and A. Tschiesner. Lightweight, heavy impact, how carbon fiber and other lightweight materials will develop across industries and specifically in automotive, advanced industries. Technical report, McKinsey & Company, 2012.

[10] M. Favaloro. Thermoplastic composites in aerospace—the future looks bright. composites world. https://compositesworld.com/columns/thermoplastic-composites-in-aerospace-past-present-and-future. (accessed: 01.03.2021).

[11] G. Gardiner. Thermoplastic composite demonstrators – eu roadmap for future airframes. composites world. https://www.compositesworld.com/articles/thermoplastic-composite-demonstrators-eu-roadmap-for-future-airframes. (accessed: 01.03.2021).

[12] C. Sauer. *Challenges in Maintenance and Repair of Composites*. Lufthansa Technik, 2007.

[13] C. Soutis and P.T. Curtis. Prediction of the post-impact compressive strength of cfrp laminated composites. *Composites Science and Technology*, 56(6):677–684, 1996.

[14] B. Vieille, V.M. Casado, and C. Bouvet. About the impact behavior of woven-ply carbon fiber-reinforced thermoplastic- and thermosetting-composites: A comparative study. *Composite Structures*, 101(1):9–21, 2013.

[15] M. De Freitas, A. Silva, and L. Reis. Numerical evaluation of failure mechanisms on composite specimens subjected to impact loading. *Composites Part B: Engineering*, 31(3):199–207, 2000.

[16] Nobuo Takeda, R.L. Sierakowski, and L.E. Malvern. Microscopic observations of cross-sections of impacted composite laminates. *Compos Technol rev*, 4(2):40–44, 1982.

[17] N. Cristescu, L.E. Malvern, and R.L Sierakowski. Failure mechanisms in composite plates impacted by blunt-ended penetrators. In *ASTM Special Technical Publication*, Foreign Object Impact Damage to Composites, pages 159–172, Philadelphia, Pa, 1973. ASTM.

[18] G. Clark. Modeling of impact damage in composite laminates. *Composites*, 20(3):209–214, 1989.

[19] G. A. O. Davies and P Robinson. Predicting failure by debonding/delamination. *AGARD, Debonding/Delamination of Composites*, 28(1):7–24, 1992.

[20] Z. Ji, Z. Guan, and Z. Li. A progressive damage model for predicting permanent indentation and impact damage in composite laminates. *Applied Composite Materials*, 24(5):1029–1048, 2017.

[21] E. Panettieri, D. Fanteria, M. Montemurro, and C. Froustey. Low-velocity impact tests on carbon/epoxy composite laminates: A benchmark study. *Composites Part B: Engineering*, 107(1):9–21, 2016.

[22] L.E. Malvern, C.T. Sun, and D. Liu. Delamination damage in central impacts at subperforation speeds on laminated kevlar/epoxy plates. *ASTM STP*, 1012(-):387–405, 1989.

[23] M. De Freitas and L. Reis. Failure mechanisms on composite specimens subjected compression after impact. *Composite Structures*, 42(4):365–373, 1998.

[24] G. Belingardi and R. Vadori. Influence of the laminate thickness in low velocity impact behavior of composite material plate. *Composite Structures*, 61(1-2):27–38, 2003.

[25] X.C. Sun, L.F. Kawashita, A.S. Kaddour, M.J. Hiley, and S.R. Hallett. Comparison of low velocity impact modelling techniques for thermoplastic and thermoset polymer composites. *Composite Structures*, 203(1):659–671, 2018.

[26] F. Schimmer, S. Ladewig, N. Motsch, J.r Hausmann, and I. Ehrlich. Comparison of low-velocity impact damage behavior of unidirectional carbon fiber-reinforced thermoset and thermoplastic composites. *Key Engineering Materials*, 809(1):9–14, 2019.

[27] W.J. Cantwell and J. Morton. Geometrical effects in the low velocity impact response of cfrp. *Composite Structures*, 12(1):39–59, 1989.

[28] H.Y. Nezhad, A. Auffray, C.T. McCarthy, and R. O'Higgins. Impact damage response of carbon fibre-reinforced aerospace composite panels. In *ICCM International Conferences on Composite Materials*, Copenhagen, Denmark, 2015. International Committee on Composite Materials.

[29] P. Bajurko. Comparison of damage resistance of thermoplastic and thermoset carbon fibre-reinforced composites. *Journal of Thermoplastic Composite Materials*, 2019.

[30] H. Liu, J. Liu, Y. Ding, J. Zheng, X. Kong, J. Zhou, L. Harper, B.R.K. Blackman, A.J. Kinloch, and J.P. Dear. The behaviour of thermoplastic and thermoset carbon fibre composites subjected to low-velocity and high-velocity impact. *Journal of Materials Science*, 55(33):15741–15768, 2020.

[31] T. Lu, X. Chen, H. Wang, L. Zhang, and Y. Zhou. Comparison of low-velocity impact damage in thermoplastic and thermoset composites by non-destructive three-dimensional x-ray microscope. *Polymer Testing*, 91, 2020.

[32] B. Vieille, V.M. Casado, and C. Bouvet. Influence of matrix toughness and ductility on the compression-after-impact behavior of woven-ply thermoplastic- and thermosetting-composites: A comparative study. *Composite Structures*, 110(1):207–218, 2014.

[33] Y.P. Siow and V.P.W. Shim. An experimental study of low velocity impact damage in woven fiber composites. *Journal of Composite Materials*, 32(12):1178–1202, 1998.

[34] D. Whisler and H. Kim. Effect of impactor radius on low-velocity impact damage of glass/epoxy composites. *Journal of Composite Materials*, 46(25):3137–3149, 2012.

[35] F.J. Yang and W.J. Cantwell. impact damage initiation in composite materials. *Composites Science and Technology*, 70(2):336–342, 2010.

[36] N.R. Adsit and J.P. Waszczak. Effect of near-visual damage on the properties of graphite/epoxy. In *ASTM Special Technical Publication*, Composite Materials: Testing and Design, pages 101–117, Philadelphia, Pa, 1979. ASTM.

[37] M.P. Delaney, S.Y.K. Fung, and H. Kim. Dent depth visibility versus delamination damage for impact of composite panels by tips of varying radius. *Journal of Composite Materials*, 52(19):2691–2705, 2018.

[38] M.R. Wisnom. The role of delamination in failure of fibre-reinforced composites. *Philosophical Transactions of the Royal Society A: Mathematical, Physical and Engineering Sciences*, 370(1965):1850–1870, 2012.

[39] G. Davies, P. Irving, and C. Soutis. *Impact, post-impact strength, and post-impact fatigue behavior of polymer composites*. Elsevier, 2019.

[40] B. Yang, Y. Chen, J. Lee, K.a Fu, and Y. Li. In-plane compression response of woven cfrp composite after low-velocity impact: Modelling and experiment. *Thin-Walled Structures*, 158(1), 2021.

[41] Z. Cheng and J. Xiong. Progressive damage behaviors of woven composite laminates subjected to lvi, tai and cai. *Chinese Journal of Aeronautics*, 33(10):2807–2823, 2020.

[42] H. Tuo, Z. Lu, X. Ma, C. Zhang, and S. Chen. An experimental and numerical investigation on low-velocity impact damage and compression-after-impact behavior of composite laminates. *Composites Part B: Engineering*, 167(1):329–341, 2019.

[43] A. Soto, E.V. González, P. Maimí, F. Martín de la Escalera, J.R. Sainz de Aja, and E. Alvarez. Low velocity impact and compression after impact simulation of thin ply laminates. *Composites Part A: Applied Science and Manufacturing*, 109(1):413–427, -.

[44] M.A. Caminero, I. García-Moreno, and G.P. Rodríguez. Experimental study of the influence of thickness and ply-stacking sequence on the compression after impact strength of carbon fibre reinforced epoxy laminates. *Polymer Testing*, 66(1):360–370, 2018.

[45] J.C. Prichard and P.J. Hogg. The role of impact damage in post-impact compression testing. *Composites*, 21(6):503–511, 1990.

[46] D. Zhang, X. Zheng, J. Zhou, and W. Zhang. Bridging the low-velocity impact energy versus impact damage and residual compression strength for composite laminates. *Journal of Reinforced Plastics and Composites*, 0(0):1–13, 2020.

[47] S. Rivallant, C.R Bouvet, E. Abi Abdallah, B. Broll, and J.J. Barrau. Experimental analysis of cfrp laminates subjected to compression after impact: The role of impact-induced cracks in failure. *Composite Structures*, 111(1):147–157, 2014.

[48] I.F. Villegas. Ultrasonic welding of thermoplastic composites. *Frontiers in Materials*, 6(1):291, 2019.

[49] H. Potente. Ultrasonic welding - principles theory. *Materials and Design*, 5(5):228–234, 1984.

[50] Z. Zhang, X. Wang, Y. Luo, Z. Zhang, and L. Wang. Study on heating process of ultrasonic welding for thermoplastics. *Journal of Thermoplastic Composite Materials*, 23(5):647–664, 2010.

[51] A. Benatar and T.G. Gutowski. Ultrasonic welding of peek graphite apc-2 composites. *Polymer Engineering Science*, 29(23):1705–1721, 1989.

[52] I.F. Villegas. Strength development versus process data in ultrasonic welding of thermoplastic composites with flat energy directors and its application to the definition of optimum processing parameters. *Composites Part A: Applied Science and Manufacturing*, 65(1):27–37, 2014.

[53] ASTM International. Standard test method for measuring the damage resistance of a fiber-reinforced polymer matrix composite to a drop-weight impact event. 2005.

[54] G Davies and X Zhang. Impact damage prediction in carbon composite structure. *International Journal of Impact Engineering*, 16(1):149–170, 1995.

[55] T. Zhao, C. Broek, G. Palardy, I.F. Villegas, and R. Benedictus. Towards robust sequential ultrasonic spot welding of thermoplastic composites: Welding process control strategy for consistent weld quality. *Composites Part A: Applied Science and Manufacturing*, 109(1):355–367, 2018.

# Appendix A

## A.1 Impact data

The tables below show more detailed impact data of all impacts performed during this project. The data also includes drop height, impact velocity and maximum impact force.

| Impact # | Specimen | Impactor radius | Impactor weight | Height [mm] | Velocity [m/s] | Energy [J] | Energy [J/mm] | Fpeak [N] | Damaged area [mm^2] |
|---|---|---|---|---|---|---|---|---|---|
| 1 | 1.1 | 40 | 1925 | 691 | 3.21 | 9.91 | 2.29 | 7889.45 | 0 |
| 2 | 1.1 | 40 | 1925 | 1391 | 4.50 | 19.49 | 4.51 | 9649.07 | 0 |
| 3 | 1.1 | 40 | 3727.5 | 1078 | 4.17 | 32.47 | 7.52 | 11745.20 | 3136 |
| 4 | 1.2 | 40 | 3727.5 | 835 | 3.71 | 25.63 | 5.88 | 13245.20 | 0 |
| 5 | 1.3 | 40 | 3727.5 | 966 | 4.00 | 29.84 | 6.89 | 14625.00 | 2170 |
| 6 | 1.4 | 40 | 3727.5 | 855 | 3.79 | 26.77 | 6.18 | 13375.00 | 3456 |
| 7 | 1.5 | 40 | 3727.5 | 586 | 3.06 | 17.41 | 4.08 | 10129.80 | 0 |
| 8 | 1.5 | 40 | 3727.5 | 606 | 3.24 | 19.60 | 4.59 | 11206.80 | 0 |
| 9 | 1.5 | 40 | 3727.5 | 604 | 3.25 | 19.75 | 4.62 | 11504.80 | 0 |
| 10 | 1.5 | 40 | 3727.5 | 604 | 3.25 | 19.64 | 4.60 | 11399.10 | 2851 |
| 11 | 1.6 | 20 | 3515 | 642 | 3.28 | 18.90 | 4.31 | 10629.80 | 671.2 |
| 12 | 1.7 | 20 | 3515 | 534 | 2.96 | 15.38 | 3.51 | 9644.26 | 713.2 |
| 13 | 1.8 | 20 | 3515 | 433 | 2.67 | 12.48 | 2.92 | 9024.07 | 0 |
| 14 | 1.8 | 20 | 3515 | 423 | 2.71 | 12.90 | 3.01 | 9264.50 | 697.2 |
| 15 | 1.9 | 20 | 3515 | 474 | 2.85 | 14.24 | 3.27 | 9961.60 | 0 |
| 16 | 1.10 | 20 | 3515 | 508 | 2.95 | 15.34 | 3.52 | 10394.30 | 0 |
| 17 | 1.11 | 15 | 3560.8 | 502 | 2.93 | 15.27 | 3.53 | 8639.45 | 572.2 |
| 18 | 1.12 | 15 | 3560.8 | 299 | 2.34 | 9.75 | 2.31 | 3211.55 | 0 |
| 19 | 1.12 | 15 | 3560.8 | 370 | 2.49 | 11.00 | 2.61 | 5576.90 | 0 |
| 20 | 1.12 | 15 | 3560.8 | 370 | 2.43 | 10.48 | 2.49 | 5442.32 | 0 |
| 21 | 1.12 | 15 | 3560.8 | 364 | 2.42 | 10.44 | 2.48 | 3947.13 | 0 |
| 22 | 1.12 | 15 | 3560.8 | 429 | 2.72 | 13.17 | 3.13 | 7927.90 | 753.2 |
| 23 | 2.12 | 20 | 3515 | 506.97 | 2.92 | 15.03 | 3.50 | 10865.40 | 0 |
| 24 | 2.11 | 20 | 3515 | 529.549 | 3.00 | 15.86 | 3.69 | 10346.20 | 772 |
| 25 | 3.1.1 | 20 | 3515 | 536 | 3.08 | 16.72 | 3.84 | 10754.80 | 555.5 |
| 26 | 3.1.2 | 20 | 3515 | 537 | 3.07 | 16.55 | 3.80 | 11730.80 | 757.5 |
| 27 | 3.1.3 | 20 | 3515 | 518 | 2.96 | 15.38 | 3.53 | 11394.30 | 782.5 |
| 28 | 3.1.4 | 20 | 3515 | 441 | 2.73 | 13.07 | 3.00 | 9798.11 | 0 |
| 29 | 3.1.4(2) | 20 | 3515 | 441 | 2.79 | 13.65 | 3.13 | 10351.00 | 0 |
| 30 | 3.1.4(3) | 20 | 3515 | 441 | 2.74 | 13.21 | 3.03 | 10173.10 | 0 |
| 31 | 3.1.4(4) | 20 | 3515 | 441 | 2.73 | 13.14 | 3.01 | 10110.60 | 0 |
| 32 | 3.1.4(5) | 20 | 3515 | 474 | 2.81 | 13.90 | 3.19 | 10423.10 | 0 |
| 33 | 3.1.4(6) | 20 | 3515 | 474 | 2.84 | 14.17 | 3.25 | 9562.53 | 647 |
| 34 | 3.1.5 | 20 | 3515 | 522 | 2.95 | 15.28 | 3.50 | 11254.80 | 0 |
| 35 | 3.1.5(2) | 20 | 3515 | 522 | 2.97 | 15.55 | 3.57 | 9201.95 | 554 |
| 36 | 3.2.1 | 20 | 3515 | 534 | 3.06 | 16.41 | 3.76 | 11221.20 | 0 |
| 37 | 3.2.2 | 20 | 3515 | 534 | 3.02 | 16.07 | 3.69 | 11110.60 | 0 |
| 38 | 3.2.1(2) | 20 | 3515 | 534 | 3.01 | 15.93 | 3.65 | 10754.80 | 0 |
| 39 | 3.2.2(2) | 20 | 3515 | 534 | 2.99 | 15.69 | 3.60 | 10591.40 | 736 |
| 40 | 3.2.3 | 20 | 3515 | 553 | 3.03 | 16.14 | 3.70 | 10461.60 | 622 |
| 41 | 3.2.4 | 20 | 3515 | 534 | 3.05 | 16.38 | 3.76 | 11293.30 | 0 |
| 42 | 3.2.5 | 20 | 3515 | 535 | 3.01 | 15.90 | 3.65 | 10802.90 | 0 |
| 43 | 3.2.1(3) | 20 | 3515 | 521 | 2.98 | 15.62 | 3.58 | 11134.60 | 0 |
| 44 | 3.2.4(2) | 20 | 3515 | 521 | 2.93 | 15.10 | 3.46 | 10250.00 | 0 |
| 45 | 3.2.5(2) | 20 | 3515 | 521 | 2.98 | 15.59 | 3.57 | 10668.30 | 803 |
| 46 | 3.3.1 | 20 | 3515 | 553 | 3.02 | 16.07 | 3.69 | 10726.00 | 0 |
| 47 | 3.3.2 | 20 | 3515 | 553 | 3.01 | 15.93 | 3.65 | 10514.50 | 0 |
| 48 | 3.3.3 | 20 | 3515 | 552 | 3.00 | 15.83 | 3.63 | 10264.50 | 672 |
| 49 | 3.3.4 | 20 | 3515 | 566 | 3.07 | 16.59 | 3.80 | 11110.60 | 0 |
| 50 | 3.3.5 | 20 | 3515 | 566 | 3.09 | 16.79 | 3.85 | 9875.03 | 693 |
| 51 | 3.4.1 | 20 | 3515 | 566 | 3.06 | 16.45 | 3.77 | 11144.30 | 0 |
| 52 | 3.4.2 | 20 | 3515 | 566 | 3.09 | 16.79 | 3.85 | 11033.70 | 0 |
| 53 | 3.4.3 | 20 | 3515 | 566 | 3.14 | 17.28 | 3.96 | 11019.30 | 820 |
| 54 | 3.4.4 | 20 | 3515 | 566 | 3.08 | 16.65 | 3.82 | 10072.10 | 806 |
| 55 | 3.4.5 | 20 | 3515 | 566 | 3.06 | 16.41 | 3.76 | 11187.50 | 0 |
| 56 | 3.5.1 | 20 | 3515 | 543 | 3.00 | 15.79 | 3.62 | 11687.50 | 0 |
| 57 | 3.5.2 | 20 | 3515 | 543 | 3.01 | 15.97 | 3.66 | 11533.70 | 0 |
| 58 | 3.5.3 | 20 | 3515 | 543 | 3.04 | 16.21 | 3.72 | 11802.90 | 0 |
| 59 | 3.5.4 | 20 | 3515 | 553 | 3.08 | 16.65 | 3.82 | 11908.70 | 0 |
| 60 | 3.5.5 | 20 | 3515 | 553 | 3.06 | 16.41 | 3.76 | 12019.30 | 0 |
| 61 | 3.2.1(4) | 20 | 3515 | 475 | 2.86 | 14.34 | 3.29 | 11605.80 | 387 |
| 62 | 3.2.4(3) | 20 | 3515 | 534 | 2.98 | 15.65 | 3.59 | 9427.91 | 0 |
| 63 | 3.3.1(2) | 20 | 3515 | 566 | 3.02 | 16.07 | 3.69 | 9043.30 | 0 |
| 64 | 3.3.2(2) | 20 | 3515 | 564 | 3.12 | 17.07 | 3.91 | 9668.30 | 0 |
| 65 | 3.3.4(2) | 20 | 3515 | 565 | 3.05 | 16.38 | 3.76 | 9485.60 | 0 |
| 66 | 3.4.1(2) | 20 | 3515 | 566 | 3.07 | 16.59 | 3.80 | 8466.37 | 526 |

**Figure A1:** Impact data of all impacts

| Impact # | Specimen | Impactor radius | Impactor weight | Height [mm] | Velocity [m/s] | Energy [J] | Energy [J/mm] | Fpeak [N] | Damaged area [mm^2] |
|---|---|---|---|---|---|---|---|---|---|
| 67 | 3.4.2(2) | 20 | 3515 | 565 | 3.10 | 16.90 | 3.88 | 7899.06 | 654 |
| 68 | 3.4.5(2) | 20 | 3515 | 533 | 3.05 | 16.34 | 3.75 | 8798.10 | 586 |
| 69 | 3.5.1(2) | 20 | 3515 | 537 | 3.03 | 16.14 | 3.70 | 8456.76 | 580 |
| 70 | 3.5.2(2) | 20 | 3515 | 523 | 2.95 | 15.31 | 3.51 | 8153.87 | 718 |
| 71 | 3.5.3(2) | 20 | 3515 | 506 | 2.92 | 14.97 | 3.43 | 9105.80 | 0 |
| 72 | 3.5.4(2) | 20 | 3515 | 524 | 3.04 | 16.21 | 3.72 | 8793.30 | 696 |
| 73 | 3.5.5(2) | 20 | 3515 | 524 | 3.02 | 16.00 | 3.67 | 7620.21 | 431 |
| 74 | 3.2.4(4) | 20 | 3515 | 554 | 3.10 | 16.90 | 3.88 | 8596.18 | 610 |
| 75 | 3.3.1(3) | 20 | 3515 | 554 | 3.12 | 17.07 | 3.91 | 7798.10 | 611 |
| 76 | 3.3.2(3) | 20 | 3515 | 554 | 3.10 | 16.86 | 3.87 | 8264.45 | 774 |
| 77 | 3.3.4(3) | 20 | 3515 | 534 | 3.00 | 15.86 | 3.64 | 9384.64 | 0 |
| 78 | 3.5.3(3) | 20 | 3515 | 520 | 2.99 | 15.76 | 3.61 | 8043.29 | 676 |
| 79 | 3.3.4(4) | 20 | 3515 | 535 | 3.04 | 16.28 | 3.73 | 7807.72 | 842 |
| 80 | 2.1 | 20 | 3515 | 541 | 3.17 | 17.65 | 4.05 | 9375.03 | 860 |
| 81 | 2.2 | 20 | 3515 | 550 | 3.14 | 17.38 | 3.99 | 10105.80 | 404.6 |
| 82 | 2.3 | 20 | 3515 | 541 | 3.15 | 17.48 | 4.01 | 10677.90 | 778.3 |
| 83 | 2.4 | 20 | 3515 | 542 | 3.17 | 17.69 | 4.06 | 10466.40 | 770.4 |
| 84 | 2.5 | 20 | 3515 | 543 | 3.18 | 17.72 | 4.07 | 10158.70 | 856.6 |
| 85 | 2.6 | 20 | 3515 | 542 | 3.08 | 16.62 | 3.81 | 9206.76 | 682 |
| 86 | 2.7 | 20 | 3515 | 542 | 3.09 | 16.79 | 3.85 | 10298.10 | 1103.8 |
| 87 | 1.2 | 20 | 3515 | 551 | 3.02 | 16.07 | 3.69 | 8798.10 | 701.8 |
| 88 | 1.9 | 20 | 3515 | 542 | 3.07 | 16.55 | 3.80 | 9975.99 | 609.6 |
| 89 | 1.10 | 20 | 3515 | 543 | 3.06 | 16.45 | 3.77 | 9754.84 | 646.4 |

**Figure A2:** Impact data of all impacts (continued)

# Appendix B

## B.1 Welding sequence to determine the duration for the final repairs

| Specimen ID | $F_w$ | $A_w$ | $F_c$ | Welding duration | Welding energy | Degradation |
|---|---|---|---|---|---|---|
| 3.3.4 | 600N | $70\mu m$ | 600N | 2.0 sec | 1585 J | No |
| 3.1.3 | 600N | $70\mu m$ | 600N | 2.5 sec | 1695 J | No |
| 3.1.4 | 600N | $70\mu m$ | 600N | 3.0 sec | 2040 J | Yes |
| 3.1.2 | 600N | $70\mu m$ | 600N | 3.5 sec | 1810 J | No |

**Table B1:** Set of welding parameters used to determine welding duration for the final repairs

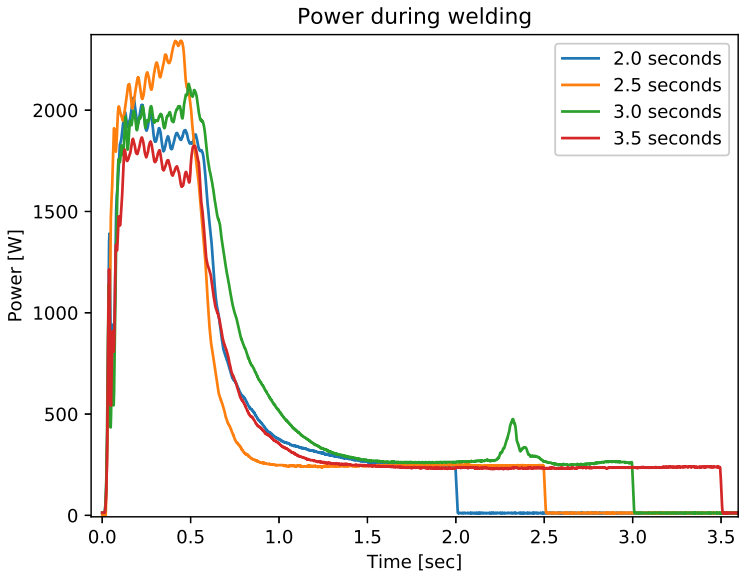


**Figure B1:** Power curves of the welds to determine the welding duration for the final repairs

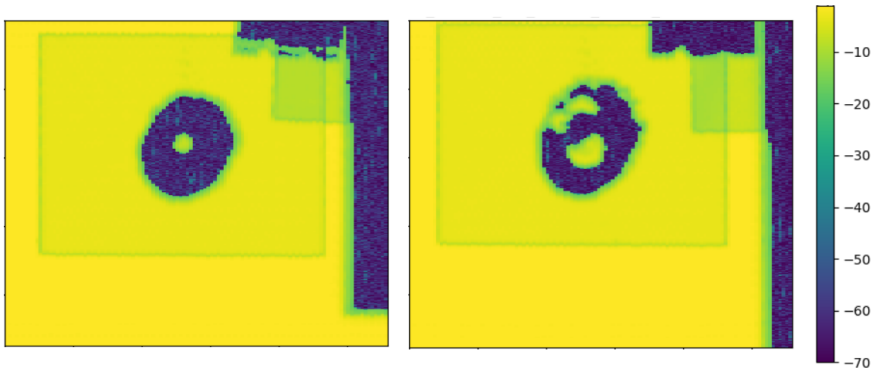


**(a)** 2.0 seconds

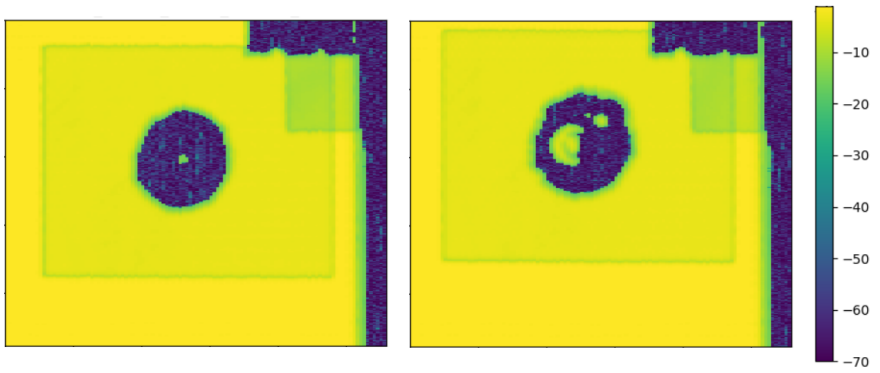


**(b)** 2.5 seconds

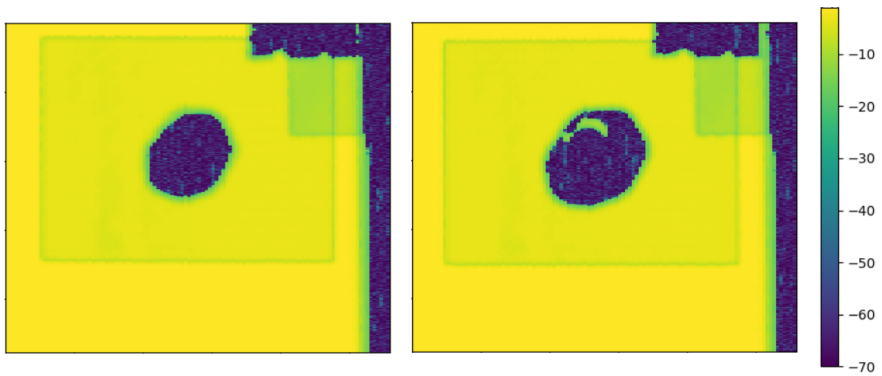


**(c)** 3.0 seconds

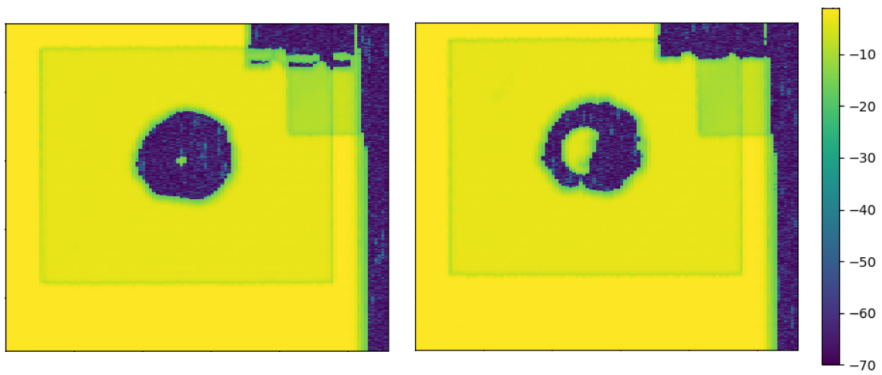


**(d)** 3.5 seconds

**Figure B2:** C-scans of the specimens which are welded to determine the welding duration for the final repairs. Left: before welding. Right: after welding.

# Appendix C

## C.1 Fiber damage inside damaged specimens

The figures show the extent of fiber damage on the non-impacted side of specimen 1.2 and 1.9.

**Figure C1:** Fiber damage on the non-impacted side of specimen 1.2

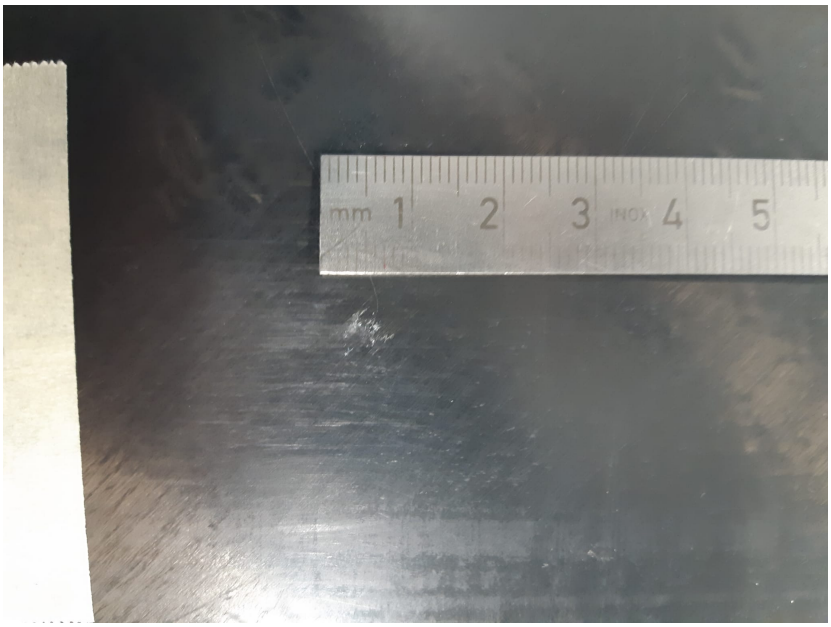


**Figure C2:** Fiber damage on the non-impacted side of specimen 1.9

## C.2 DIC data of all specimens

The figures below show the DIC data of all tested specimens. These include pristine, damaged, welded and pressed specimens.

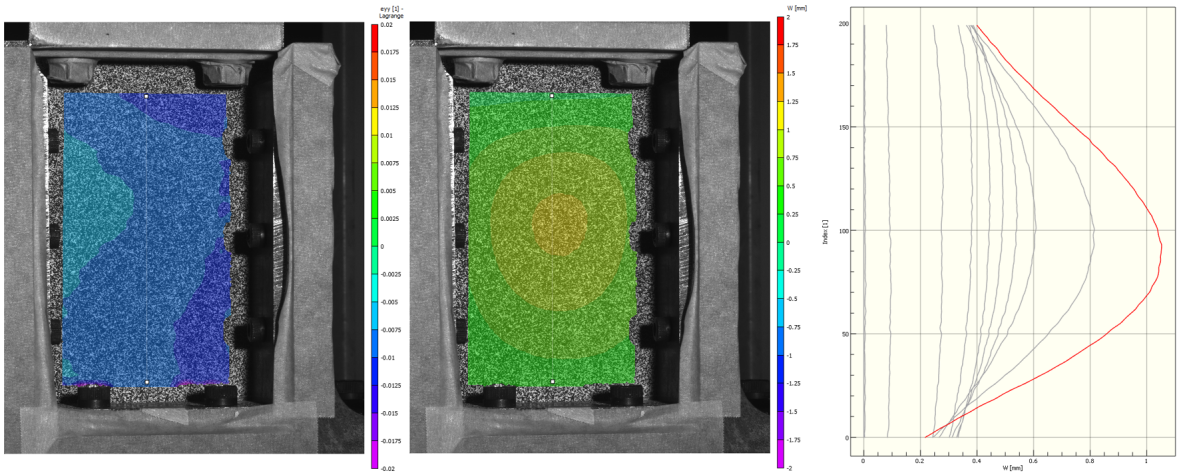

**(a)** 2.8

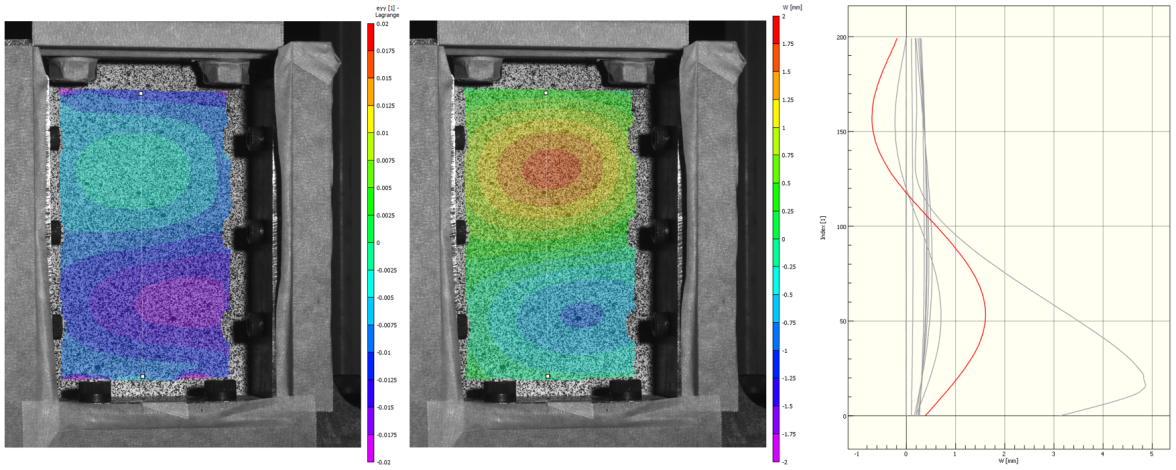

**(b)** 2.9

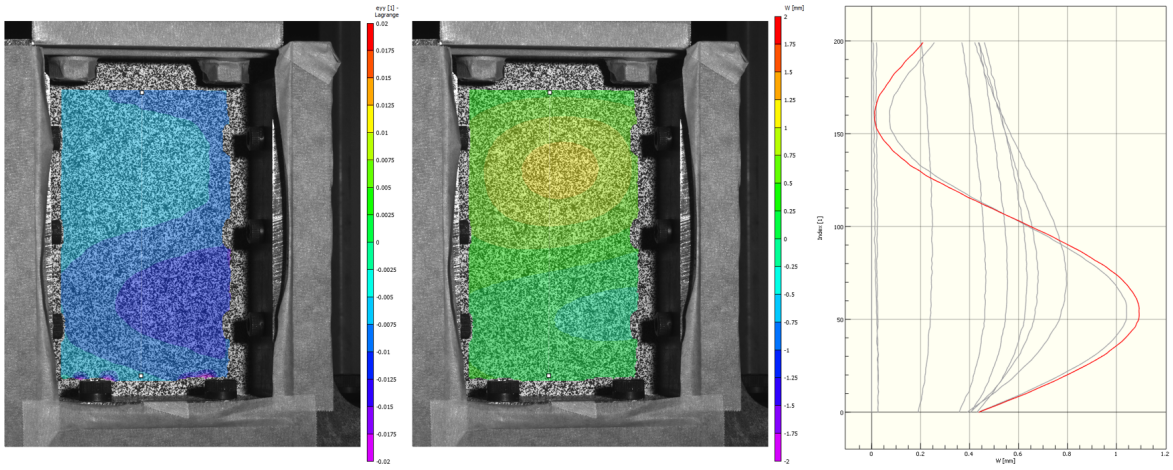

**(c)** 2.10

**Figure C3:** DIC data for pristine specimens. Left: Distribution of strain in y-direction just before failure , Middle: distribution of displacement in z-direction just before failure , Right: displacement in z-direction over the line that runs vertically through the middle of the specimen, progressing throughout the whole test.

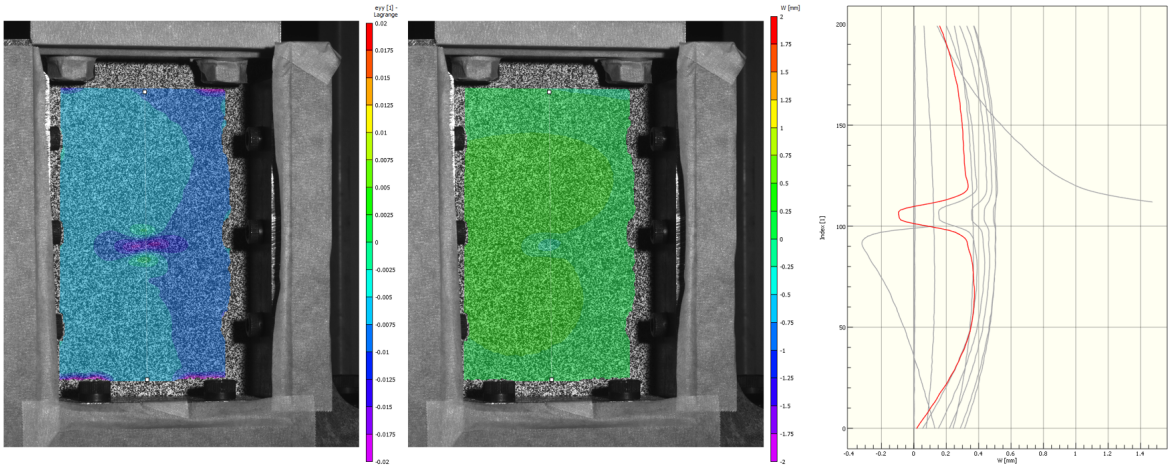

(a) 1.2

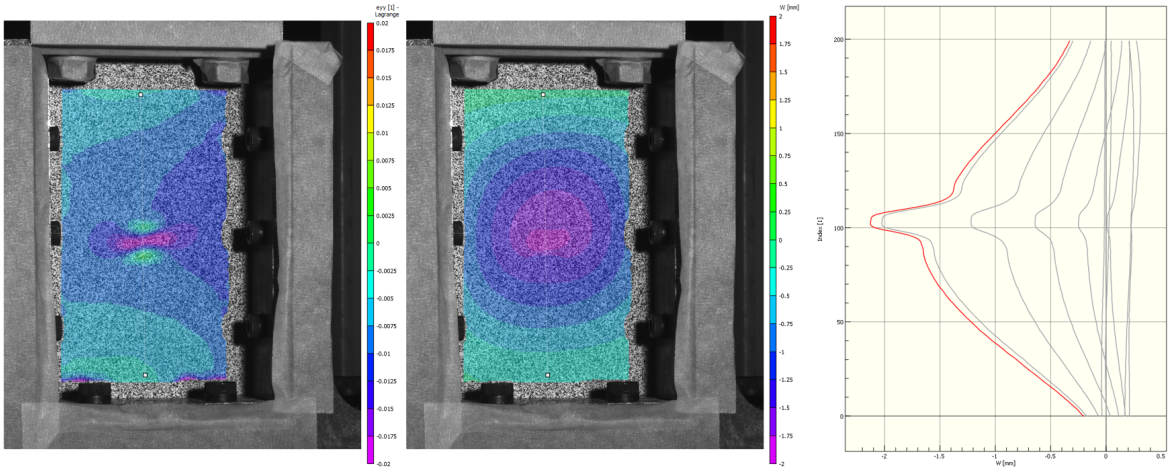

(b) 1.7

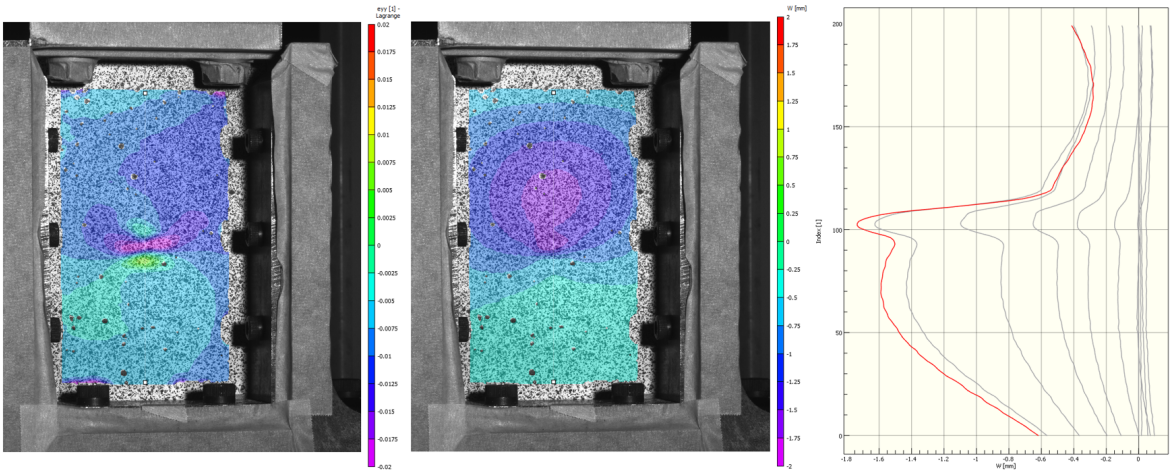

(c) 1.9

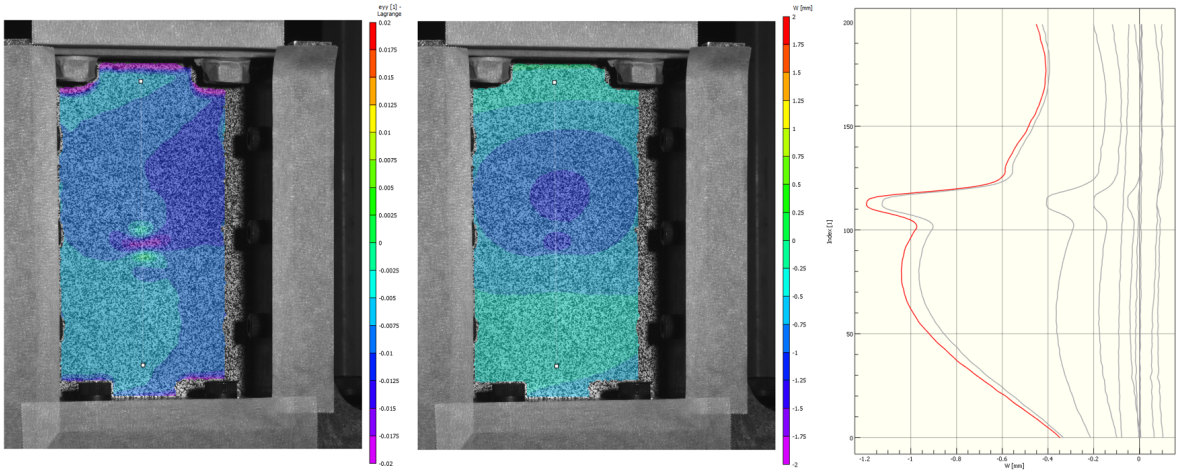

(d) 2.2

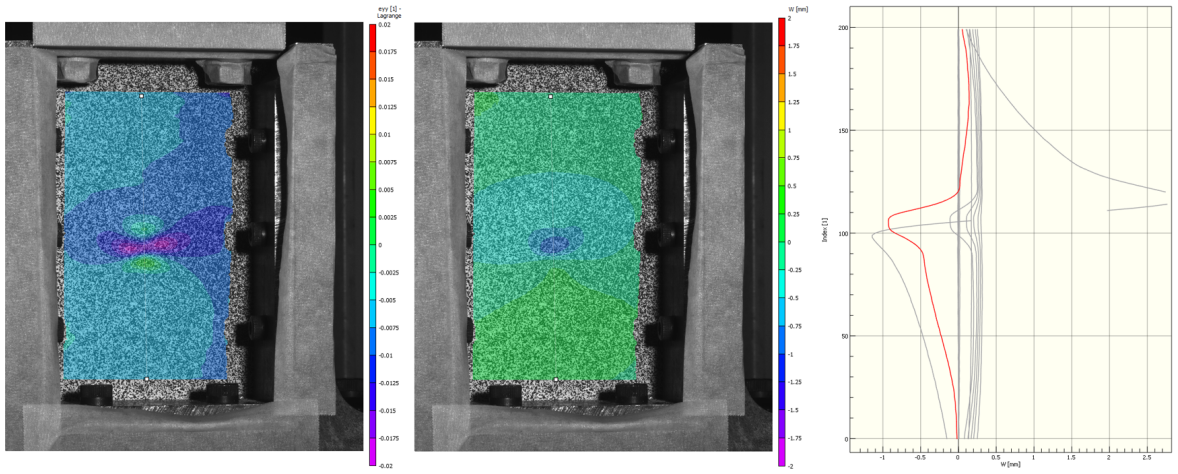

(e) 2.7

**Figure C4:** DIC data for damaged specimens. Left: Distribution of strain in y-direction just before failure , Middle: distribution of displacement in z-direction just before failure , Right: displacement in z-direction over the line that runs vertically through the middle of the specimen, progressing throughout the whole test.

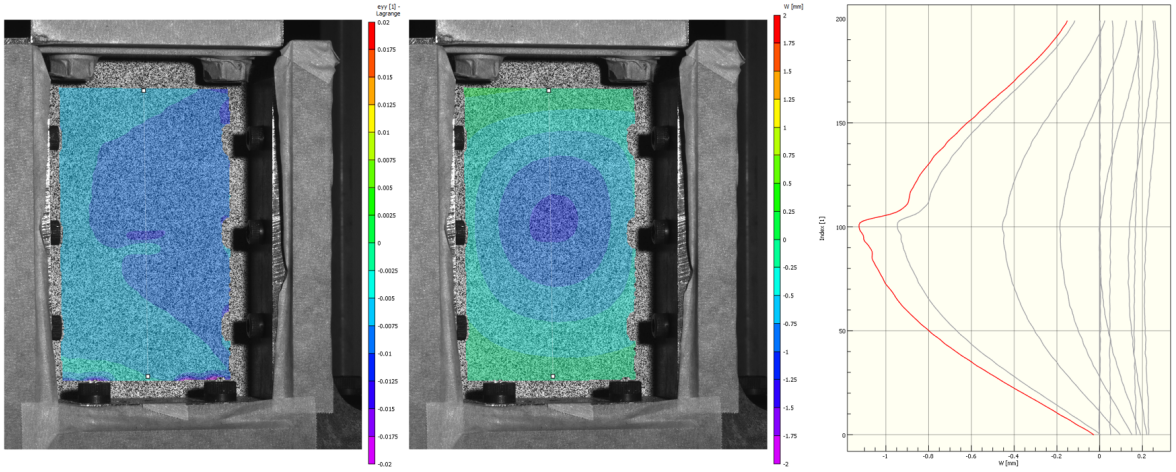

**(a)** 1.6

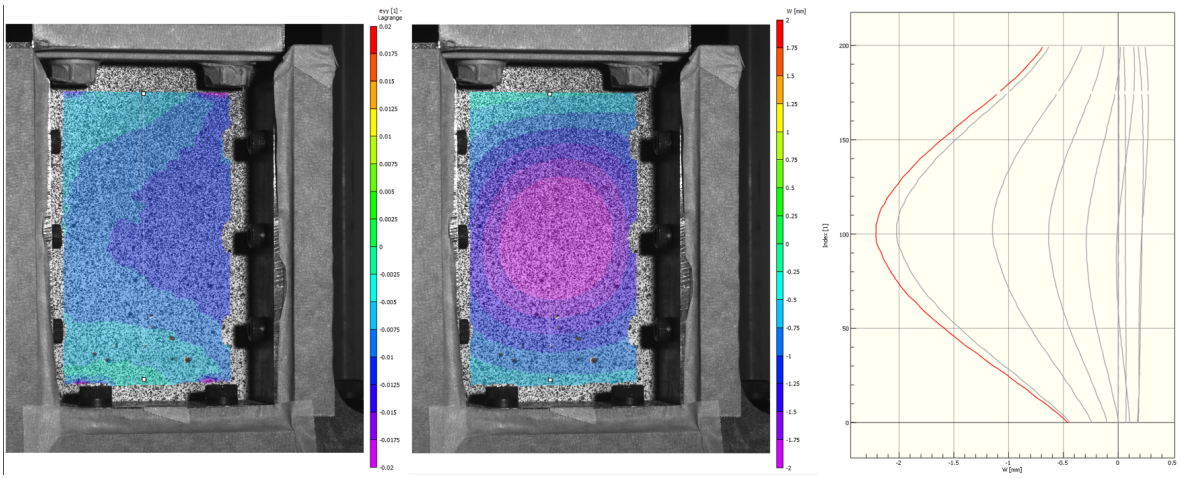

**(b)** 1.10

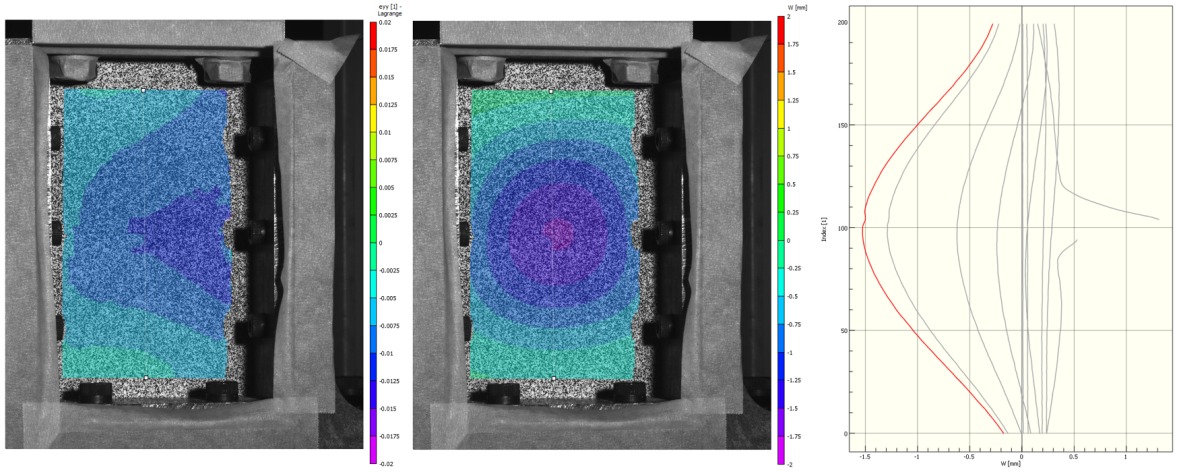

**(c)** 1.11

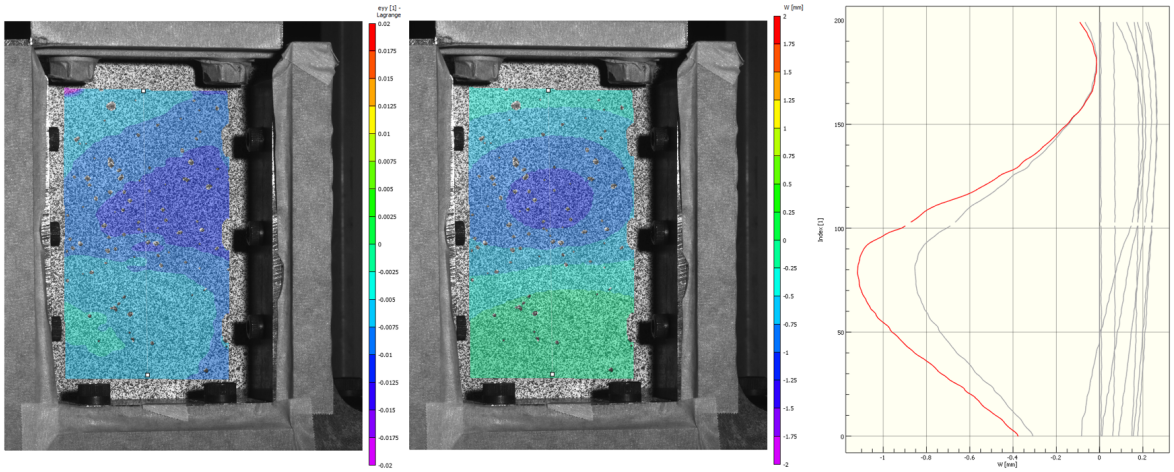

(d) 2.1

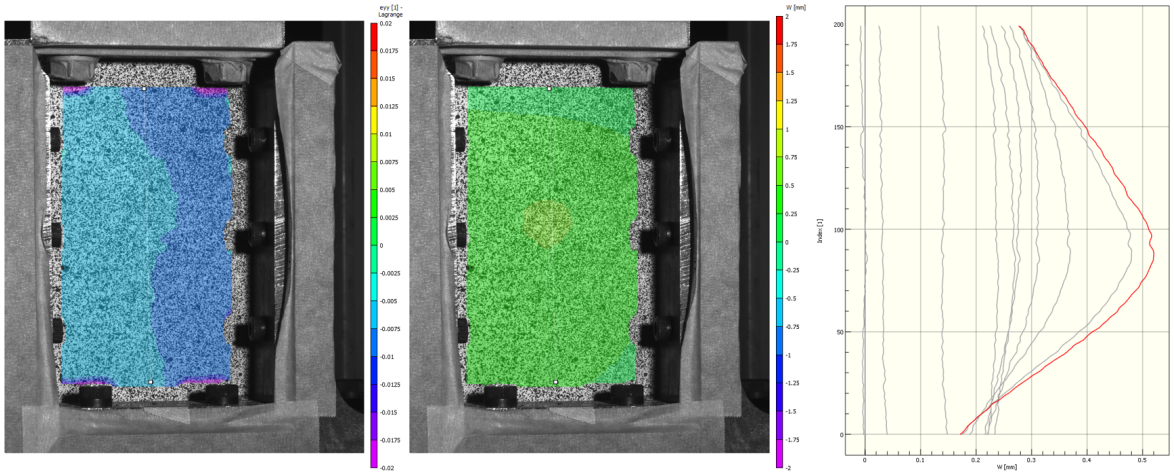

(e) 2.3

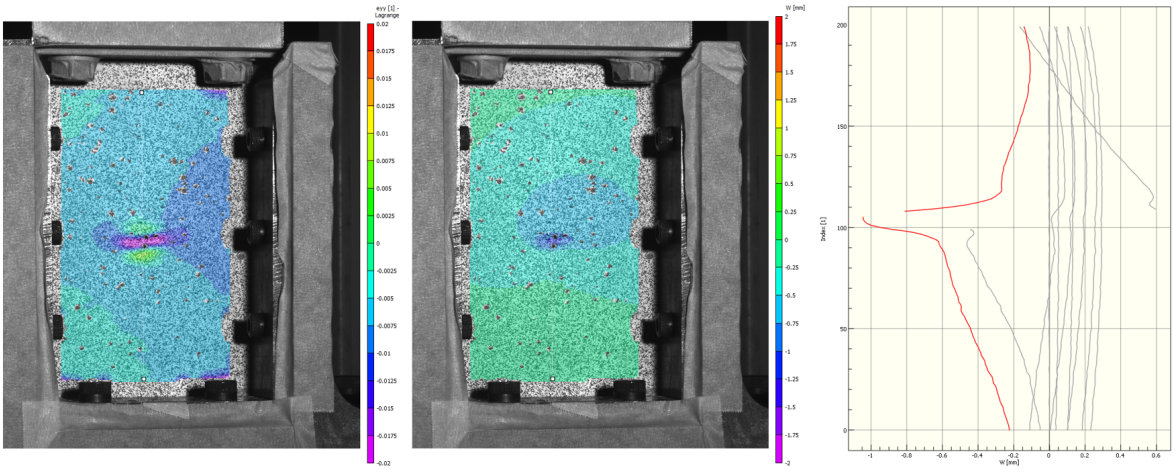

(f) 2.4

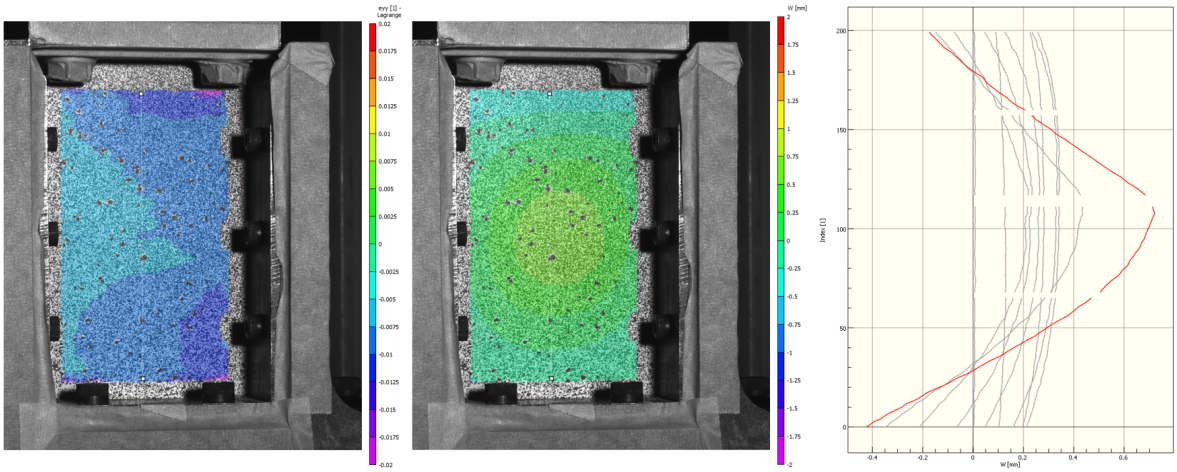

(g) 2.6

**Figure C5:** DIC data for welded specimens. Left: Distribution of strain in y-direction just before failure , Middle: distribution of displacement in z-direction just before failure , Right: displacement in z-direction over the line that runs vertically through the middle of the specimen, progressing throughout the whole test.

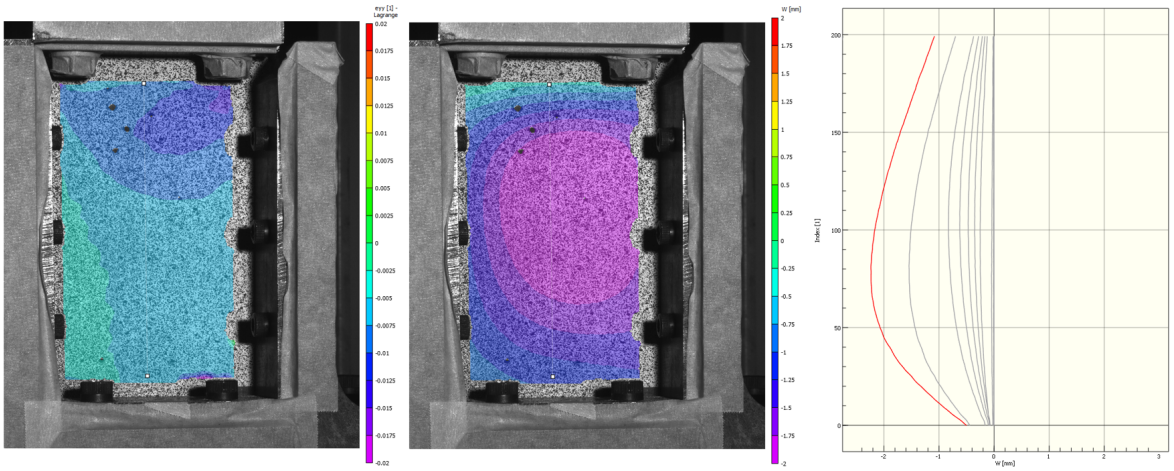

**(a)** 1.4

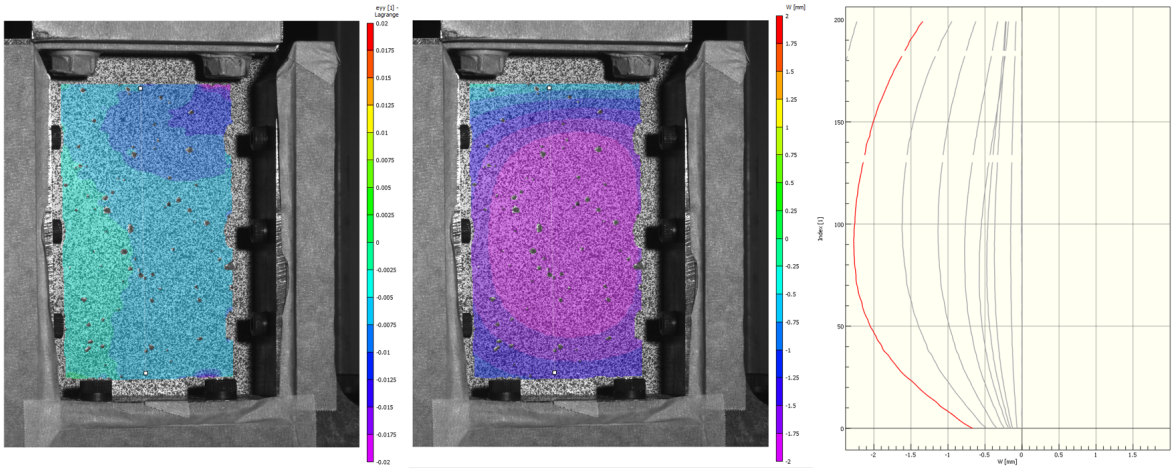

**(b)** 1.5

**Figure C6:** DIC data for pressed specimens. Left: Distribution of strain in y-direction just before failure , Middle: distribution of displacement in z-direction just before failure , Right: displacement in z-direction over the line that runs vertically through the middle of the specimen, progressing throughout the whole test.